# The performance of tungsten carbide end-mills in micro-milling of Ti-6Al-4V under nitrogen cooling

by

Maria Elizabeth Engelbrecht

Thesis presented in partial fulfilment of the requirements for the degree of Master of Engineering in the Faculty of Industrial Engineering at Stellenbosch University
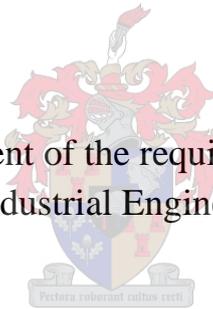
Supervisors: Mr. T.G. Dirkse van Schalkwyk

Dr G.A. Oosthuizen

Prof N. Sacks

March 2016

-

DECLARATION

By submitting this thesis electronically, I declare that the entirety of the work contained therein is my own, original work, that I am the sole author thereof (save to the extent explicitly otherwise stated), that reproduction and publication thereof by Stellenbosch University will not infringe any third party rights and that I have not previously in its entirety or in part submitted it for obtaining any qualification.

Date: March 2016

i

ACKNOWLEDGEMENTS

ABSTRACT

A strong demand exists from various industries to fabricate miniature devices and components with complex microscale features from a wide range of materials including Ti-6Al-4V. The need exists to improve the micro-machining process of using tungsten carbide end-mills to micro-mill Ti-6Al-4V. Key performance indicators are the rate of tool wear, tool life, surface finish as well as the forces experienced when machining.

In this research, the performance of tungsten carbide end-mills were investigated when micro-milling Ti-6Al-4V under nitrogen gas cooling. A rotatable central composite design of experiments was applied to generate the run-order of the experiments.

Tungsten carbide end-mills with a diameter of 1.5 mm were used to micro-mill Ti-6Al-4V. Each experimental run consisted of machining 6 slots of 70 mm each. The experimental variables were cutting speed, feed rate and depth of cut.

The tungsten carbide micro-tools were analysed before and after cutting to see the effect of the experimental conditions and Ti-6Al-4V workpiece material on the micro-tools. Cutting forces were also measured throughout the whole experimental procedure using an ATI Net F/T Gamma Sensor to measure forces and deduce the effects of the experimental conditions on the forces experienced by the tungsten carbide micro-tools at the tool workpiece interface. After each experimental run, the metal chips were gathered for analysis. The Ti-6Al-4V workpieces underwent microscopy to document the tool wear by measuring the width of the machined slots as well as atomic force microscopy to measure the surface roughness of each experiment.

The purpose of the experiments were to find settings for the three control factors that will maximise tool life and simultaneously minimise all the other responses. In order to achieve this, a mathematical model was fitted for each of the responses in terms of the three control factors. Once the models were established, numerical methods were used to find the optimal settings. For spindle speed (15000 – 17000 RPM), feed rate per tooth (20 – 28 μm) and depth of cut (93.75 – 156.25 μm), the results of the models predicted that an optimal solution can be found. To produce the best tool life, the values of the three factors should be 17000 RPM for spindle speed, 156.25 μm for depth of cut and 28 μm for feed per tooth. This yielded an overall desirability of 0.780. However, by increasing the limits of the three factors slightly to outside the experimental space the model can predict an even better solution. For ranges of spindle speed (15000 – 20000 RPM), feed rate per tooth (20 – 35 μm) and depth of cut (93.75 – 250 μm) the best tool life of 1800 mm was found at 19000 RPM for spindle speed, 243.10 μm for depth of cut and 34.80 μm for feed per tooth. This yielded a desirability of

1.000. Since the predicted optimal parameters lie outside of the experimental space it is suggested that future studies should explore this region.

OPSOMMING

Daar is 'n sterk aanvraag uit verskeie industrië om miniatuur toestelle en komponente met komplekse mikroskaal eienskappe te fabriseer uit 'n wye reeks materiale, insluitende Ti-6Al-4V. Daar bestaan 'n behoefte om die mikrofrees proses van Ti-6Al-4V, met die gebruik van tungsten karbied mikro beitels te verbeter. Die hoof faktore om te ondersoek is die tempo van beitel slytasie, oppervlak gladheid en die kragte betrokke by die masjineringsproses.

Hierdie navorsing fokus op hoe tungsten karbied mikro beitels vaar wanneer hulle Ti-6Al-4V sny terwyl hulle deur koue stikstof gas verkoel word. 'n Roteerbare sentrale saamgestelde ontwerp van eksperimente was saamgestel om die ekperimentele lopie volgorde te bepaal.

Tungsten karbied mikro beitels met 'n diameter van 1.5 mm was gebruik om Ti-6Al-4V te mikrofrees. Elke eksperimentele lopie het bestaan uit 6 gemasjineerde gleuwe van 70 mm elk. Die eksperimentele veranderlikes was snyspoed, voertempo per tand en sny diepte.

Die tungsten karbied mikro beitels is geanaliseer voor en na die snywerk om die effek van die eksperimentele kondisies en die Ti-6Al-4V op die beitels waar te neem. Snykragte is deur die duur van die eksperimente geneem deur gebruik van 'n ATI Net F/T Gamma Sensor om die effekte van die eksperimentele kondisies by die beitel-werkstuk interaksie area waar te neem. Na elke eksperimentele lopie is die metaal snysels versamel om ook geanaliseer te word. Die Ti-6Al-4V plate is onder 'n mikroskoop ondersoek om die wydte van die gemasjineerde gleuwe te meet. Die plate is ook deur 'n atomiese krag mikroskoop ondersoek om die oppervlak gladheid van die gleuwe te meet.

Die doel van die eksperimente was om die masjien stelbare stellings vir die drie veranderlikes te kry wat die beitel lewe maksimeer en terselfde tyd al die ander meetbare faktore minimeer. 'n Wiskundige model is op al die meetbare faktore gepas in terme van die drie veranderlike waardes. Na die model opgestel is, is statistiese metodes gebruik om die optimale stellings te bepaal. Die resultate van die model het aangedui dat daar vir snyspoed ((15000 – 17000 RPM), voertempo per tand (20 – 28 µm) en sny diepte (93.75 – 156.25 µm) 'n optimale oplossing voorspel kan word. Om die beste beitel lewe te bereik moet snyspoed gestel word teen 17000 RPM, voertempo per tand moet 28 µm wees en 'n diepte van 156.25 µm moet gesny word. Hierdie stellings het 'n totale begeerlikheid van 0.780. Nietemin, deur die drie faktore se waardes 'n klein bietjie na buite die eksperimentele area te verstel kan moontlik selfs 'n beter oplossing opgelewer word. Die resultate van die ander voorspelde model het aangedui dat daar vir snyspoed ((15000 – 20000 RPM), voertempo per tand (20 – 35 µm) en sny diepte (93.75 – 250 µm) 'n beter optimale oplossing voorspel kan word. Om die beste beitel lewe van 1800 mm te bereik moet snyspoed gestel word teen 19000 RPM, voertempo per tand moet 34.80 µm

wees en 'n diepte van 243.10 μm moet gesny word. Hierdie stellings het 'n totale begeerlikheid van 1.00. Aangesien die voorspelde optimale waardes buite die eksperimentele area is word daar voorgestel dat toekomstige studies hierdie area moet ondersoek.

TABLE OF CONTENTS

TABLES OF CONTENTS

TABLES OF CONTENTS

LIST OF FIGURES

LIST OF TABLES

NOMENCLATURE

Acronyms

ANOVA	Analysis of Variance
BCC	Body Centred Cubic
BHN	Brinell Hardness Humber
CCD	Central Composite Design
CI	Confidence Interval
CNC	Computer Numerical Control
CSV	Comma-Separated Values
DOE	Design of Experiments
EDS	Energy Dispersive X-ray Spectroscopy
ELI	Extra low interstitial
FCC	Face-Centred Cubic
G-Code	CNC Programming Language
HCP	Hexagonal Close-Packed
HRA	Rockwell Hardness
IM	Ingot Melting
MIM	Metal Injection Moulding
PcBN	Polycrystalline Cubic Boron Nitride
PCD	Polycrystalline Diamond
PM	Powder Metallurgy
PMMA	Polymethyl Methacrylate
RPM	Revolutions Per Minute
SEM	Scanning Electron Microscope
ST	Solution Treated

Greek Symbols

α	Alpha - The low temperature allotrope of a metal with a hexagonal, close-packed crystal structure
β	Beta - The high temperature allotrope of a metal with a body-centred cubic crystal structure

Other Symbols

a_p	Depth of Cut [mm]
D	Diameter [mm]
f_z	Feed Per Tooth [mm]
k_e	Number of Experimental Runs in CCD
n	Rotational Speed [rev/min]
n_c	Number of Centre Runs in CCD
S_a	Surface Roughness [nm]
v_c	Cutting Speed [m/min]
v_f	Feed Rate [mm/min]

Units

GPa	Gigapascal
Hz	Hertz
kPa	Kilopascal
MPa	Megapascal

Elements

C	Carbon
Co	Cobalt
Cr	Chromium
Cu	Copper
Fe	Iron
Hf	Hafnium
Mo	Molybdenum
N	Nitrogen
NaCl	Sodium Chloride
Nb	Niobium
O	Oxygen
Si	Silicon
Sn	Tin
Ta	Tantalum
Ti	Titanium
TiAlCrN	Titanium Aluminium Chromium Nitride

xvii

TiAlN   Titanium Aluminium Nitride

TiC   Titanium Cobalt

TiCN   Titanium Carbo Nitride

TiN   Titanium Nitride

V   Vanadium

WC   Tungsten Carbide

WC-Co   Tungsten Carbide Cobalt

Zr   Zirconium

GLOSSARY

Abrasion wear	A wear pattern that occurs due to the chips rubbing across the surface of the tool.
Adhesion	It is a condition where some of the work piece material welds to the cutting edge.
Alpha-beta structure	A microstructure containing α and β as the principal phases at a specific temperature.
Binder	A substance added to the powder to increase the strength of the compact and cement together powder particles that alone would not sinter into a strong object.
Cemented carbide	Material that is manufactured by combining tungsten carbide (WC) powders and binder cobalt powders (Co).
Chip	The material removed when machining.
Chip thickness	The maximum thickness of the metal chip removed by machining.
Corrosion	The deterioration of a metal by a chemical or electrochemical reaction with its environment.
Cutting Parameters	Parameters that fully characterise the mechanics of the material removal process. These include cutting speed, feed per tooth and axial depth of cut.
Cutting Speed	The velocity of the cutting edge of the tool relative to the stationary equipment.
Depth of cut	Describe the thickness of the work piece material that is to be removed by the cutting edge when machining.
Feed Per Tooth	The distance that the cutting edge penetrates the workpiece per tooth pass. Also known as the uncut chip thickness.
Hardness	A measure of the resistance of a material to surface indentation or abrasion; may be thought of as a function of the stress required to produce some specified type of surface deformation. There is no absolute scale for hardness.
Machinability	The relative ease of machining a metal.

Melting point   The temperature at which a pure metal, compound, or eutectic changes from solid to liquid. The temperature at which the liquid and solid are in equilibrium.

Micro-milling   The milling of components with two of more feature dimensions in the sub-millimetre range.

Microstructure   Refers to the phases and grain structure present in a metallic component.

Ploughing   The process of sliding and deforming instead of cutting through material.

Spindle   A rotation axis of a machine, on which a cutting tool is mounted.

CHAPTER 1
Introduction

There are various types of cutting tool materials currently on the market for use in machining, including carbide, high-speed steel, cast cobalt alloy, ceramic-based alumina, diamond and others (Ghani, et al., 2012). The use of straight tungsten carbide cutting tools is superior in almost all machining processes of titanium alloys and it is the preferred material for machining titanium and its alloys (Rahman, et al., 2002). Carbide-based cutting tools have been the most extensively used tool in the machining industry since they were introduced in Germany in the 1920s to realise the high-wear-resistance requirement of the mould industry (Ghani, et al., 2012). Carbide-based cutting tools are produced from the mixture of a carbide compound and a soft, ductile metal binder. This mixture is compressed before being sintered, making the resulting material hard and highly resistant and resilient to heat. Cutting tools composed of tungsten carbide (WC) with a cobalt (Co) binder were the first to be fabricated in the industry (Ghani, et al., 2012). In micro-machining it is critical to have precision cutting tools for micro cutting operations, since the surface quality and feature size of the microstructures are dependent on them.

A strong demand exists from various industries to fabricate miniature devices and components with complex microscale features from a wide range of materials including Ti-6Al-4V (Dornfeld, et al., 2006; Ehmann, et al., 2005; McKeown, 1987). Current industries involved include the medical, aerospace, military and transport industries (Filiz, et al., 2007). Miniature devices within the medical field include implantable devices that are used to replace damaged or diseased tissues, to perform targeted drug delivery, to monitor and correct functional abnormalities as well as performing tissue-tissue connections (Ouellette, 2001; Lavan, et al., 2003). These devices are required to be miniature in size and manufactured from biocompatible materials due to their functional needs together with their biological compatibility considerations (Ratner & Bryant, 2004; Davis, 2003).

The main biomaterials used include stainless steels, cobalt-based alloys and titanium and its alloys (Balazic, et al., 2007; Niinomi, 2003; Elias, et al., 2008). As a biomaterial, titanium is the newest metallic biomaterial in both the medical and dental fields and together with its alloys has demonstrated success as a biomedical device (Elias, et al., 2008).

Titanium and its alloys satisfy the property requirements for a biomaterial for biomedical applications better than any other competing material (Balazic, et al., 2007). Titanium alloys have excellent specific strength and corrosion resistance, no allergic problems and the best biocompatibility among metallic biomaterials (Niinomi, 2003).

1

The Ti-6Al-4V alloy is generally classified as difficult to machine because of its thermo-mechanical properties. The main challenge when machining titanium is to overcome the short tool life which prevents people from using high cutting speeds. Titanium has low thermal conductivity and high chemical affinity towards the cobalt binders that are found in most cutting tool materials. The low thermal conductivity increases the temperature at the cutting edge of the tool. The interface between titanium chips and cutting tools is quite small, which results in high cutting zone stresses. There is a strong tendency for titanium chips to pressure-weld to cutting tools and lastly, the low modulus of elasticity of titanium alloys and its high strength at elevated temperatures impair its machinability (Ezugwu & Wang, 1997; Che-Haron, 2001; Ghani, et al., 2012).

There are several ways to improve the machinability of titanium. These include the use of standard coolants or lubricants (Ezugwu & Wang, 1997), cryogenic cooling (Hong, et al., 2001), and the use of alternate cutting tool materials (Settineri & Faga, 2008) such as coated carbide cutting tools. The high temperatures experienced in the cutting zones has been traditionally tried to be controlled by using cutting fluids. Cutting fluids perform as coolant and lubricant. The coolant effect reduces the temperature in the cutting zone and the lubrication action decreases cutting forces. Thus, when using cutting fluids, the friction coefficient between tool and chip becomes lower in comparison to dry machining (El Baradie, 1996; Diniz & Micaroni, 2002; Vieira, et al., 2001). Instead of cutting fluids, some gases have also been used in machining including oxygen, carbon dioxide and gaseous and liquid nitrogen (Cakir, et al., 2004; Stanford, et al., 2009; Su, et al., 2007)

1.1. Problem Statement

The need exists to improve the micro-machining process of using tungsten carbide end-mills to micro-mill Ti-6Al-4V. Key performance indicators are the rate of tool wear, tool life, surface finish as well as the forces experienced when machining. This project will focus on the performance of tungsten carbide end-mills when micro-milling Ti-6Al-4V under nitrogen gas cooling.

1.2. Research Objective

In this research, the performance of tungsten carbide end-mills is investigated when micro-milling Ti-6Al-4V under nitrogen gas cooling. The main objective of the research is to find an optimal set of machine settings, for micro-milling with tungsten carbide end-mills. Tungsten carbide end-mills with a diameter of 1.5 mm are used to micro-mill Ti-6Al-4V. Each experimental run consists of machining 6 slots of 70 mm each. The experimental variables are cutting speed, feed rate and depth of cut. The tungsten carbide micro-tools are analysed before and after cutting to see the effect of the experimental conditions and Ti-6Al-4V workpiece material on the micro-tools. Cutting forces are

also measured throughout the whole experimental procedure using an ATI Net F/T Gamma Sensor to deduce the effects of the experimental conditions on the forces experienced by the tungsten carbide micro-tools at the tool workpiece interface. During each experimental run, the metal chips are gathered for analysis. After each experimental run, the Ti-6Al-4V workpieces undergo microscopy to document the tool wear by measuring the width of the machined slots as well as atomic force microscopy to measure the surface roughness of each experiment.

1.3. Research Approach

The approach for this project is to prepare a thorough literature review with the end goal of designing an experimental procedure to investigate the performance of tungsten carbide end-mills when micro-milling Ti-6Al-4V under nitrogen gas cooling. Once the experimental design is finalised, the experiments are to be completed. The next step will be data analysis together with the discussion of the results. The last step in the process will be to draw conclusions from all the results and observances.

Chapter 1 outlines the significance of micro-milling operations using tungsten carbide end-mills on Ti-6Al-4V in the medical field as well as the difficulties experienced when machining this metal. Chapter 2 presents a literature review of the current understanding of the factors involved in this project and their influence on machining performance. Chapter 3 presents the experimental design and methodology used during the experimental investigation of this project. The results from the investigations are presented and discussed in Chapters 4. Conclusions and recommendations for future work are presented in Chapter 5.

CHAPTER 2
Literature Review
2.1. Tungsten Carbide

Tungsten carbide (WC) is a chemical compound that contains equal parts of tungsten and carbon atoms. In its most basic form, tungsten carbide is a fine grey powder, but it can be pressed and formed into shapes for use in various industries such as: cutting tools, industrial machinery, abrasives, armour-piercing rounds, jewellery and various other tools and instruments (Atkins & Shriver, 2010).

Tungsten carbide is a compound that does not occur in nature. In the late 1890's it was fabricated for the first time by the Frenchman Henri Moissan. It took another two decades for the technological and commercial importance of the development of tungsten carbide to be recognised (Groover, 2013).

In the early 1900s tungsten became an important metal for incandescent lamp filaments. These filaments were produced by wire drawing and the traditional tool steel draw dies of the period were unsatisfactory for drawing tungsten wire due to excessive wear. There was a need for a much harder material and tungsten carbide was known to possess such hardness. In Germany, 1914, H. Voigtlander and H. Lohmann developed a fabrication process for hard carbide draw dies by sintering parts pressed from powders of tungsten carbide and/or molybdenum carbide.

Also in Germany, during the early and mid-1920s, the breakthrough leading to the modern technology of cemented carbides is linked to the work of K. Schrüter. He used tungsten carbide powders mixed with about 10% of a metal from the iron group and sintered the mixture at a temperature close to the melting point of the metal. He settled with cobalt as the best binder. This hard material was first marketed in Germany as "Widia" in 1926. Schrüter's patents were assigned to the General Electric Company under the trade name "Carboloy" and was first produced in 1928 (Groover, 2013).

Widia and Carboloy were used as cutting tool materials, with cobalt content in the range of 4% to 13%. These cutting tools were effective in the machining of cast iron and many nonferrous metals, but not in the cutting of steel. When machining steel the tools would wear rapidly by cratering. During the early 1930s, carbide cutting tool grades with tungsten carbide and titanium cobalt (TiCo) were developed for steel cutting. In 1931, the German firm Krupp started production of Widia X, which had a composition of 84% WC, 10% TiC, and 6% Co. In 1932, Carboloy Grade 831 was introduced in the United States. It contained 69% WC, 21% TiC, and 10% Co (Groover, 2013).

2.1.1. Properties

Tungsten carbide has a high melting point at 2 870 °C and its boiling point is at 6 000 °C when under a pressure equivalent to one standard atmosphere (101.3 kPa) (Pohanish, 2008). It has a thermal conductivity of 80 $Wm^{-1}K^{-1}$, and a coefficient of thermal expansion of ~ 5.5 x $10^{-6}K^{-1}$ (Upadhyaya, 2001).

Tungsten carbide is extremely hard, ranking 9 on Mohs scale, a Vickers number of 1700–2400 HV (Groover, 2013) and 18-22 GPa at 300 K (Kurlov & Gusev, 2013). It has a Young's modulus of approximately 700 GPa, which is twice as large as the modulus of other carbides (Cardarelli, 2008; Groover, 2013; Kurlov & Gusev, 2013). Further, tungsten carbide has a bulk modulus of 439 GPa and a shear modulus of 270 GPa (Kurlov & Gusev, 2013). It has an ultimate tensile strength of 344 MPa (Cardarelli, 2008), an ultimate compression strength of about 2.7 GPa and it has a Poisson's ratio of 0.31 (Kurlov & Gusev, 2013).

Table 1 below shows some properties of tungsten carbide according to the various percentages of tungsten carbide, cobalt and other carbides in the mixture (Upadhyaya, 2001).

Table 1: Properties of selected tungsten carbide hard metals (Upadhyaya, 2001)

Properties and Composition	Type 1	Type 2	Type 3	Type 4	Type 5
Composition, wt %					
• WC	94	85.3	74	78.5	60
• Co	6	12	25	11.5	9
• Other carbides (TiC, TaC, NbC)	-	2.7	-	10	31
Properties					
Density g cm^{-3}	14.9	14.2	12.9	13.0	10.6
Hardness HV_{30}	1580	1290	780	1380	1560
Bend strength, MPa	2000	2450	2900	2250	1700
Elastic modulus, MPa	630	580	470	560	520
Fracture toughness, MPa √m	9.6	12.7	14.5	10.9	8.1
Thermal conductivity $Wm^{-1}K^{-1}$	80	65	50	60	25
Thermal expansion coefficient $x10^{-6}K^{-1}$	5.5	5.9	7.5	6.4	7.2

2.1.2. Structure

Carbides of Group IV-VI transition *d*-metals belong to strongly nonstoichiometric interstitial compounds. Transition metals from the subgroups IVa and VI (Ti, Zr, Hf, V, Nb & Ta) form cubic carbides MC_y with carbon with the β1 – type rock salt (NaCl) structure. Metals of the subgroups Va

and VIa (V, Nb, Ta, Cr, Mo & W) form additional lower hexagonal carbides M_2C_y with the *L*'3 (W_2C) structure. The structures of these compound have a characteristic feature of having present the face-centred cubic (FCC) or hexagonal closely-packed (HCP) metallic lattice. Carbon atoms are located in the centre of octahedral or trigonal interstitials of the metallic lattice. The metallic sub-lattice symmetry, however, differs from that of transition metallic lattices. Thus the crystal structure of metals changes with the formation of carbides. Group IV metals (Ti, Zr & Hf), which have the hexagonal closely-packed structure, forms carbides with the face-centred cubic metallic sub-lattices. Metals with the body centred cubic (BCC) structure (V, Nb, Ta, Cr, Mo & W) form carbides with the cubic or hexagonal metallic sub-lattices, of which the cubic form is shown in Figure 1 (Kurlov & Gusev, 2013).
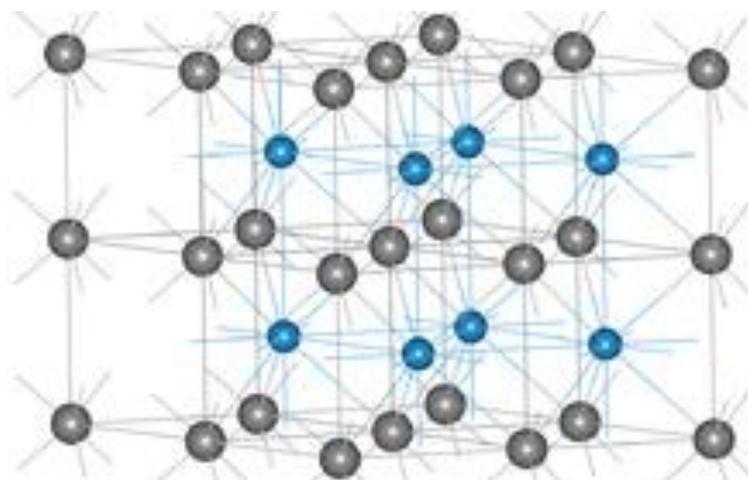
Figure 1: α - WC structure with the carbon atoms shown in grey (Kurlow & Gusev 2013).

Thus, there are two forms of tungsten carbide, a hexagonal form, α-WC and a cubic high-temperature form, β-WC, which has the rock salt structure. The hexagonal form can be visualized to be made up of a simple hexagonal lattice of metal atoms of layers lying directly over one another, with carbon atoms filling half the spaces giving both tungsten and carbon a regular trigonal prismatic with 6 carbon atoms attached to each tungsten atom. From the unit cell dimensions the following bond lengths can be determined; the distance between the tungsten atoms in a hexagonally packed layer is 291 pm, the shortest distance between tungsten atoms in adjoining layers is 284 pm, and the tungsten carbon bond length is 220 pm (Kurlov & Gusev, 2013).

2.1.3.   Tungsten carbide micro-tools

Tungsten carbide is a very important tool and die material due to its hardness, strength and wear resistance over a wide range of temperatures. These tools typically consist of tungsten-carbide particles that are bonded together in a cobalt matrix.

Powder metallurgy techniques are used to make these carbides. The first step in the process is to blend together the powders of tungsten and carbide in a ball mill or rotating mixer. The mixture, consisting of approximately 94% Tungsten (W) and 6% Carbon by weight, is heated to 1500 °C in a vacuum-induction furnace. This process causes the tungsten to be carburised and forms tungsten carbide in a fine powder form. Cobalt as a binding agent is then added to the tungsten carbide powder mixture together with an organic fluid (hexane). This new mixture is then ball milled to produce a uniform and homogenous mixture with particle sizes ranging from 1 to 5 μm. This process can take several hours or even days to be completed. After a uniform and homogenous mixture is achieved the mixture is dried and consolidated by cold compaction using pressures of about 200 MPa. The desired part or tool is then sintered in a hydrogen atmosphere or vacuum furnace at temperatures between 1350°C to 1600°C, depending on its composition. At these temperatures the cobalt is in a liquid phase and acts as a binder for the carbide particles. The tungsten carbide and cobalt powders can also be hot pressed at the sintering temperature using graphite dies (Kalpakjian & Schmid, 2006).

Throughout the manufacturing of a part or tool, the tungsten carbide undergoes a linear shrinkage of about 16% during sintering. This corresponds to a volume shrinkage of about 40%. The amount of cobalt present, ranging from 6 to 16%, significantly affects the properties of tungsten carbide tools. The strength, hardness and wear resistance of tungsten carbide decreases as the cobalt content increases, while the toughness of the tungsten carbide increases due to the higher toughness of cobalt. Tungsten carbide tools generally are used for cutting steels, cast irons, and abrasive nonferrous materials and have largely replaced high speed steel tools due to their better performance (Kalpakjian & Schmid, 2006).

In micro-machining it is critical to have precision cutting tools for micro cutting operations, since the surface quality and feature size of the microstructures are dependent on them. Currently, the geometries of micro-milling tools are created by scaling down macro tools but due to the increasing miniaturisation of components, it is becoming ever more complex to produce the required tools (Cardoso & Davim, 2012). In addition, several researchers have shown that micro-tools respond in a different way to cutting influences than macro tools do (Filiz, et al., 2008; Perez, et al., 2007). Conventional milling tools vary widely in size and design for different applications. In end-milling, the common issues are tool deflection and uneven distribution of cutting force among the cutting edges of the tools. The forces are concentrated on one side of the tool and cause the tool to bend in the direction of the workpiece feed. The extent of deflection depends greatly on the rigidity of the tool and the distance it extends from the spindle. The deflection is directly proportional to the cube

of the extension and the smaller the tool diameter, the more prone it is to deflection thus it has a greater effect in micro-milling due to the extremely small tool diameters (Saffar, et al., 2008).

The tool's diameter and cutting edge radius determines the achievable feature size and surface quality of the machined part (Sun & Cheng, 2010). The cutting edge radius of the tool determines the cutting tool sharpness and its influence on minimum chip thickness and it determines the effective rake angle of the tool. If the diameter of micro-tools can decrease even further, the size of features on miniature components could be comparable to those produced with the lithographic techniques (Chae, et al., 2006).

As far as the tool materials are concerned they include monocrystalline diamond, high speed steel, polycrystalline diamond (PCD), polycrystalline cubic boron nitride (PcBN) and coated and uncoated tungsten carbide. As can be seen in Figure 2, tungsten carbide is the most common choice due to its hardness, high toughness and relatively low price (Camara, et al., 2012; Chae, et al., 2006; Gietzelt & Eichhorn, 2012).

Diamond tools are often used for ultra-precision machining, but have a limited ability to machine ferrous materials. The high chemical affinity between diamond and ferrous materials causes severe wear, limiting its use to nonferrous micro-mechanical machining operations (Kalpakjian & Schmid, 2006; Shabouk & Nakamoto, 2002). Therefore, micro-tools such as micro-end-mills and drills are generally made from tungsten carbide, which has high hardness and strength at high temperatures (Kalpakjian & Schmid, 2006). To improve the wear resistance characteristics of micro-tools, very small grain size tungsten carbide (i.e. <600 nm) is fused together to form the tool. Cobalt is typically used as a binder and its content influences tool hardness. Smaller cobalt content makes the carbide harder, but at the expense of higher brittleness (Chae, et al., 2006).

Tungsten carbide cutting tools are generally used due to their hardness and strength over a broad range of temperatures. This range of temperatures can be seen in Figure 3 (Attanasio, et al., 2013).
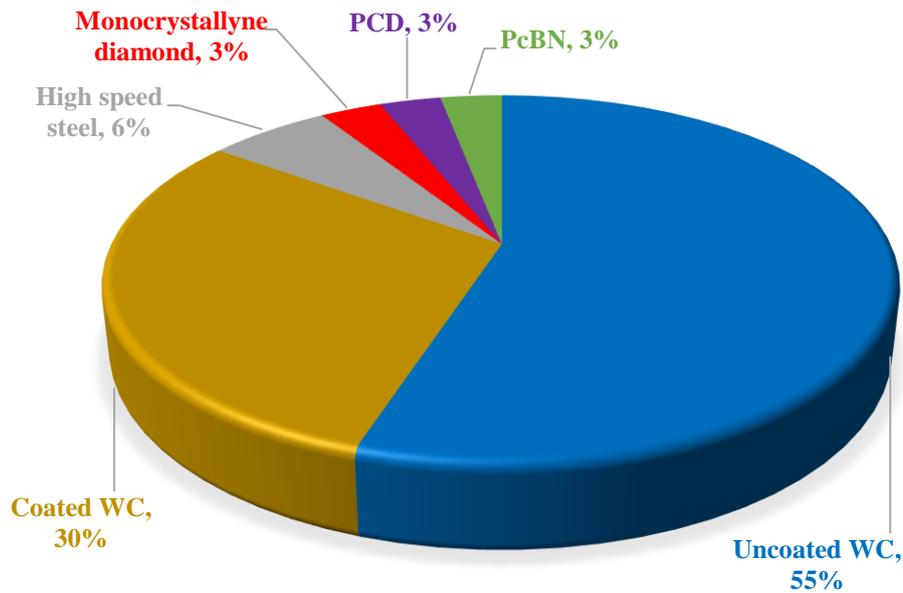
Figure 2: Principal tool materials used in micro-machining adapted from (Camara, et al., 2012)
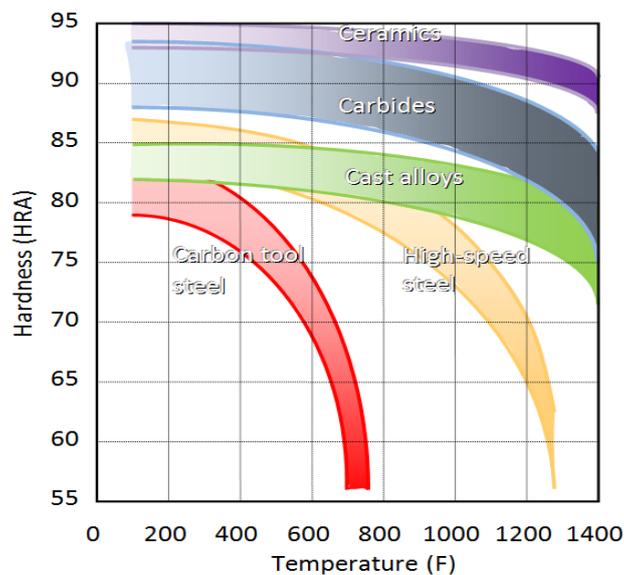
Figure 3: Hardness of cutting tool materials as a function of temperature adapted from (Attanasio, et al., 2013)

As mentioned before, the size of precision micro-cutting tools determines the limit of the size and accuracy of microstructure features. Smaller tools have decreased thermal expansion relative to their size, increased static stiffness from their short structure, increased dynamic stability from their higher natural frequency and potential for decreased cost due to smaller quantities of material (Monroy-Vazquez, et al., 2013). Commercially available micro-end-mills can be as small as 50 μm in diameter, with their helix angle fabricated by grinding. Figure 4 depicts a typical two-fluted micro-end-mill. Micro-tools of less than 50 μm need a zero helix angle to improve their rigidity and to mitigate the limitations of fabrication techniques (Benavides, et al., 2001; Schaller, et al., 1999). Onikura et al.

(2000) used ultrasonic vibration grinding to reduce the grinding forces and produced an 11 μm diameter micro-carbide tool (Onikura, et al., 2000). Schaller et al. (1999) fabricated micro-tungsten carbide tools using diamond-grinding disks (Schaller, et al., 1999).

Figure 4: A typical two-fluted tungsten carbide micro-end-mill (SGS Tool Company, 2015)

2.1.3.1. Coatings

In the early 1990s, the use of coatings to reduce tool wear and friction became more common and most of these coatings are referred to by their chemical composition, such as TiN (Titanium nitride), TiCN (Titanium carbo nitride), TiAlN (Titanium aluminium nitride) or TiAlCrN (Titanium aluminium chromium nitride), among others. Nowadays, TiAlN is the principal coating material applied to tungsten carbide cutters, but the other coatings, can also be applied successfully (Camara, et al., 2012).

The principle purpose of coating is to extend tool life by reducing tool wear. However, in cases of a thick coating layer the cutting edge radius is increased and consequently higher cutting forces are induced which renders the coating improvement regarding tool wear obsolete. The formation of coating droplets must be avoided during coating in order to prevent the coating resulting in worse machining properties (Piljek, et al., 2014). The majority of tool coatings are quite uniform and below 1 μm in thickness, and therefore rounding of the cutting edge can be neglected in some cases (Gietzelt & Eichhorn, 2012). However, the size of micro-end-mills makes coating deposition challenging especially around the cutting edges. The requirements on the coatings for micro-machining tools are not only the desirable properties such as high hardness, high toughness and high chemical/erosive and abrasive wear resistance, but they must also be dense, have a fine microstructure and present a smooth surface to the workpiece, with a reduced coefficient of friction compared to that of the uncoated tool (Aramcharoen, et al., 2008).

2.1.3.2. Tool failure

Tool failure a major issue in micro-machining, especially when dealing with hard and difficult to cut materials such as hardened steels, heat resistant alloys, ceramics and glasses. The life time of micro-tools is unpredictable and depends strongly on the workpiece material (Camara, et al., 2012; Gietzelt & Eichhorn, 2012). The smaller the tools are the smaller their thermal expansion rate is relative to

their size, their static stiffness is increased due to their compact structure and they have the potential for decreased cost due to smaller quantities of material utilised in their production (Chae, et al., 2006; Sun & Cheng, 2010). However, they are also more fragile and experience larger deflection which can manifest as tool run-out and chatter marks on the workpiece. Catastrophic tool failure may also occur as a result of chip clogging, failure by fatigue or failure caused by tool wear (Camara, et al., 2012; Dornfeld, et al., 2006). Chip clogging is the result of a poor chip evacuation process, and causes a rapid increase in cutting force and stress which leads to tool breakage. This mechanism is very unpredictable and happens extremely rapidly (Tansel, et al., 2000). Failure by fatigue may occur as a result of tool deflection and high spindle speeds employed.

Tool wear causes an increase in cutting edge radius and burr formation leading to elevation of the cutting forces to levels high enough to cause failure of the tool shaft (Camara, et al., 2012). Due to the small size of micro-tools the tool condition cannot be predicted based on visual inspection of the tool alone. Other strategies employed in micro-machining include predicting the tool condition based on monitoring of cutting forces (Dornfeld, et al., 2006), burr formation (Camara, et al., 2012), and acoustic emission (Mian, et al., 2011). Additionally, tool failure may occur as a consequence of cracks and impurities formed during the manufacturing process and covered by the coating (Gietzelt & Eichhorn, 2012).

In micro-milling an interesting phenomenon is seen related to the axial depth of cut and tool life. In conventional end-milling, increasing the depth of cut increases the resultant cutting force necessary for material removal. This increase in the required cutting force, increases the rate at which the tool cutting edge wears, leading to more rapid tool failure and reduced tool life (Essman, 2012). Zaman, et al. (2004), have suggested that the opposite could be true for micro-end-milling, up to a certain extent. They found that the tool life of micro-end-mills was greater for a larger depth of cut, as long as the depth of cut remained below that of the diameter of the tool (Zaman, et al., 2004). This can be explained geometrically by considering Figure 5 below. From the figure it can be seen that the ratio of depth of cut to the tool diameter is relatively higher in micro-end-milling (right) than in conventional milling (left). In this figure the unwrapped helix of a conventional tool and a micro-tool are shown and the amount of helix face involved in cutting for a certain depth of cut is compared in both cases. In the figure, d is the axial depth of cut, $a_1 + b_2$ is the length of the unwrapped helix face for a conventional end-mill (diameter D_2) and $a_2 + b_2$ is the unwrapped helix face of a micro-end-mill (diameter D_1). Thus,

$$\frac{b_2}{(a_1+b_2)} < \frac{b_2}{(a_2+b_2)} \text{ as } a_1 > a_2. \tag{1}$$

Therefore, the proportion of the helix face that is engaged for a certain depth of cut is relatively more in micro-milling than in conventional milling shown in Equation 1. This results in less idle distance traversed by the cutting edge for one rotation of the tool leading to reduced intensity on the cutting edge against the workpiece (Zaman, et al., 2004). This increase in tool life for an increased axial depth of cut is only up to a certain extent. According to Sreeram, et al. (2006), this phenomenon is only applicable while the axial depth of cut is below that of the tool diameter, beyond which the cutting force becomes too great, resulting in tool failure (Sreeram, et al., 2006).
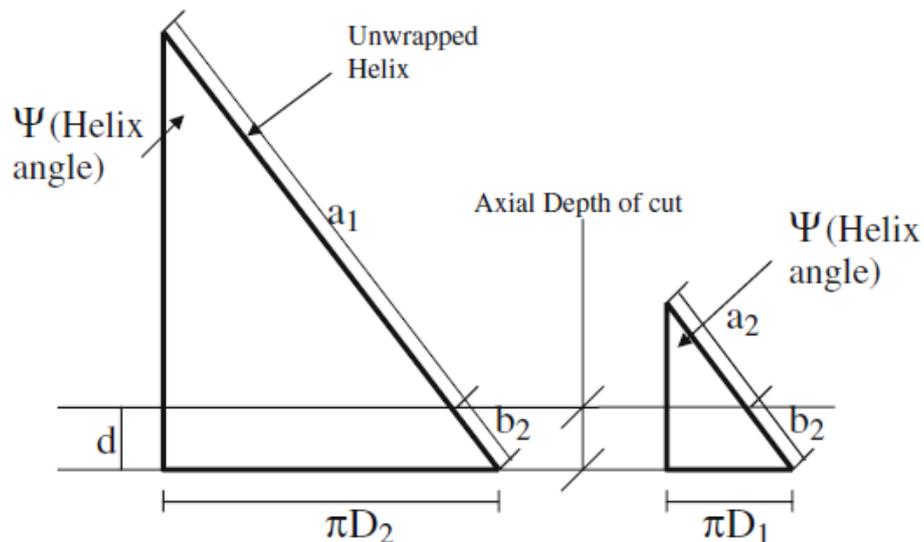
Figure 5: Ratio of depth of cut to tool diameter in conventional and micro-milling (Sreeram, et al., 2006)

2.1.3.3.   Tool wear and burrs

Tool wear is the gradual failure of cutting tools that occur during regular machining operations. The rate of tool wear depends on the tool and workpiece materials, tool geometry, process parameters and the characteristics of the machine used. The main wear mechanisms in micro-milling include abrasion and adhesion (Attanasio, et al., 2013). Abrasion is the reduction of the tool diameter during the cutting process due to the friction experienced by the cutting tool as the workpiece is fed past. Adhesion is when the chips that form during the cutting process is in effect welded to the cutting tool and thus affects the dimension of the tool as well as the cutting forces experienced by the tool during machining.

The small depth of cut in micro-machining significantly increases friction between the tool and the workpiece, resulting in thermal growth and wear. This results in an increased tool radius, decreases the quality of the produced part and increases the rate at which the tool fails (Liu & Mittal, 1996; Xiao, et al., 2003). Additionally, the suppression of burr development in micro-machining is very

important because post-processing cannot always be applied to remove burrs on miniature fabricated parts. While tool wear monitoring has been extensively studied on the macro-scale, limited work has been conducted at the micro-scale. Tansel et al. (2000) developed neural networks to predict tool wear using cutting force and wear data (Tansel, et al., 2000). The neural networks estimated tool condition in the micro-machining of aluminium and steel and found slower tool wear rates for aluminium than for steel. This phenomenon is in agreement with tool wear of soft and hard workpiece cutting observed by Weule et al. (2001). The neural network approach, however, requires extensive experimental data and is often inconsistent for different material and cutting conditions (Weule, et al., 2001). Rahman et al. (2001) investigated the micro-milling of copper. They concluded the wear of a 1 mm diameter tool depended on the tool helix angle and the depth of cut. Their experiments found that a small depth of cut of 150 μm has a higher tool wear rate than a larger depth of cut of 250 μm. They interpreted this result to occur due to a continuous chip being removed up the helix of the micro-tool which increased the force on its rake face (Rahman, et al., 2001).

Prakash et al. (2001) and Dow et al. (2004) empirically predicted tool life (Prakash, et al., 2001; Dow, et al., 2004). Using coated micro-end-mills, Prakash et al. (2001) found that the flank wear at the end of the cutting edge is highest, and that the feed rate and cutting speed have a more significant influence over the micro-cutting tool than the axial depth of cut. Dow et al. (2004) observed that as cutting tools wear, the edge of the cutting tool becomes flat. This flat area can be monitored with a scanning electron microscope (SEM) image of the tool edge. The influence of the tool size on tool wear was investigated by Weinert et al. (2004), who also used an SEM to measure the tool wear (Weinert & Petzoldt, 2004).

In micro-milling, the kinematics of the tool as it exits from the workpiece significantly affects burr formation due to the plastic deformation of chips rather than shearing (Byrne, et al., 2003). Weule et al. (2001) reported that burrs frequently occur when micro-machining hard materials because of increased tool wear (Weule, et al., 2001). Schaller et al. (1999) examined ways to remove burrs from brass and stainless steel micro-parts. To minimise burrs forming, they coated brass with a cyanacylate polymeric material. The polymeric material filled voids around the edges of the workpiece, where burrs form, allowing the cutting tool always to be engaged with the workpiece or the cyanacylate layer. After machining, the cyanacylate was removed with acetone in an ultrasonic bath (Schaller, et al., 1999).

2.2. Titanium and its Alloys

2.2.1. Metallurgy

Titanium is a transition metal with an incomplete shell in its electronic structure. This enables it to form solid solutions with most substitutional elements with a size factor of ±20%. Titanium has a high melting point of 1678°C in its elemental form (Long, et al., 1998).

Titanium undergoes an allotropic transformation at 882.5°C (Komanduri & Reed, 1983) where it changes from the alpha phase to beta phase which are the hexagonal close-packed (HCP) and body-centred cubic (BCC) structures respectively (Machado & Wallbank, 1990; Guillemot, 2005; Weiss & Semiatin, 1998). The transformation temperature is strongly influenced by the addition of certain elements. Elements that produce an increase in the temperature of transformation are aluminium (Al), oxygen (O), nitrogen (N) and carbon (C) and known as alpha stabilizers. Elements that produce a decrease in temperature of transformation are known as beta stabilizers and include molybdenum (Mo), vanadium (V), niobium (Nb), copper (Cu) and silicon (Si). Other elements have little influence on the transformation temperature and are known as neutral elements such as tin (Sn) and zirconium (Zr) (Machado & Wallbank, 1990; Guillemot, 2005; Balazic, et al., 2007; Geetha, et al., 2009). Titanium alloys are classified into four main groups:

➢ Unalloyed titanium

These alloys present excellent corrosion resistance but have low strength properties. Increases in strength can be achieved by the addition of small amounts of oxygen (O) and iron (Fe) (Machado & Wallbank, 1990).

➢ Alpha and near-alpha alloys

Alpha alloys contain alpha stabilizers and present excellent creep resistance; near-alpha alloys are alpha alloys that contain limited quantities of beta stabilizers but behave more like conventional alpha alloys (Machado & Wallbank, 1990; Geetha, et al., 2009). These alloys exhibit superior corrosion resistance with their use as biomedical materials being principally limited by their low ambient temperature strength (Long, et al., 1998). Alpha titanium alloys have thus far not been involved in the development of biomedical applications (Guillemot, 2005).

➢ Alpha-beta alloys

This group represents a mixture of "alpha" and "beta" phases at room temperature and contains additions of both alpha and beta stabilizers. This group of alloys is the largest used in the aerospace industries, and Ti-6Al-4V is its most common alloy (Machado & Wallbank, 1990).

Alpha-beta alloys exhibit higher strength due to the presence of both alpha and beta phases. Their specific properties depend upon composition, the relative proportions of the alpha/beta phases, and the alloy's prior thermal treatment and thermo-mechanical processing conditions (Long, et al., 1998). Alpha-beta alloys have the greatest commercial importance for biomedical application, since Ti-6Al-4V and Ti-6Al-4V ELI (extra low interstitial) are widely used as loadbearing orthopaedic implants due to their relatively good fatigue resistance and biological inactivity. These alloys however suffer from a large degree of biomechanical incompatibility, due to their relatively high elastic modulus compared to that of bone tissue (Guillemot, 2005).

➤ Beta alloys

This group contains significant quantities of beta stabilizers and is characterized by high hardenability but also a higher density (Machado & Wallbank, 1990). Beta alloys (metastable or stable) are titanium alloys with high strength, good formability and high hardenability. Beta alloys also offer the unique possibility of combined low elastic modulus and superior corrosion resistance (Long, et al., 1998). Metastable beta titanium alloys contain enough beta stabilizing elements to displace the martensite start line (Ms) at room temperature, consequently avoiding the formation of martensite alpha upon quenching (Guillemot, 2005).

The Ti-6Al-4V alloy is still the most commonly used alpha-beta titanium biomedical alloy and is normally used in an annealed condition. The metastable biomedical alloys are preferred in solution treated (ST) and, ST and aged conditions. The alpha-beta treated structures have higher strength, higher ductility and higher low cycle fatigue while the beta treated structures have higher fracture toughness. In general, the strength of an alloy increases with increasing beta stabilizer content (Geetha, et al., 2009).

According to the definition proposed at the Consensus Conference of the European Society for Biomaterials (1986), biomaterials are defined as nonviable materials used in a medical device, intended to interact with biologic systems; they possess a combination of characteristics including chemical, mechanical, physical and biologic properties that render them suitable for safe, effective and reliable use within a physiologic environment, an environment that is both extremely hostile and yet sensitive to unforgiving of irritating foreign bodies. These materials must be able to ensure the functional requirements (e.g., strength, fatigue strength and rigidity) and continue performing these functions for a long period of time (>20 years) without deterioration of the material itself or undesirable effects induced in the body tissues (Geetha, et al., 2009).

2.2.2.   Properties

Biomedical titanium alloys applied as biomaterial in hard tissue replacement must exhibit a low elastic modulus combined with enhanced strength, good fatigue resistance and good workability. The mechanical behaviour or titanium alloys are directly related to composition and thermo-mechanical processing (Balazic, et al., 2007). Table 2 shows some mechanical properties of selected titanium base materials that have been developed for medical applications (Niinomi, 1998).

The specific mechanical properties decide the type of material that will be selected for a specific application. The properties of prime importance are hardness, tensile strength, modulus of elasticity and elongation (Geetha, et al., 2009).

Mechanical strength of the alloys can be increased by adding alloying elements, which may lead to solid solution strengthening, or even precipitation of second phases. By using ageing processes, metastable structures obtained by rapid quenching from beta field may give rise to fine precipitates, which considerably increases the mechanical strength (Balazic, et al., 2007). Titanium alloys present a high strength-to-weight ratio, which is higher than with most of the steels. While commercially pure titanium has yield strength between 170 (grade 1) and 485 MPa (grade 4), titanium alloys may present values higher than 1500 MPa (Leyens & Peters, 2003).

The elastic modulus or Young's modulus corresponds to the stiffness of a material and is associated to the way interatomic forces vary with distance between atoms in the crystal structure. A comparison between both crystal structures of titanium has led to the conclusion that HCP structure presents higher values of elastic modulus than the BCC structure. Hence, addition of beta-stabiliser elements allows beta phase stabilisation and hence, low elastic modulus alloys. While commercially pure titanium shows elastic modulus values close to 105 GPa, Ti-6Al-4V type alpha-beta alloy presents values between 101 and 110 GPa, beta type titanium alloys may present values as low as 55 GPa (Niinomi, 1998). When compared with common alloys used as biomaterials, such as 316 L stainless steel (190 GPa) and Co-Cr alloys (210-253 GPa), low elastic modulus titanium alloys display a more compatible elastic behaviour to that of the human bone. In general, as the elastic modulus decreases, so does the mechanical strength and vice versa.

Table 2: Selected titanium based alloys developed for medical applications (Niinomi, 1998).

Material	Tensile Strength [MPa]	Yield Strength [MPa]	Elongation	Elastic Modulus [GPa]
Alpha type				
Pure Ti grade 1	240	170	24	102.7
Pure Ti grade 2	345	275	20	102.7
Pure Ti grade 3	450	380	18	103.4
Pure Ti grade 4	550	485	15	104.1
Alpha-beta type				
Ti-6Al-4V	895-930	825-869	6-10	110-114
Ti-6Al-4V ELI	860-965	795-875	10-15	101-110
Ti-6Al-7Nb	900-1050	880-950	8.1-15	114
Ti-5Al-2.5Fe	1020	895	15	112
Beta type				
Ti-13Nb-13Zr	973-1037	836-908	10-16	79-84
Ti-12Mo-6Zr-2Fe	1060-1100	1000-1060	18-22	74-85
Ti-15Mo	874	544	21	78
Ti-15Mo-5Zr-3Al	852-1100	838-1060	18-25	80
Ti-15Mo-2.8Nb-0.2Si	979-999	945-987	16-18	83
Ti-35.3Nb-5.1Ta-7.1Zr	596.7	547.1	19	55
Ti-29Nb-13Ta-4.6Zr	911	864	13.2	80

2.2.3. Machinability

Titanium alloys are among the most widely used and promising materials for medical implants. The selection of a titanium alloy for implantation is determined by a combination of the most desirable characteristics including immunity to corrosion, biocompatibility, shear strength, density and osteointegration (Rack & Qazi, 2006).

Machinability is defined by the Webster dictionary (Gove & others, 1963) as "the quality or state of being machinable"; "machinable" is defined as "capable of or suitable for being machined"; and to "machine" is defined as "to turn, shape, plane, mill, or otherwise reduce or finish by machine-operated tools," (Yang & Richard Liu, 1999).

Generally, there are three main aspects of machinability namely: tool life, surface finish, and power required to cut (Yang & Richard Liu, 1999). Part accuracy and the chip form or chip breakability are also used to assess machinability. The best criterion for rating machinability under normal conditions is the machining cost per part and under special conditions where machine capacity is limited and production output is of major concern, the proper machinability criterion is the number of parts per unit time (Yang & Richard Liu, 1999). Research by Kahles et al. (1985), shows that power requirements of cutting titanium alloys are lower than those of cutting steels and Nickle and Cobalt-based alloys (Kahles, et al., 1985). Their result is similar with the findings of Motonishi et al. (1987),

who state that no definite relation between cutting force and hardness and tensile strength of the titanium materials exists. They conclude that it cannot be said that the magnitude of cutting force causes difficulty in cutting (Motonishi, et al., 1987).

With regards to tool life however, the machinability of titanium and its alloys is poor. The tool wears fast and the cutting speed must be kept low, which gives rise to high machining cost per part (Yang & Richard Liu, 1999). Table 3 shows some machining time ratios for various types of titanium alloys compared to AISI 4340 steel at 300 Brinell Hardness Number (BHN). As can be seen, in most cases it takes longer to machine titanium and its alloys than it does to machine AISI 4340 steel.

Table 3: Machining time ratios for various titanium alloys compared to AISI steel at 300 BHN (Yang & Richard Liu, 1999).

Titanium alloy	Turning (Carbide Tool)	Face milling (Carbide Tool)	Drilling (HSS Tool)
Commercially pure 175 BHN	0.7:1	1.4:1	0.7:1
Alpha Ti-8Al-1Mo-1V 300 BHN	1.4:1	2.5:1	1:1
Alpha-beta Ti-6Al-4V 365 BHN	2.5:1	3.3:1	1.7:1
Beta Ti-13-V-11Cr-3Al 400 BHN	5:1	10:1	10:1

In previous research completed it was reported that it takes over three times as long to manufacture parts from titanium as to manufacture them from aluminium alloys (Wang, et al., 2007). It can also be seen from Table 3 that the hardness has a big impact on the machinability. This phenomenon is also reported in (Trucks, 1987) who claims that the machining characteristics of titanium alloys change significantly at hardness levels of 38 Rockwell (C scale). It is also seen in this table that alloy type has an impact on the machinability and (Trucks, 1987) reports similar results. When ranked in a descending order in terms of machinability, the materials are commercially pure titanium, alpha alloys, alpha-beta alloys, and beta alloys.

It is reported by (Ezugwu & Wang, 1997) that progress in the machining of titanium alloys has not kept pace with advances in the machining of other materials. This is due to their high temperature strength, very low thermal conductivity, relatively low modulus of elasticity and high chemical reactivity. Therefore, success in the machining of titanium alloys depends largely on the overcoming of the principal problems associated with the inherent properties of these materials (Ezugwu & Wang, 1997).

2.2.3.1. Processes of machining

Processes of machining titanium alloys involve conventional machining operations such as: turning, face milling, high speed cutting, milling and drilling; forming operations such as: cold and hot

forming, hydroforming and forging as well as alternative machining operations such as: laser cutting, water jet cutting, direct metal laser sintering, powder metallurgy (PM), ingot melting (IM) and metal injection moulding (MIM) (Niinomi, 2002; Balazic, et al., 2007).

2.2.3.2.   Specific machining problems

It is frequently reported that one or more factors are those most responsible for the poor machinability of titanium and its alloys. However, many characteristics operate together to cause this metal to be classified as a difficult to machine material. The reasons for the poor machinability of titanium and its alloys include the following:

➢   The high strength is maintained to elevated temperatures generated in machining and this opposes the plastic deformation needed to form a chip (Machado & Wallbank, 1990).

➢   Titanium's chip is very thin thus it has an unusually small contact area with the tool (one-third that of the contact area of a steel at the same feed rate and depth of cut (Machado & Wallbank, 1990; Siekmann, 1955; Zlatin & Field, 1973). This causes high stresses on top of the tool, although cutting forces are reported to be similar to steel and hence the power consumption in machining is approximately the same (Machado & Wallbank, 1990). The combination of a small contact area and the low thermal conductivity results in very high cutting temperatures. The cutting speed of the titanium must be low to avoid too short tool life. The high unit pressure resulting from the thin chip, high surface friction and high heat generated could give rise to pressure welding and galling (Yang & Richard Liu, 1999).

➢   It has a high coefficient of friction between the chip and the tool face; however Zlatin and Field (1973) showed this to be in line with that obtained in machining many steels (Zlatin & Field, 1973).

➢   There is strong chemical reactivity of titanium at the cutting temperature ($> 500°C$) with almost all tool materials available (Machado & Wallbank, 1990; Yang & Richard Liu, 1999). High affinity of titanium and its alloys for the interstitial oxygen and nitrogen gives rise to the pick-up of interstitials of the heated outer surface layer of the workpiece during machining, which contributes partially to the hardening of titanium and its alloys in addition to the strain hardening (Yang & Richard Liu, 1999). The active properties of titanium alloys control tool wear rate (especially crater wear) (Motonishi, et al., 1987).

➢   The adiabatic or catastrophic thermoplastic shear process by which titanium chips are formed. Titanium's low volumetric specific heat and relatively small contact area along with the presence of a very thin flow zone between the chip and the tool (approximately 8 µm compared

with 50 μm when cutting iron under the same cutting conditions cause high tool-tip temperatures of up to about 1100°C) (Machado & Wallbank, 1990).

➢ Even though the built-up edge have been said not to occur (Komanduri & Reed, 1983) have confirmed its presence at low cutting speeds, and this could lead to a poor surface finish in some operations.

➢ Low modulus of elasticity which can cause chatter, deflection and rubbing problems (Machado & Wallbank, 1990; Yang & Richard Liu, 1999). The forces perpendicular to the workpiece may increase three to four times as a result of a build-up of titanium on the wearland of the tool (the cutting forces will generally increase 25 to 50% as the tool dulls when cutting a steel) (Zlatin & Field, 1973). Because of this high thrust force and the low elastic modulus of titanium, the deflection of the workpiece can be a serious problem. Chatter is another main problem to be overcome when machining titanium alloys, especially for finish machining. When subjected to cutting pressure, titanium deflects nearly twice as much as carbon steel. The greater spring-back behind the cutting edge results in premature flank wear, vibrations and higher cutting temperatures (Ezugwu & Wang, 1997). In effect, there is a bouncing action as the cutting edge enters the cut. The appearance of chatter may also be partly ascribed to the high dynamic cutting forces in the machining of titanium. This can be up to 30% of the value of the static forces due to the adiabatic or catastrophic thermoplastic shear process by which titanium chips are formed (Komanduri & Reed, 1983).

➢ Care must be taken about titanium's tendency to ignite during machining because of the high temperatures involved (Machado & Wallbank, 1990; Yang & Richard Liu, 1999).

➢ There is a high rate of work hardening; however according to Machado and Wallbank (1990) it work-hardens to a lesser extent than steel (Machado & Wallbank, 1990).

➢ The poor thermal properties of the materials (Machado & Wallbank, 1990; Yang & Richard Liu, 1999). This problem may be more pronounced in drilling operation using conventional twist drills because cutting speed diminishes towards the centre resulting in considerable cutting forces and excessive heat (Yang & Richard Liu, 1999).

All these facts above, whether they are operating separately or in combination cause rapid wear, chipping or even catastrophic failure of the tools and hence add to the difficulty in machining titanium and its alloys.

2.2.3.3.   Chip formation and effects of cutting conditions

While most materials can form a continuous chip with relatively uniform thickness, those formed by titanium are serrated and have thus been classified as "catastrophic shear chips" (Komanduri & Brown, 1981). The strain in the chip is confined to narrow bands between the segments with very

little deformation within these segments (Machado & Wallbank, 1990; Bayoumi & Xie, 1995; Komanduri, et al., 1982). The intensive shear takes place in a narrow zone rather than in a plane as is assumed by some investigations in the analysis of orthogonal machining process (Bayoumi & Xie, 1995).

Machado and Wallbank (1990) have again explained the characteristics of the chip's segmentation by means of a model. In this model the rate of decrease in strength resulting from the local increase in temperature equals or exceeds the rate of increase in strength due to strain hardening in the primary shear zone. Shear to form the chip occurs on a particular shear plane when the stress built up by the relative tool motion exceeds the yield strength of the material. The energy associated with this deformation is converted immediately into thermal energy and because of titanium's poor thermal properties large temperature rises occur. This in turn causes the effect of temperature softening locally and thus the strain continues in the same plane instead of moving to a new plane in the colder material. As deformation proceeds the deforming shear plane rotates, thus becoming larger until the increased force due to this rotation exceeds the force needed to plastically deform colder material on a more favourable plane (Machado & Wallbank, 1990).

This process has been referred to as "catastrophic thermoplastic shear" (Recht, 1964) or "adiabatic shear" (Lemaire & Backofen, 1972; Von Turkovich, 1970) and results in a cyclic process producing a saw-tooth chip form. Although this process of chip formation can be applied to commercially pure titanium and all of its alloys, Motonishi et al. (1987) have suggested that the conditions of segmentation vary according to the microstructure and that no conspicuous serrated chip is observed in alpha alloys. They also state that a typical serrated chip is observed in the alpha-beta alloys and the adiabatic shear deformation occurs twice to form one chip serration in beta alloys (Motonishi, et al., 1987).

The shear localization has multiple effects (Machado & Wallbank, 1990; Bayoumi & Xie, 1995). First, such chips cause cyclic variation of force (both cutting and thrust) and consequent vibration or chatter in the metal cutting process and this in turn can encourage chatter to occur under unfavourable conditions, resulting in an undulating surface finish. Second, with poor thermal properties, shear localization causes an increase of the local temperature at the shear band to such a high value that it induces a phase transformation. Some non-diffusional phase transformation has been observed owing to the change in beta structure into alpha phase during chip formation. Third, this high temperature can cause a rapid chemical reaction and is most certainly responsible for the high tool wear on the rake face. Fourth, cavities have been observed in the shear band, which have a significant effect on

the mechanical properties. Fifth, shear bands are good sites for fracture and nucleation of cracks since they are usually very brittle and have different microstructures with respect to matrix materials.

The effects of cutting conditions on chip formation can be understood by the effect of those on the cutting temperature and hence the work hardening or softening rate. At low speed, thermal gradients are lower and the distance between the shear bands is less. This distance approaches zero as the velocity decreases to the critical value at which deformation becomes uniform (Recht, 1964). This critical cutting speed can be expected to decrease with increasing feed rate because the cutting temperature will increase. Thickness of the segments has been shown to decrease with a decrease in depth of cut and rake angle. The critical cutting speed, however, is explained in terms of a temperature-dependent process, and this conclusion of a purely thermally activated process may not be reliable.

The presence of a very thin "flow zone" between the chip and the tool have been confirmed and after comparing the structure in this zone and across the chip, it was concluded that the mechanisms of catastrophic thermoplastic shear also occur in the secondary shear zone of the chips (Machado & Wallbank, 1990).

2.2.3.4.   Surface integrity

Titanium is generally used as a material for parts requiring the greatest reliability, and therefore the surface integrity must be maintained. Surface integrity has been defined as the inherent or enhanced condition of a surface produced by machining. Its parameters includes residual stress, metallurgical alterations, and surface finish (Zlatin & Field, 1973).

The surface of titanium alloys is easily damaged during machining and grinding operations due to their poor machinability. The damage appears in the form of micro-cracks, built-up edge, plastic deformation, heat-affected zones, and tensile residual stresses (Yang & Richard Liu, 1999).

Parameters that has an impact on the residual stress include cutting speed, depth of cut, fluid type, coolant pressure, velocity of grinding wheel, and grit size (Yang & Richard Liu, 1999). High variations of residual stress on the same surface exist on ground surfaces and low variations of residual stress exist on single-point cut surfaces. The inherent differences in cutting point geometry between grinding and single-point cutting are believed to be primarily responsible for such differences (Yang & Richard Liu, 1999). When machining titanium in an abusive manner an overheated white layer can be produced that could be harder or softer than the base materials (Ezugwu & Wang, 1997). Under both gentle and abusive machining conditions, however, the surface residual

stresses appear compressive and their values differ according to the cutting conditions (such as the cutting speed).

Abusive grinding practices produce high-residual tensile surface stresses, whilst gentle grinding produces beneficial shallow compressive stresses (Kahles, et al., 1985). The surfaces produced under abusive conditions are also damaged by deformation and micro-cracks, which contribute to the loss of fatigue strength and stress corrosion resistance in combination with the residual stress pattern.

2.2.3.5. Cutting temperatures and stresses

The principal reasons for the rapid wear of tools is the high temperatures generated when machining titanium and the fact that this high temperature acts close to the cutting edge of the tool. Heat generation in machining Ti-6A1-4V was studied with various tool materials and a curve of the heat distribution could be produced, shown in Figure 6 (Machado & Wallbank, 1990). Data for a type of steel have also been included as a basis of comparison. When machining titanium 80% of the heat generated can be absorbed by the tool against a maximum of between 50 and 60% when machining steel. Researchers, have used metallographic methods to determine the cutting temperature distribution in high-speed steel tools when machining titanium (Smart & Trent, 1975; Wright & Trent, 1973).

The temperature gradients when compared to iron were found to be much steeper and the heat-affected zone smaller and much closer to the cutting edge than when machining titanium, even at lower speed. The highest temperatures are produced closest to the cutting edge of the tool because of the thin chips, a thin secondary shear zone and a short chip tool contact length (Machado & Wallbank, 1990).

It was also shown that the stronger the work material, in other words, the higher the amount of beta phase, the higher the temperature production is during machining at the same cutting conditions. The cutting forces when machining titanium are in line with those obtained in the machining of steel, but because the contact area is very small, high stresses result in the immediate neighbourhood of the cutting result. The stresses on the tool when machining Ti-6A1-4V is higher than when machining Nimonic 105 and 3 to 4 times the stresses seen when machining steel. The high strength of titanium at elevated temperatures also contributes to these high stresses and these strengths only decrease considerably above 800°C. Both the high temperature and the high stresses developed at the cutting edge of the tool may cause plastic deformation and/or accelerate the wear of the tools (Machado & Wallbank, 1990). In order to minimize the stresses, a cutting fluid must be applied as a basic rule.

The application of a cutting fluid while functioning as a lubricant primarily acts as a coolant, reducing tool temperatures and therefore stresses experienced at the tool-workpiece interface.
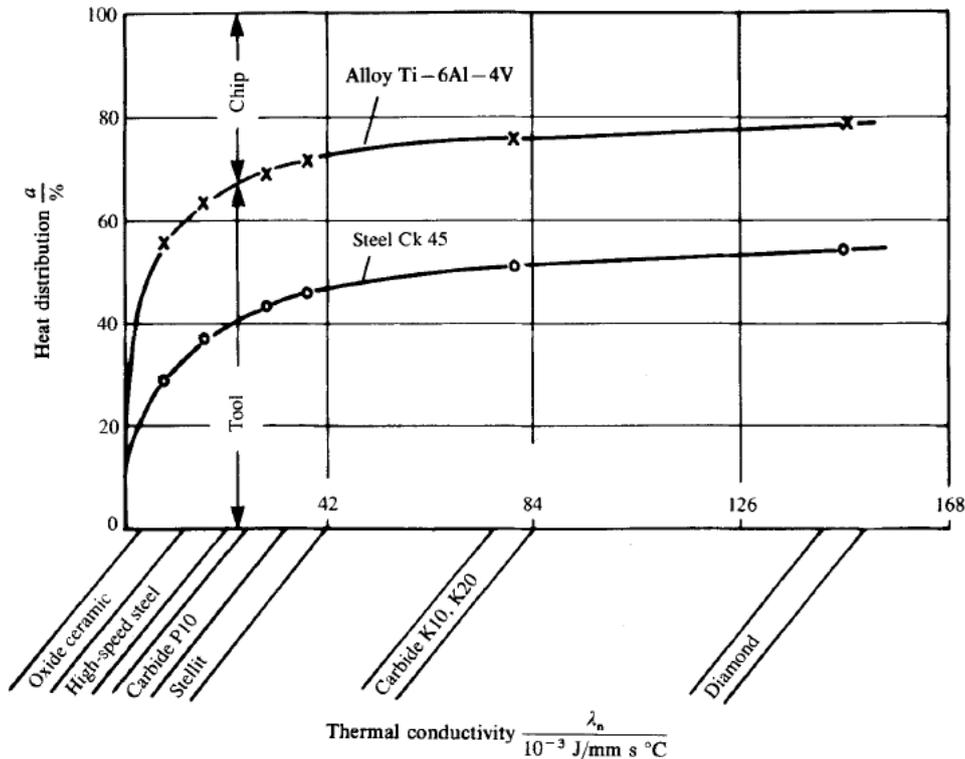
Figure 6: Distribution of the heat generated when machining titanium and steel (Machado & Wallbank, 1990).

2.3. Nitrogen Gas Cooling and Machining

As described in the previous section, titanium and its alloys are classified as hard-to-machine materials due to their inherent physical and mechanical properties. Due to the low thermal conductivity of titanium, the chip cannot effectively dissipate the heat generated when cutting and a large proportion ($> 70\%$) of the heat is conducted into the cutting tool. This leads to rapid increase in cutting temperatures with increase in cutting speed compared to that observed during machining of aluminium alloys (Ezugwu & Wang, 1997). The high temperatures combined with the high chemical reactivity of titanium with almost all of the cutting tool materials causes a significant reduction in tool life with an increase in cutting speed. It also negatively affects machined parts quality, such as dimensional accuracy and surface quality (Shaw, 2005). Therefore, the machining of titanium alloys is a high-cost process due to long cycle times and tool costs. Optimisation of the machining parameters can lead to minimising the overall costs by increasing productivity without dramatic loss

of tool life (Perez, et al., 2000). Effective cooling methods can significantly contribute to improving tool life by minimising the friction and lowering the cutting temperature (Sun & Cheng, 2010).

The high temperatures experienced in the cutting zones has traditionally been controlled by using cutting fluids. Cutting fluids perform as coolant and lubricant. The coolant effect reduces temperature in cutting zone and the lubrication action decreases cutting forces. Thus, when using cutting fluids, the friction coefficient between tool and chip becomes lower in comparison to dry machining (El Baradie, 1996; Diniz & Micaroni, 2002; Vieira, et al., 2001). However, conventional coolant delivery techniques are limited in their ability to penetrate into the region adjacent to the cutting edge at high cutting speeds because coolants tend to vaporise at the high temperatures that are generated close to the tool edge, forming a high- temperature blanket (Ezugwu, 2004; Ezugwu, et al., 2003).

Unfortunately, conventional cutting fluids cause environmental and health problems. Process-generated pollution in machining has been primarily coming from cutting fluid waste. The disposal of these fluids became important environmental and economic issues to be considered in the machining industry, due to the expensive cost of disposal. Improper disposal of cutting fluids results in ground, water or air pollution. In addition, the costs related to cutting fluids are higher than those related to labour and overhead (Cakir, et al., 2004). Environmental and resource problems are forcing the companies and organizations to implement strategies to reduce the use of cutting fluids in their production activities (Byrne & Scholta, 1993; Klocke & Eisenblatter, 1997; Sokovic & Mijanovic, 2001; Sreejith & Ngoi, 2000).Therefore, in theory, it seems to be a better option to eliminate cutting fluid usage in its entirety. This option has been widely investigated and dry machining has become a reliable choice in machining of some materials. However, some engineering materials still require cutting fluid application in their machining operations because of surface quality and dimensional accuracy (Diniz & Micaroni, 2002; El Baradie, 1996; Sreejith & Ngoi, 2000; Vieira, et al., 2001).

Instead of cutting fluids some gases have also been used in machining. Considering the negative impact of cutting fluids on the environment and operator health, alternative environmentally friendly solutions such as gaseous lubricants have been developed, including oxygen, carbon dioxide, gaseous and liquid nitrogen (Cakir, et al., 2004; Stanford, et al., 2009; Su, et al., 2007) , water vapour (Liu, et al., 2004; Liu, et al., 2007) and cold air generated by vortex tube (Liu & Chou, 2007) or refrigerator (Su, et al., 2007). Cryogenic air at high pressure can easily penetrate into the cutting edge to reduce the cutting temperature (Sun, et al., 2010).

The use of gases as a replacement for cutting fluids have been used since the 1930s. Wister applied nitrogen gas during machining processes in 1936 and his study concluded that nitrogen gas formed a

film on the tool surface, chips were easily moved away from the tool face friction was reduced in the tool-workpiece-chip interface (Shaw, 2005). Pahlitzsch (1953) reported that a higher tool life was obtained when using carbon dioxide and nitrogen gases in machining (Pahlitzsch, 1953). Çakir et al. (2004) researched the effect of gas application in machining and compared results to dry and wet machining. They used carbon dioxide, nitrogen and oxygen gases in the machining of AISI1040 steel. The machining experiments were conducted at constant cutting speed and three different cutting depths and feeds. Cutting force, thrust force, surface roughness, friction coefficient and shear angle were examined during their comparison. They found that gas application in low feed produced a lower cutting force comparing to wet machining (Cakir, et al., 2004). To investigate inhibiting chips burning during the high-speed milling of Ti-6Al-4V, Ke et al. (2009) ejected nitrogen gas with 0.7 MPa pressure cutting zone. They found that the high speed flowing of nitrogen gas sped up the chip removal, prevented the chips from burning and a reduced cutting force (Ke, et al., 2009).

Su et al. (2006) investigated the influence of compressed cold nitrogen gas on tool wear in high- speed end-milling of Ti-6Al-4V and evaluated the effectiveness of cooling/lubrication conditions in terms of tool life. They found that the application of compressed cold nitrogen gas in high-speed end-milling of Ti-6Al-4V can provide not only environment friendliness but also great improvement of tool life (Su, et al., 2007).

Sun et al. (2010) researched the effects of using nitrogen gas on cutting force, chip temperature and chip formation. They found a significant reduction in chip temperature with both compressed air and cryogenic compressed air cooling at all cutting speeds which lead to a smaller chip built-up edge and lower tool wear. They also noted that increases in cutting forces with nitrogen gas cooling in respect to cutting length is significantly lower than that when dry machining (Sun, et al., 2010).

2.4. Micro-milling

2.4.1. Process

Conventional milling or macro milling is described as a machining operation where a workpiece of suitable material is fed past a rotating cylindrical tool with multiple cutting edges. The axis of rotation of the tool is perpendicular to the direction of the feed (Groover, 2007).

Micro-milling is similar to conventional milling as it also operates by feeding a workpiece past a rotating cylindrical tool, however the micro-milling process has several significant features that differentiate it from the macro end-milling process.

In literature, micro-milling is defined by various authors relating to tool size, machine size, workpiece size and feature size (Aramcharoen, et al., 2008; Gafford, et al., 2010; Heamawatanachai & Bamberg, 2010). Micro-milling was first related to the micrometre by Masuzawa and Tönshoff (1997), which indicates the machining of dimensions between 1 and 999 μm (Masuzawa & Tönshoff, 1997). Masuzawa (2000) later suggested that a more flexible approach is needed to define micro-milling which takes into consideration factors such as the personal view point, machining method and material used (Masuzawa, 2000). Key aspects that have an influence on the micro-milling process is shown in Figure 7.
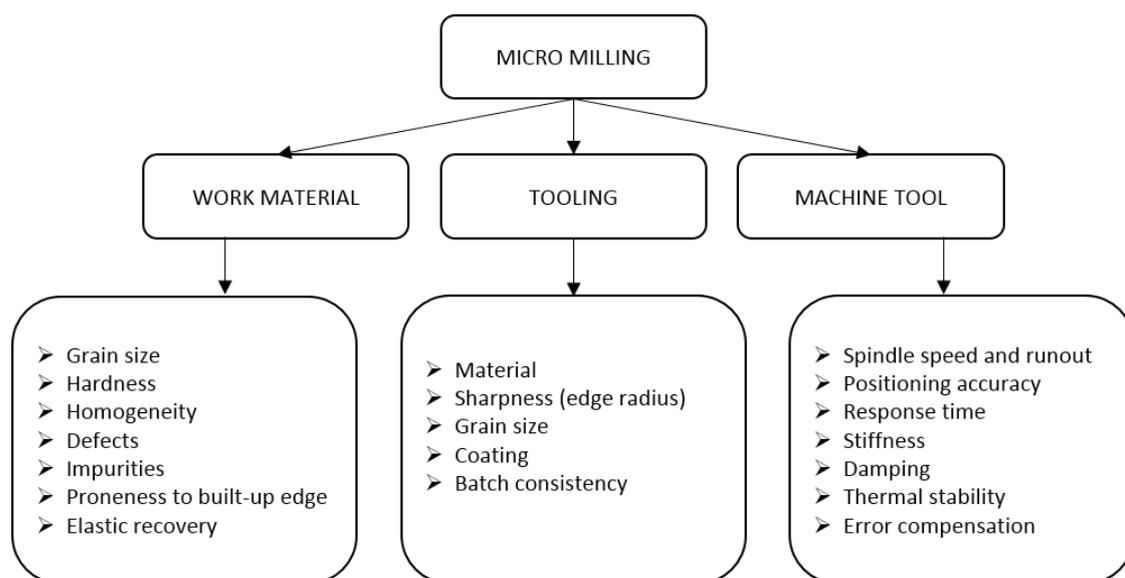
Figure 7: Key aspects affecting micro-milling adapted from (Alting, et al., 2003)

Scaling down the end-milling process from conventional sizes (100 μm/tooth feed rates and 1 mm depths of cut) to micro-milling sizes (1 μm/tooth feed rates and 100 μm depths of cut), different properties dominate the micro-milling process compared to those that are usually observed in conventional milling (Vogler, et al., 2004). Dhanorker and Özel (2008) describes that the fundamental difference between micro-milling and conventional milling arises due to the scale of the operation, even though the two processes are kinematically the same (Dhanorker & Ozel, 2008). Other differences include that the ratio of feed per tooth to radius of the cutting edge is much greater in micro-milling than conventional milling. This often leads to an error in predicting cutting forces.

The effect of the cutting edge radius is not negligible seeing as it affects the chip forming mechanism. Minimum chip thickness is a function of this parameter, and determines the transition between two cutting conditions; where chips are produced and where ploughing takes place (Dhanorker & Ozel, 2008). Also, if the runout of the tool tip is more than a few microns it will greatly affect the accuracy of micro-milling as opposed to conventional milling. Further, it cannot be assumed that the

microstructure of the workpiece material is homogeneous. As tool size becomes smaller, its effect becomes more important (Vogler, et al., 2004).

According to Cardoso and Davim (2012), the most important inputs in the micro-milling process is the tools (characteristics and materials), machine tools (spindle technology, tool holder, rigidity) and the machining parameters (cutting speed, feed rate and feed per tooth) (Cardoso & Davim, 2012). Issues that need to be addressed with micro-milling are the minimum chip thickness, size effect, cutting temperatures and cutting forces. These effects influences tool wear and tool failure, which in turn, influences the burr formation and therefore the overall surface quality of the micro-milled workpiece (Cardoso & Davim, 2012).

2.4.2.   Applications

The miniaturization technologies that are currently emerging are potential key technologies that will change the way that people are currently interacting with the physical world.

Some applications of micro-milling across a broad range of fields is summarized in Table 4 below.

Table 4: Typical applications of micro-milling in the different market sectors (Coetzee, 2012; Essman, 2012; Micro Manufacturing Portal Project, 2015).

Market	Typical Applications
Biomedical	➢ Implantable systems ➢ Micro fluidics ➢ Micro-tools for surgery ➢ Micro drug delivery systems ➢ Lab on chip ➢ Moulds for orthodontics (dental brackets) ➢ Hearing aids diagnostic systems ➢ Smart pills ➢ Microchip electrophoresis devices ➢ Cataract lenses ➢ Retinal micro-tacks
Automotive	➢ Injection nozzles ➢ Electrodes for cutting inserts ➢ Gyroscopes and accelerometers ➢ Engine management ➢ Security ➢ Sensors
Aerospace	➢ Miniature devices for rockets ➢ Mould for miniature planetary gear wheels ➢ Adaptors ➢ Sensors ➢ Health and monitoring systems ➢ Smart materials
Electronics & Information Technology	➢ Test membrane for PC chip manufacturing ➢ Components for measuring devices ➢ Electrodes for various industries ➢ Displays ➢ Printer Heads ➢ Auto ID Systems ➢ Radio frequency modules ➢ Micro mirrors ➢ Optical switches
Energy	➢ Micro combustion engines ➢ Solar Cells ➢ Wind energy ➢ Hydrogen fuel cells ➢ Advanced batteries ➢ Micro fuel cells
Telecommunications	➢ Easy assembly moulds for multi-fibre connectors for single and multimode applications ➢ Joining elements for device parts

2.4.3.   Micro-milling Ti-6Al-4V

Ti-6Al-4V is widely used for manufacturing micro parts in various industries due to its superb mechanical properties, high strength-to-weight ratio, corrosion resistance and biocompatibility. It is however classified as a difficult-to-machine material due to its strong affinity with tool materials and low thermal conductivity which can lead to excessive tool wear (Armendia, et al., 2010; Ulutan & Ozel, 2011).

Attanasio et al. (2013) researched the effect that the material microstructures of Ti-6Al-4V had on the micro-milling process. Four different microstructures (namely bimodal, fully equiaxed, fully lamellar and mill annealed) were obtained through recrystallization annealing treatments carried out at different times and temperatures. They found that it is fundamental to correctly select the right material microstructure when micro-milling Ti-6A-4V parts and that a fully lamellar structure guarantees a better tool status and cutting conditions (Attanasio, et al., 2013).

Kim et al. (2014) studied the characteristics of the micro end-milling process of Ti-6Al-4V in terms of milling forces, burr formation, chip morphology, and tool wear with varying machining parameters (spindle speed and feed per tooth), while other parameters were fixed. With regards to the milling forces, the average resultant milling force increased linearly together with the increase in feed per tooth but did not show any clear trend with the spindle speed changes. They found that low feed per tooth (1 μm/tooth) could cause irregular and large top burrs. Regarding chip morphology, they found that long and connected chips were observed at the lowest feed per tooth of 1 μm/tooth. When the feed per tooth was increased, short and thick arc-shaped chips were generated. Regarding tool wear, they found that a blunt radius of the cutting edge and significant tool wear were observed at the lowest feed per tooth of 1 μm/tooth (Kim, et al., 2014).

2.4.4.   Cutting Parameters

Spindle speed, feed rate and feed per tooth are the most important machining parameters in micro-milling. Many studies have been done to show to which extent these parameters influence the quality of the machined parts and the consequences on the tool (Cardoso & Davim, 2012).

Vogler et al. (2004) studied the influence of the tool edge condition and the workpiece microstructure. They performed experiments with 508 μm diameter end-mills on workpiece materials with different microstructures over a range of feed rates. Four materials were selected for the experimentation; two specially prepared, single phase materials (pure Ferrite and Pearlite) and two multi-phase materials with different compositions of the two single phase materials (Ferritic and Pearlitic). They performed 5 mm long full slot immersion end-milling cuts in order to study the interaction between ploughing

and process condition effects on the surface roughness of the slot floor under several conditions. They kept the spindle speed constant at 120 000 RPM and changed the cutting edge radius, axial depth of cut and feed rate variables. The cutting edge radius was varied between 2 and 5 μm; the axial depths of cut was varied between 50 and 100 μm and the feed rates were varied between 0.25, 0.5, 1, 2 and 3 μm/flute (Vogler, et al., 2004).

Filiz et al. (2007) used micro-end-mills of 254 μm in diameter to perform micro-machining experiments on 99.99% pure Copper using a miniature milling machine. The machine was equipped with a 160 000 RPM air-turbine, air-bearing spindle with a 3.125 mm precision collet. The micro-end-mills used during the experimentation were micro-grain tungsten carbide tools, fabricated by diamond grinding. The micro-tools were two-fluted with a 254 μm diameter and a 30° helix angle. Their experimental study included full immersion slot cutting with an axial depth of cut of 30 μm. The feed rates were varied between 0.75, 1.5, 3, and 6 μm/flute and three cutting speeds of 40, 80, and 120 m/min were considered. The range of feed rates was specifically selected to include the ploughing, indentation, and minimum chip thickness effects in the data. They varied the spindle speed according the feed rates: 50,000 RPM for 0.75 μm/ flute, 100,000 RPM for 3 μm/flute and 150,000 RPM for 6 μm/flute (Filiz, et al., 2007).

Dhanorker and Özel (2008) performed experimental and modelling studies on meso/micro-milling of AL 2024-T6 aluminium and AISI 4340 steel to predict chip formation and temperature areas. Their study included size effects and minimum chip thickness. During this study 2-flute tungsten carbide on cobalt matrix (WC-Co) end-mills with a 30° helix angle were used. The tools had diameters of 1.5875 mm and 3.175 mm respectively. A fixed spindle speed of 60 000 RPM was used to conduct the experiments. The cutting speeds used in the experiments were 22.62m/min and 59.85 m/min respectively and the feed per tooth varied from 0.265 μm to 4 μm. They observed large force variations as the diameter of the cutter decreased and the spindle speed increased (Dhanorker & Ozel, 2008).

Filiz et al. (2008) explored the use of the mechanical micro-milling process for fabrication of micro-scale piercing elements from biocompatible materials. They used two custom made, special geometry, tools with cutting diameters of 254 μm and 101.6 μm respectively and investigated the effects of feed, speed, and axial depth of cut on the performance of the tools when cutting polymethyl methacrylate (PMMA). The experiments were done using spindle speeds of 50 000 and 100 000 RPM respectively, two feeds of 1 and 5 μm/flute and two axial depths of cut of 10 and 20 μm. They concluded that the

spindle speed has the most prominent effect for all force components, and an increase in spindle speed caused an increase in forces experienced (Filiz, et al., 2008).

2.4.5. Cutting Forces

The majority of researchers investigating micro-machining processes have used cutting force measurements for monitoring or improving the quality of machined products (Liu, et al., 2004; Tansel, et al., 1998; Tansel, et al., 2000; Jun, 2005; Li, et al., 2000). The performance of micro-end-mills is significantly influenced by small vibrations and excessive forces. These factors are disadvantageous to the durability of the tools and the control of component tolerances and it is challenging to detect damage to cutting edges and broken tool shafts (Alting, et al., 2003; Tansel, et al., 1998; Tansel, et al., 2000). Excessive cutting force limits the accuracy and the depth of cut due to deflection of tool and workpiece and this defines the bending stress that determines the feed rate and introduces the built-up edge (Chae, et al., 2006; Weule, et al., 2001; Kim, et al., 2004; Vogler, et al., 2003). Reducing the cutting force in micro-machining operations significantly improves material removal rate; decreases tool deflection and tool wear; extends tool life; delays tool failure and narrows workpiece tolerance limits (Chae, et al., 2006).

To accurately measure very small cutting forces is extremely challenging due to even small amounts of noise giving false cutting force signals. The frequency bandwidth of force sensors is inadequate for the majority of micro-machining systems due to the very high rotational speeds used for micro-milling processes (Chae, et al., 2006).

As in conventional machining, micro-machining cutting force consists mainly of normal and tangential components. This is usually called shearing/cutting and ploughing/thrust force, respectively. The cutting force is directly related to chip formation. Since cutting force also determines the tool deflection and bending stress as mentioned, the tool edge radius is often larger than the chip thickness to prevent plastic deformation or breakage of the tool (Chae, et al., 2006). The minimum chip thickness leads to an increase in shearing forces and ploughing of the machined surface which contributes to increasing cutting force, burr formation and surface roughness (Bissacco, et al., 2006; Ducobu, et al., 2012).

Cutting forces in micro-machining is significantly influenced by problems that are generally minor in conventional machining regarding tool/workpiece interactions such as tool wear, run-out (unbalance) and chatter (instability) (Chae, et al., 2006; Camara, et al., 2012; Dornfeld, et al., 2006; Sun & Cheng, 2010; Gietzelt & Eichhorn, 2012). In micro-milling, chips may not form when the depth of cut is less than a critical chip thickness. The smaller the uncut chip thickness, the greater the

impacts on the tool wear and cutting force will be (Piljek, et al., 2014). Chae et al. (2006) also reported that feed rate directly affects cutting forces and with excessive forces large tool deflection results as well as accelerated tool wear and tool breakage (Chae, et al., 2006). Tool run-out is caused when the tool deflects due to a misalignment of the axis of symmetry between the tool and the tool holder or spindle. Tool run-out contributes significantly to noise in force measurements, surface roughness and severe vibrations which causes burr formation (Piljek, et al., 2014). Chatter is a self-excited vibration between a cutting tool and a workpiece in both conventional milling and micro-milling (Afazov, et al., 2012). It introduces excessive vibrations that can lead to catastrophic failure and burr formation due to the interaction between the cutting tool and workpiece (Piljek, et al., 2014).

To reduce cutting forces and extend tool life, laser assisted micro-milling or vibration assisted micro-milling can be applied when machining difficult to cut materials (Chae, et al., 2006; Camara, et al., 2012; Dornfeld, et al., 2006). Kumar et al. (2012) reported that the usage of laser assisted micro-machining provides more consistent tool life, however larger burr heights and poorer surface finish were observed and attributed to the impact of thermal softening (Kumar & Melkote, 2012). Kumabe et al (1989) introduced ultrasonic vibration machining (Kumabe, et al., 1989) and the process was later improved by Moriwaki et al. (1991 &1995), through elliptical ultrasonic vibration which produced improved cutting performance and surface quality (Moriwaki & Shamoto, 1991; Moriwaki & Shamoto, 1995). Vibration assisted micro-machining also improves machining of ferrous metals with diamond tools by means of reduced tool wear (Weule, et al., 2001).

2.4.6. Chip formation

With conventional milling, it is assumed that the cutting tool edge is perfectly sharp and that there is no contact between the tool's clearance face and machined surface. Chips are then formed by shearing of the material in front of the tool tip. Such an assumption, however, cannot be made for micro-milling due to the highly effective negative rake angle caused by the small depth of cut being of the same order of magnitude as the tool edge radius (Piljek, et al., 2014). A schematic representation of the negative rake angle can be seen in Figure 8 below.
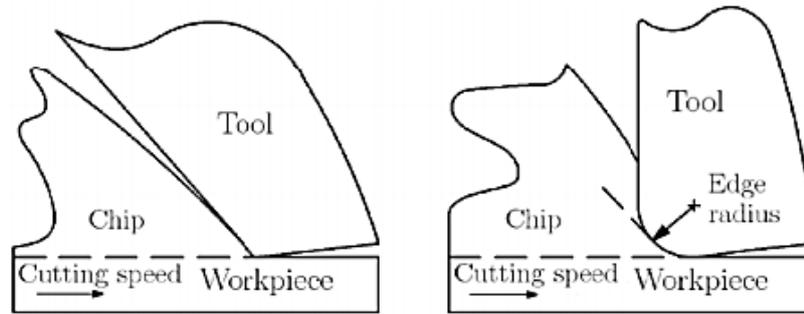
Figure 8: Schematic representation of the negative rake angle observed in micro-milling (Dornfeld, et al., 2006).

A highly negative rake angle leads to ploughing of the machined surface and elastic return of the workpiece. The spring back section occurring under the flank face of the tool leads to friction which raises the specific cutting energy (Ducobu, et al., 2013). Due to the negative rake angle of the tool a minimum chip thickness is in effect during micro-milling. Minimum chip thickness is the minimum undeformed chip thickness below which chips may not form when machining the workpiece (Chae, et al., 2006; Sun & Cheng, 2010).

In conventional milling shear takes place along the shear plane, in micro-milling the shear stress rises continuously around the cutting edge due to the negative rake angle of the tool and material seems to be ploughed and deformed rather than sheared (Chae, et al., 2006; Ducobu, et al., 2013; Sun & Cheng, 2010; Woon & Rahman, 2010). Therefore, micro-milling processes are greatly influenced by the ratio of the depth of cut to the cutting edge radius causing a significant influence to the cutting process by a small change in the depth of cut. This ratio defines the active material removal mechanism such as cutting, ploughing, or sliding and thus the resultant surface quality (Chae, et al., 2006; Sun & Cheng, 2010).

Figure 9 from Ding et al. (2012) illustrates the chip formation with respect to the cutting tool edge radius (Re) and the uncut chip thickness (h). When the uncut chip thickness is larger than the minimum chip thickness [Figure 9 (a)], elastic deformation is reduced significantly and the entire depth of cut is removed as a chip. As the uncut chip thickness approaches the minimum chip thickness [Figure 9 (b)], chips are formed by shearing of the workpiece, with some elastic deformation still occurring. As a result, actual depth of cut is less than the desired depth. When the uncut chip thickness is smaller than the minimum chip thickness [Figure 9 (c)], only elastic deformation occurs and no workpiece material will be removed by the cutter (Ding, et al., 2012).
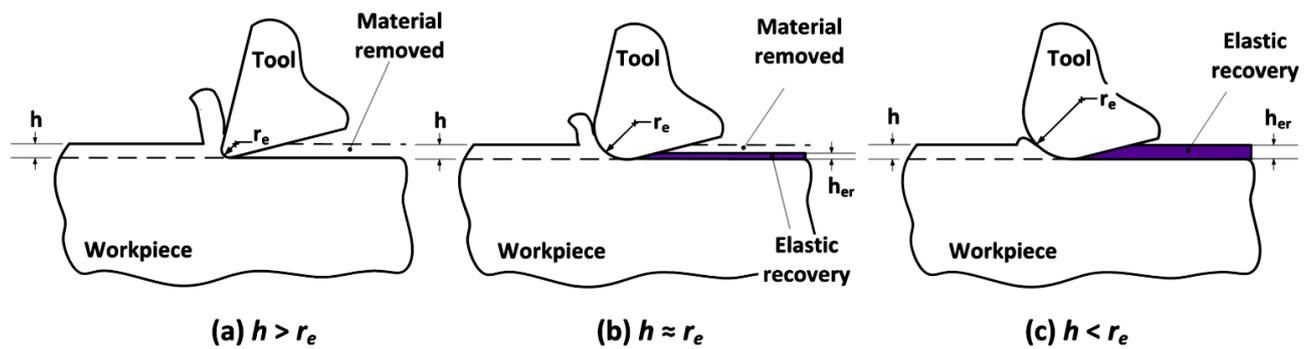
Figure 9: Schematic diagram of the effect of the minimum chip thickness (Ding, et al., 2012).

The smaller the uncut chip thickness is in comparison to the minimum chip thickness the greater increase can be seen in slipping forces and ploughing of the machined surface which also contributes to the increase in cutting forces, burr formation and surface roughness (Bissacco, et al., 2006).

Understanding of the minimum chip thickness is essential in the selection of appropriate machining parameters to ensure a proper cutting procedure and to avoid ploughing and sliding of the tool (Chae, et al., 2006; Dornfeld, et al., 2006; Sun & Cheng, 2010). In micro-milling, when the feed per tooth is smaller than the minimum chip thickness, several tool rotations are needed to form a chip (Ducobu, et al., 2012). During this research Ducobu et al. (2012) also show that the stability of micro-milling can be feed dependent which is contrary to macro milling.

It is very difficult to measure the minimum chip thickness directly during the micro-milling process, in spite of knowing the tool edge radius, therefore it is obtained by experimental results or through numerical simulations (Piljek, et al., 2014). The minimum chip thickness to be used when micro-milling depends primarily on the ratio of uncut chip thickness to the cutting tool edge radius and secondly on the workpiece material properties and the friction between the tool and workpiece material (Dornfeld, et al., 2006). Estimation of the minimum chip thickness is one of the present challenges in micro-milling. Minimum chip thickness cannot be expressed as a precise and single value but rather as a range of values with unclear limits (Ducobu, et al., 2013). Minimum chip thickness was estimated to be between 5 % and 40 % of the tool edge radius depending on the material machined (Chae, et al., 2006; Dornfeld, et al., 2006; Ducobu, et al., 2013; Woon & Rahman, 2010).

2.4.7.   Surface finish

Surface finish is especially critical in micro-milling as the machining operation is typically intended to produce components with high quality surfaces. Three dimensional assessments of the finished components are usually carried out using optical equipment and scanning electron microscopy (Camara, et al., 2012; Sun & Cheng, 2010; Gietzelt & Eichhorn, 2012). The surface quality is

evaluated by evaluating the surface roughness and burr formations. In conventional milling a smaller uncut chip thickness generates a smaller surface roughness, however when micro-milling there exist a critical depth of cut below which surface roughness starts to increase. This phenomenon shows a strong influence of size effects on surface generation, therefore when chip removal size decreases the cutting parameters, workpiece material properties and issues of tool edge geometry becomes dominant factors with strong influences on the resultant accuracy, surface quality and integrity of the machined component (Chae, et al., 2006; Sun & Cheng, 2010).

Vogler et al. (2004) studied the surface roughness in the micro-milling process and they found that surface roughness is strongly affected by the tool edge radius and the feed rate. During their experiments the authors observed that when using a tool with a 2 μm edge radius and reducing the feed rate to a certain value, the surface roughness started to increase. They concluded that this observation indicates that an optimal feed rate exists that will produce the smallest surface roughness value. The authors further claimed that the existence of the optimal feed rate was due to the minimum chip thickness effect resulting in tool passes that do not remove any material as the feed rate is reduced (Vogler, et al., 2004).

Cardoso and Davim (2012) performed a comprehensive study on surface roughness of micro-milled surfaces using optimization micro-milling. They varied the machined surfaces, feed rate as well as machining strategies. In this research, Al 2011 aluminium alloy was used and the tool used to machine the workpiece was a cemented carbide K10, 0.8 mm diameter end-mill. During the experimentation four feed rates (2, 4, 6, and 8 μm/flute) and one spindle speed 6,500 RPM were considered. The three machining strategies that they used were: constant overlap spiral, parallel spiral and parallel zigzag. They found that the constant overlap spiral strategy was the one that presented the best results and the burrs produced with the parallel spiral strategy were much more pronounced (Cardoso & Davim, 2012).

Lee et al. (2000) studied the effect of the feed rate, cutting speed and depth of cut on the surface roughness when machining aluminium. The results indicated that the effect of the cutting speed and depth of cut was by far smaller than the feed rate (Lee, et al., 2000).

Damazo et al. (1999) reported that the surface roughness depends on the machining parameters used, the tool condition and the nature of the workpiece, for instance the grain size. They reported that the surface quality can be improved by increasing the rigidity and accuracy of the equipment (Damazo, et al., 1999).

Research done by Li et al. (2008) propose that the surface roughness of a machined part should be the criterion for characterising tool wear. Their experiments indicated that the variation in surface roughness as machining progresses is strongly related to the tool wear progression. The researchers stated that micro-tool geometry, minimum chip thickness as well as the effect of tool wear plays an important role in surface roughness generation of the machined part. They came to the conclusion that the effect of tool wear on surface roughness was significant (Li, et al., 2008).

Weule et al. (2001) determined the achievable surface roughness of steel (SAE 1045) as a function of minimum chip thickness including the cutting edge radius. They predicted the achievable surface roughness based on the spring back of elastically deformed material. They also conducted experiments regarding the relationship between machining parameters, material condition and surface quality. They concluded that in addition to the ratio of feed rate to edge radius, the cutting speed and material hardness are other relevant factors which have a significant influence on the surface roughness. They suggested that in order to generate smaller surface roughness a higher cutting velocity and harder workpiece materials are preferable.

In addition the researchers observed that, in contrast to surface roughness, burrs most frequently occurred when cutting hard materials. This is assumed to be a result of faster tool wear which increases the cutting edge radius leading to burr formation (Weule, et al., 2001). Mian et al. (2011) confirmed a significant influence of cutting speed to the surface roughness and observed that the same applies for the burr root thickness (Mian, et al., 2011). In addition to size effects, the resulting accuracy and surface quality is directly related to the machine tools and cutting tools properties where issues such as tool wear, tool deflection, tool run-out and chatter lead to additional surface deterioration (Camara, et al., 2012; Chae, et al., 2006; Mian, et al., 2011; Sun & Cheng, 2010).

The most unfavourable situation occurs when machining workpiece materials with high ductility. Micro-milling a material with high ductility causes long and continuously snarled chips to form which easily interferes with tool engagement which creates burrs and contribute to poor surface quality (Dornfeld, et al., 2006; Gietzelt & Eichhorn, 2012). When the ratio of the depth of cut to the cutting edge radius is small, high biaxial compressive stress pushes material toward the free surface and generates large top burrs (Bissacco, et al., 2006). Micro-milling may result in increased surface roughness with burrs due to the ploughing dominated cutting and side flow of the deformed material when the cutting edge becomes worn and blunter (Liu, et al., 2004). Burr formation is probably the principal damage noticed on machined surfaces. Burr formation at micro scale is similarly to surface roughness also affected with size effects (Piljek, et al., 2014). Sugawara investigated the effect of the

drill diameter on burr formation and concluded that as the drill size decreases the cutting ability increases and burr size is reduced (Sugawara, 1980). Also, the kinematics of the tool as it exits from the workpiece significantly influences burr formation due to plastic deformation of the chips rather than shearing (Byrne, et al., 2003). Schaller et al. drastically reduced burr formation by coating the surface with cyanoacrylate polymeric material. After machining, the cyanoacrylate is removed with acetone in an ultrasonic bath (Schaller, et al., 1999).

Researchers found that tool coatings did not result in any substantial improvement on surface roughness (Camara, et al., 2012; Mian, et al., 2011). To minimize burr size, the best results are obtained when using tools coated with TiN, TiCN and CrTiAlN (Camara, et al., 2012).

According to Mian et al. (2011) the relationship between surface roughness and cutting conditions is similar to that between burr size and cutting conditions. Both depend on the ratio of undeformed chip thickness to cutting edge radius, feed rate and cutting speed. They state however, that the best process performance in terms of surface roughness and burr formation are not essentially obtained at the same cutting conditions (Mian, et al., 2011).

CHAPTER 3
Research Methodology

3.1. Experimental Design

3.1.1. Experimental Factor Selection

Selecting the correct experimental input variables is dependent on the factors that potentially affect the various responses of tool wear, tool life, cutting force, chip formation, burr formation and surface finish. These variables are categorised and illustrated in the cause and effect diagram in Figure 10 below.
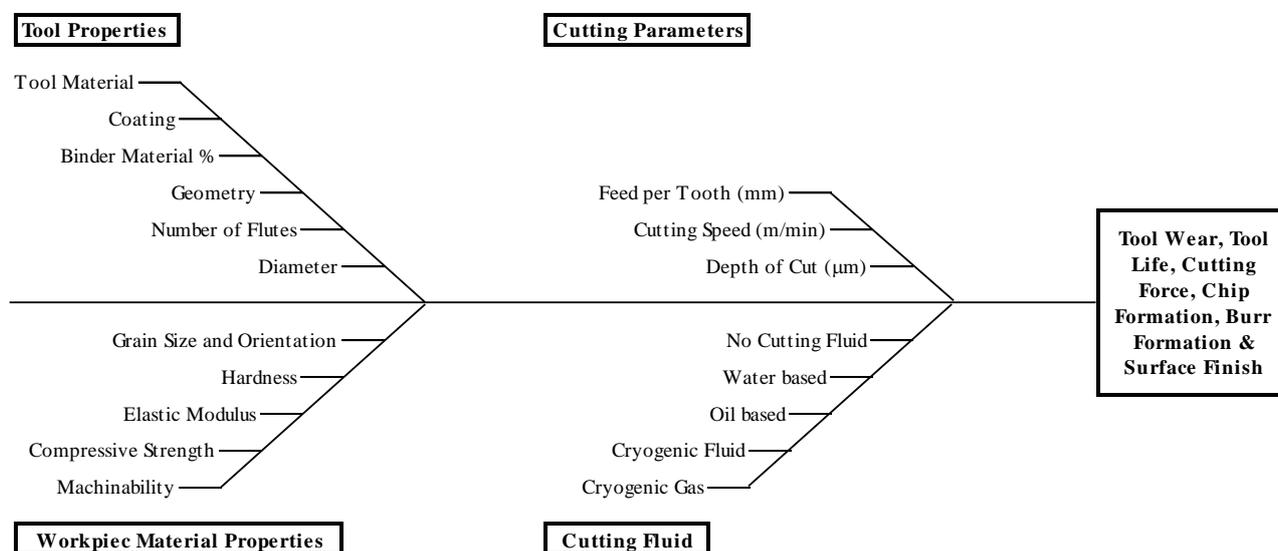
Figure 10: Experimental response cause and effect diagram showing all the variables involved in machining

There are various responses which may or may not influence the responses as illustrated above. To thoroughly test all of these factors through experimentation using a full factorial experimental design at two levels would require an impossible effort in terms of time and cost constraints of this project. A design like this using all the factors above would require 2^{19} = 524 288 experiments. Therefore, it is clearly necessary to reduce the number of experimental factors. This can be done by narrowing the scope of the investigation. For the purpose of this project, the workpiece has been predefined as Ti-6Al-4V, grade 5. The properties and specifications of the Ti-6Al-4V bar used for the experiments are listed in Table 5. The initial bar received was wire-cut into 10 smaller slabs for use during the experiments.

Table 5: Ti-6Al-4V workpiece material properties

Specification	Description
Material	Ti-6Al-4V
Supplier	Sierra Alloys
Product Code	MIL T-90451
Grade	5
Condition	Annealed
Vickers Hardness (HV)	342.3
Rockwell Hardness (HRC)	34.7
Tensile Strength (N/mm$_2$)	1100.25
Chemical Composition	Al (6%) – Fe (0.25%) – O (0.2%) – Ti (90%) – V (4%)
Initial bar Dimensions (W x L x H)	101.68 mm x 73.20 mm x 92.3 mm
Working bar Dimensions (W x L x H)	70 mm x 100 mm x 8 mm

The scope of the experiments can be further reduced by using only one type and size of end-mill. For this project a tungsten carbide micro-tool with 1.5 mm diameter was selected to conduct the experiments. The specifications of the selected tool is listed in Table 6.

Table 6: Tungsten Carbide micro-tool specifications

Specification	Description
Manufacturer	Performance Micro Tools
Type	Stub-nose end-mill
Part Number	SS-2-0591-S
Diameter	1.5 mm
Tolerance on Diameter	± 0.0508 mm
Flute length	3.0226 mm
Shank Diameter	3.175 mm
Overall Length	38.1 mm
Number of Flutes	2
Material	Tungsten carbide
Price	R 143.00 each

To reduce the scope of the experiments even further, it was necessary to decide on which type of cutting fluid would be suitable. From literature and due to the experimental setup including very expensive equipment under the machined Ti-6Al-4V plates as well as preferring to machine the Ti-6Al-4V plates in a practically inert environment it was decided to use cryogenic nitrogen gas in all of the experiments. The specifications of the liquid nitrogen and nitrogen gas dual regulator tank used in the experiments are listed in Table 7.

Table 7: Liquid nitrogen and nitrogen gas dual regulator tank specifications

Specification	Description
Diameter	508 mm
Height	1562 mm
Weight	124 kg
Evaporation Rate (% per day)	1.9 %
Gas Flow Rate	9.2 m³/hour
Gas Capacity	99 m³

By limiting the project to only use one workpiece material, one cutting tool and one cutting fluid, all with fixed material properties, the only experimental factors that remain are:

➢ Feed per tooth [μm] (machine input is feed rate)

➢ Cutting speed [m/min] (machine input is spindle speed [rev/min])

➢ Depth of cut [μm]

Thus the number of experimental combinations are reduced significantly. Validation for using only these experimental factors can be found in literature. Prakash et al. (2002) characterised tool life in terms of feed per tooth, cutting speed and depth of cut using a 1 mm micro-end-mill machining pure copper (Prakash, et al., 2001). Filiz et al. (2007) investigated the micro machinability copper using 254 μm diameter tungsten carbide end-mills varying cutting speed and feed per tooth and using a constant depth of cut of 30 μm (Filiz, et al., 2007).

3.1.2.　Design of Experiments

Design of experiments (DOE) is a systematic method to determine the relationship between input and response variables of a process. Using DOE is paramount in enabling experiments to capture as much information regarding the relationship between input and response variables as possible. This includes first order main and interaction effects as well as second order main effects where necessary. DOE also enables experiments to be conducted economically by getting all the information required in as few experimental runs as possible. The efficiency of an experimental design is described by the amount of information obtained for a certain number of experimental runs. The more information and the fewer runs, the greater the efficiency of an experimental design. There are various useful experimental designs used in practice. Each of these designs has its own benefits and shortcomings and one should attempt to select the best possible DOE according to one's experimental circumstances. In deciding which DOE to use for this project, consultations were arranged with the Statistical Department of Stellenbosch University as well as with Dr Nico Laubscher from Industat.

From both these consultation sessions it was decided to use a response surface method design, specifically a rotatable central composite design in planning the various experiments.

3.1.3.   Central Composite Design

According to Myers et al. (2009) the central composite design (CCD) is the most popular class of second-order designs (Myers, et al., 2009).

The CCD consists of the following points:

➢ *F* two-level factorial points, where $F = 2^{k_e}$ and k_e is the number of experimental factors.
➢ *2k_e* axial points and
➢ *n_c* centre runs

Firstly, the *F* two-level full factorial runs are completed. This represents a variance-optimal first order model that includes two factor interaction terms. This enables the first order main effects as well as first order two factor interaction effects to be estimated from the resulting data. Thereafter, the *n_c* centre runs are completed. The centre runs provide insight into whether or not there is non-linearity in the system. If non-linearity is present, the *2k_e* axial runs allow the pure quadratic terms to be estimated. Myers et al. (2009), describes the roles of the three components in the following way:

➢ The *F* two-level full factorial runs contribute significantly to the estimation of linear terms and two-factor interaction terms. These points are the sole contributors to the estimation of the interaction terms.
➢ The *2k_e* axial points contribute significantly to the estimation of the second order terms, namely the quadratic terms. Without axial points, only the sum of the second order terms could be estimated.
➢ The *n_c* centre runs also contribute to the estimation of the quadratic terms, but more importantly, provide an internal estimate of statistical error within the experiment.

It is useful to represent the experimental design in the form of a matrix. This is known as the design matrix. Each column in the design matrix represents one experimental factor. For the purpose of this project, three factors have been identified, namely cutting speed, v_c [m/min], feed per tooth, f_z [μm] and depth of cut, a_p [μm]. Each row in the design matrix represents a combination of factor values to be tested, otherwise known as an experimental run. The design matrix indicates the configuration of the factors at different levels as well as the sequence of experimental runs. A design matrix (coded

values) is shown in Figure 11 below for a three factor CCD. There are $2^3 = 8$ full factorial runs, $2x3 = 6$ axial runs and 6 centre runs.

$$
\begin{array}{ccc}
V_c & f_z & a_p \\
\end{array}
$$

$$
\begin{bmatrix}
-1 & -1 & -1 \\
1 & -1 & -1 \\
-1 & 1 & -1 \\
1 & 1 & -1 \\
-1 & -1 & 1 \\
1 & -1 & 1 \\
-1 & 1 & 1 \\
1 & 1 & 1 \\
-\alpha & 0 & 0 \\
\alpha & 0 & 0 \\
0 & -\alpha & 0 \\
0 & \alpha & 0 \\
0 & 0 & -\alpha \\
0 & 0 & \alpha \\
0 & 0 & 0 \\
0 & 0 & 0 \\
0 & 0 & 0 \\
0 & 0 & 0 \\
0 & 0 & 0 \\
0 & 0 & 0 \\
\end{bmatrix}
\begin{array}{l}
\left.\rule{0pt}{4.5em}\right\} \text{8 Full factorial Runs} \\
\left.\rule{0pt}{3.2em}\right\} \text{6 Axial Runs} \\
\left.\rule{0pt}{3.2em}\right\} \text{6 Centre Runs} \\
\end{array}
$$

Figure 11: A typical CCD matrix design with 8 full factorial runs, 6 axial runs and 6 centre runs

The CCD experimental design can also be viewed in a geometric view. This helps to visualise the separate components of the design, namely the 2^3 full factorial runs, the 2×3 axial runs and the n_c centre runs. The geometric view of a CCD for $k_e = 3$ is shown in Figure 12 below, where $x_1 = v_c$ [m/min], $x_2 = f_z$ [µm] and $x_3 = a_p$ [µm].
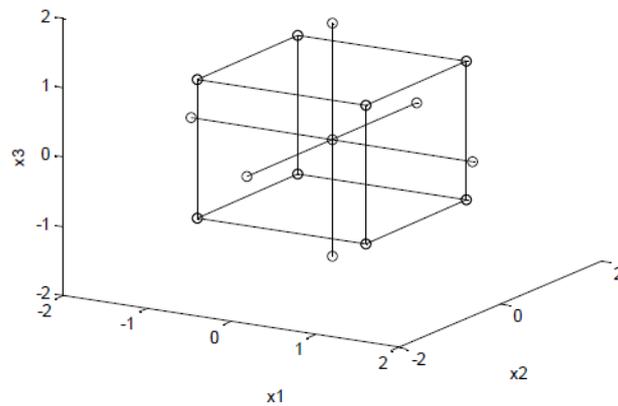
Figure 12: Geometric view of a CCD for $k_e = 3$

The flexibility of the CCD comes from the selection of the design parameters α and nc, the axial distance from the centre and the number of centre runs respectively (Myers, et al., 2009). The selection of these parameters is closely related to the rotatability of the design. Montgomery and Runger (2010), describe a rotatable design as one in which the standard deviation of the predicted response is constant at all points that are the same distance from the centre of the design. This is intended to create stability in the design in that the response is predicted with equal precision for all points that are the same distance from the centre of the design. This is despite the fact that the precision decreases with increasing distance from the centre (Montgomery & Runger, 2010).

General guidelines exist for the selection of α and by selecting the proper axial spacing α will make a CCD rotatable. Myers et al. (2009) say that rotatability is achieved by using $\alpha = \sqrt[4]{F}$ where F is the number of factorial points. In the case this project, $F = 2^3 = 8$ factorial points, which results in $\alpha = 1.68179$ (Myers, et al., 2009). The more centre runs used in the CCD the better. The general recommendation a CCD with $k_e = 3$ is 3 to 5 centre runs (Myers, et al., 2009). For the purpose of this project experiments the design parameters of $\alpha = 1.68179$ and $n_c = 6$ have been selected.

It is further necessary to select the range of values for each of the experimental factors. That is, an upper and lower bound for the cutting speed, v_c [m/min]; feed per tooth, f_z [µm] and depth of cut, a_p [µm]. These values were decided upon after consultation with Performance Micro Tools. They gave guidelines on what machining parameters are required to machine Ti-6Al-4V successfully. They suggested a feed rate of between 762 and 1524 mm/min and a depth of cut of 100 µm. Some trial experiments were done to see how the tools perform within these ranges and the experimental factor ranges that were eventually selected are summarised in Table 8 below.

Table 8: Experimental factor ranges for CCD design

Coded Values	-α	-1	Centre	1	α
Cutting Speed [m/min]	65.79	70.69	75.4	80.11	84.82
Feed per Tooth [µm]	18	20.43	24	27.57	30
Depth of Cut [µm]	93.75	106.42	125	143.58	156.25

The factors in Table 8 was used as the input for the CCD and using the Design Expert 9 software package for Stat-Ease the experimental design run chart was developed. The run chart indicates the order in which the various experiments needs to be completed. It can be seen in Table 9 below that even though experiment 20 is a centre point and indicated last on the design matrix, it needs to be completed in the 15th position when the experiments are started. The experimental run order is randomised by the software and this helps to reduce the chance that differences in experimental

materials or conditions strongly bias results. Randomisation also lets you estimate the inherent variation in materials and conditions so that you can make valid statistical inferences based on the data from your experiment.

Table 9: Experimental design run order chart

Standard Order	Run Order	Effect Label	Cutting Speed [m/min]	Feed Rate per Tooth [μm]	Depth of Cut [μm]
9	1	Axial	65.97	24.00	125.00
13	2	Axial	75.40	24.00	93.75
15	3	Centre	75.40	24.00	125.00
8	4	Factorial	80.11	27.57	143.58
6	5	Factorial	80.11	20.43	143.58
2	6	Factorial	80.11	20.43	106.42
11	7	Axial	75.40	18.00	125.00
1	8	Factorial	70.69	20.43	106.42
12	9	Axial	75.40	30.00	125.00
3	10	Factorial	70.69	27.57	106.42
5	11	Factorial	70.69	20.43	143.58
19	12	Centre	75.40	24.00	125.00
10	13	Axial	84.82	24.00	125.00
4	14	Factorial	80.11	27.57	106.42
20	15	Centre	75.40	24.00	125.00
16	16	Centre	75.40	24.00	125.00
18	17	Centre	75.40	24.00	125.00
7	18	Factorial	70.69	27.57	143.58
17	19	Centre	75.40	24.00	125.00
14	20	Axial	75.40	24.00	156.25

3.2. Experimental Procedure

3.2.1. Physical Experimental Setup

The machine used for these experiments was the Minitech 12528 5-axis milling machine from Minitech Machine Corporation. The Nakanishi E3000C spindle was used for rotating the tungsten carbide tools. It has a maximum speed of 60 000 revolutions per minute (RPM). The Mach3 CNC Controller software was used to control the milling machine and input the machining parameters. An ATI Net F/T Gamma sensor was attached on the bottom of the worktable. The force sensor measured the force continuously during each experiment. The force data was sent to an Excel CSV file on a laptop that was connected to the force sensor. The Ti-6Al-4V plates (dimensions 70 mm x 100 mm x 8 mm) were fixed to a metal clamp that was attached to the force sensor via a custom made attachment ensuring that the clamp is as flush as possible against the force sensor. The nitrogen gas pipe and

nozzle was attached to the spindle and angled so that the cryogenic nitrogen gas hits the tool-workpiece interface continuously during the experiments. The whole machine was enclosed in a clear polycarbonate structure to ensure that the milling takes place in an inert environment due to the nitrogen gas being released continuously. The various components of the experimental setup can be seen in Figures 13, 14, 15 and 16 below.

Figure 13: Experimental machine setup with various components
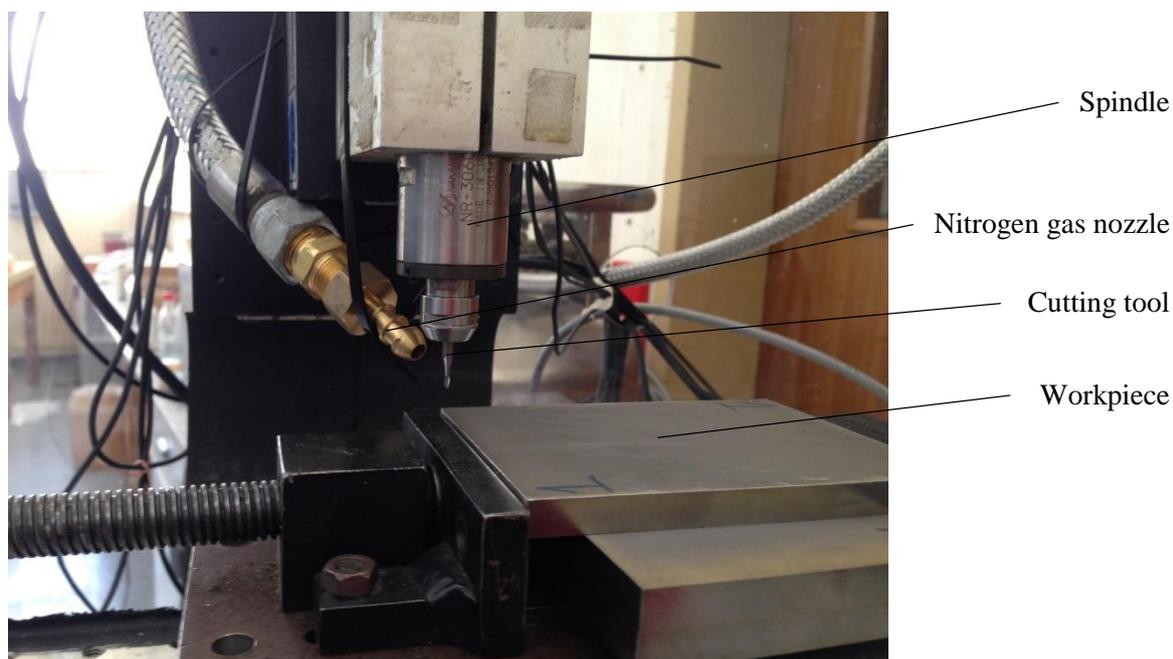
Figure 14: Close-up of the tool-workpiece and nitrogen gas interface
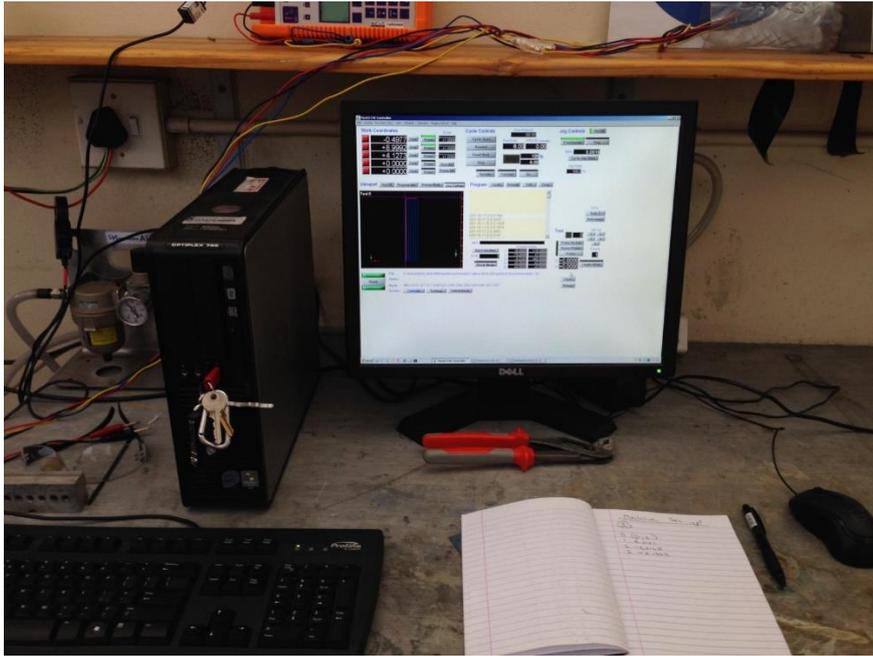
Figure 15: Mach3 CNC Controller software and setup
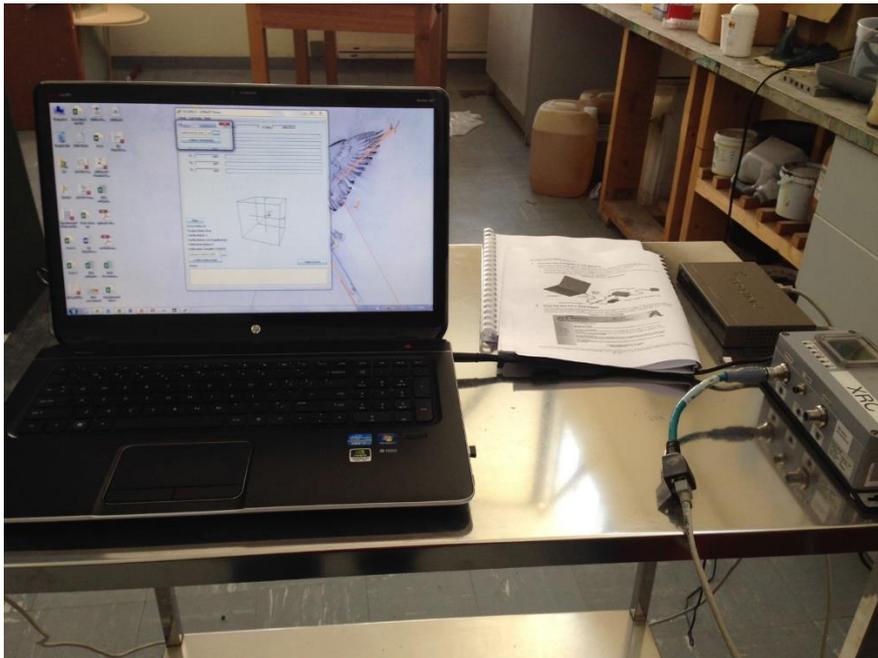
Figure 16: ATI Net F/T software and setup for force measurements

3.2.2.   Generation of the Cutting Path

Each experiment consisted of cutting 6 slots of 70 mm in length. G-Code was developed to create each experiments cutting path. To zero the tool on the workpiece it was required to factor in that the workpiece may not be perfectly aligned as it was attached to the clamp. To bypass this potential

problem, the machine coordinates were taken on all for corners of each experimental plate after it was mounted. These values were used to calculate a numerical factor by which the workpiece is sloping towards in the X-axis and Y-axis. These sloping factors were incorporated into the G-Code. An example of the G-code used for one of the experiments and the cutting path for the same experiment can be seen in Figure 17.

```
G01 X0 Y7 Z10 F768
G01 X0 Y7 Z-0.1255
G01 X0 Y-73 Z-0.1203
G01 X3 Y-73 Z-0.1131
G01 X3 Y7 Z-0.1183
G01 X6 Y7 Z-0.1111
G01 X6 Y-73 Z-0.1059
G01 X9 Y-73 Z-0.0987
G01 X9 Y7 Z-0.1039
G01 X12 Y7 Z-0.0967
G01 X12 Y-73 Z-0.0915
G01 X15 Y-73 Z-0.0843
G01 X15 Y7 Z-0.0895

G00 Z40
M30
%
```
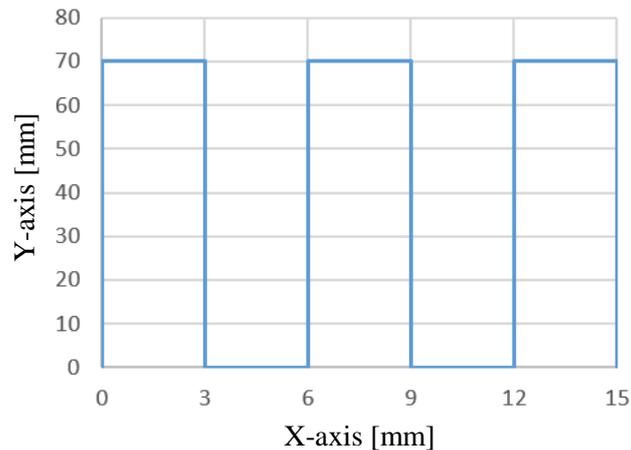

Figure 17: G-Code and cutting path of experiment 15

3.2.3. Experiments

All the experiments were completed as is set out in the experimental design run chart as is depicted in Table 9. The experiments were completed on the same day. The input of the machine consists of the spindle revolutions per minute (RPM), feed rate and depth of cut. The depth of cut was incorporated into the G-Code and the feed rate and RPM individual values were calculated using Table 9 and the formulas 2 and 3 below.

$$n = \frac{1000 \times v_c}{\pi \times D} \tag{2}$$

$$V_f = \frac{n \times b \times f_z}{1000} \tag{3}$$

Where, v_f = feed rate [mm/min], f_z = feed per tooth [µm], n = rotational speed [RPM] and b = number of teeth/flutes [2 for these experiments] and D = diameter of tool [mm]. The machine settings for each of the experiments are shown in Table 10 below.

Table 10: Calculated machine settings for each experimental run

Standard Order	Run Order	Effect Label	Spindle Speed [rev/min]	Feed Rate [mm/min]	Depth of Cut [μm]
9	1	Axial	14000	672	125.00
13	2	Axial	16000	768	93.75
15	3	Centre	16000	768	125.00
8	4	Factorial	17000	937	143.58
6	5	Factorial	17000	695	143.58
2	6	Factorial	17000	695	106.42
11	7	Axial	16000	576	125.00
1	8	Factorial	15000	613	106.42
12	9	Axial	16000	960	125.00
3	10	Factorial	15000	827	106.42
5	11	Factorial	15000	613	143.58
19	12	Centre	16000	768	125.00
10	13	Axial	18000	864	125.00
4	14	Factorial	17000	937	106.42
20	15	Centre	16000	768	125.00
16	16	Centre	16000	768	125.00
18	17	Centre	16000	768	125.00
7	18	Factorial	15000	827	143.58
17	19	Centre	16000	768	125.00
14	20	Axial	16000	768	156.25

After the whole experimental set was completed data was gathered for the following responses:

➢ Tool wear [μm/mm]

➢ Tool life [mm cut to 200 μm wear]

➢ Cutting force [Newton]

➢ Chip formation [ranked 0-2]

➢ Burr formation [% of total cut]

➢ Surface Roughness [nm]

3.2.4.   Data Gathering

The following section describes how the data for each of the responses was gathered during or after the experiments.

3.2.4.1.   Tool Life and Tool Wear

Images was taken of each tungsten carbide tool tip before and after cutting using an Olympus GX51 microscope. The tungsten carbide tool tips also underwent scanning electron microscopy (SEM) with energy dispersive X-ray spectroscopy (EDS) before and after cutting to look at the damage and

elemental composition of the tool tips and to measure tungsten carbide grain size. The Leo® 1430VP SEM was used for these measurements.

For the purpose of this study tool life was defined as the distance cut to where the tool experienced 200 μm wear. This wear was measured by measuring the width of the slots of each experiment on the Ti-6Al-4V plates. Each Ti-6Al-4V plate contained 6-8 experiments with between 1 and 6, 70 mm slots each. The width of the slots were measured in 20 mm increments across all experiments. These measurements were fitted with a mathematical model and the distance cut in millimetres from where the slot width was 1300 μm was calculated and recorded as the tool life result.

For the purpose of this study tool wear was defined as the rate at which the tungsten carbide tool tips reduce in diameter per millimetre cut. These values were also calculated from the width measurements of the slots over distance cut.

3.2.4.2.   Cutting Force

Cutting force was measured during each experiment using an ATI Net F/T Gamma sensor. The sensor was activated just before each experiment was started and measured force in the X, Y and Z axis at a rate of 7000 Hz throughout the whole experiment duration. After the experiments, the average X, Y and Z forces including the resultant force for each experiment could be calculated using the data from the sensor. Resultant force for each data entry was calculated with equation 4 below.

$$F_R = \sqrt{F_x{}^2 + F_y{}^2 + F_z{}^2} \tag{4}$$

Where F_R = resultant force [Newton], F_x = X-axis force value for data entry [Newton], F_y = Y-axis force value for data entry [Newton] and F_z = Z-axis force value for data entry [Newton].

Figure 18 below shows the configuration of the ATI Net F/T Gamma sensor.

Figure 18: ATI Net F/T Gamma sensor (ATI Industrial Automation, 2013)

3.2.4.3. Chip Formation

After each experiment the chips for that experiment was gathered and microscope images was taken of each set of chips. The chip sets were then categorised from 0 – 2 depending on what they looked like. A score of zero was given to chip sets who were relatively large and well formed. A score of 2 was given to chip sets who were extremely fragmented and broken into very small bits. A score of 1 was given to chip sets who contained elements of both.

3.2.4.4. Burr Formation

After the experiments the Ti-6Al-4V plates were imaged and the burr formation was measured for each experiment. The burr length measurements were taken along the length of the slots and documented to be able to calculate the length of cut of each experiment where burrs were formed on one or both sides of the machined slot. The total length of the burrs in millimetres were then divided by the total length of cut for each experiment to deduce a percentage of burr formation for each experiment.

3.2.4.5. Surface Finish

After the experiments the Ti-6Al-4V plates underwent atomic force microscopy with a Nanosurf® Flex AFM instrument to measure the surface roughness, S_a [nm] across various areas in the individual slots for each experiment. Each experiment were measured on 6 different areas and the average surface roughness was calculated by the Nanoscan Easyscan 2 software.

3.3. Analysis

The experiments were done by varying the values of three factors that are expected to have an influence on the performance of a tungsten carbide cutting tool when micro-milling Ti-6Al-4V with nitrogen gas cooling. The factors were:

➢ Cutting Speed (set at levels 65.79 – 84.82 [m/min]).

➢ Feed per Tooth (levels 18 – 30 [μm])

➢ Depth of Cut (106.42 – 143.58 [μm]).

The experimental design selected is a 3-factor central composite design (CCD). The design consisted of 8 factorial points (on the vertices of a cube), 6 axial points (selected so that the design is rotatable with a α-level of 1.68179) and 6 centre points giving a total of 20 experimental points in the design space. The responses that were measured are:

- ➢ R1: Tool wear [μm/mm]
- ➢ R2: Tool Life [mm cut to 200 μm wear]
- ➢ R3: Resultant Cutting Force [Newton]
- ➢ R4: Chip Formation [ranked 0-2]
- ➢ R5: Burr Formation [% of total cut]
- ➢ R6: Surface Finish [nm]

The data collected was imported from Excel to the statistical software package Design Expert 9. All the statistical analyses were done using Design Expert 9.

The purpose of the experiments were to find a set of settings for the three control factors that will maximise tool life and simultaneously minimise all the other responses. In order to achieve this, a mathematical model will be fitted for each of the responses in terms of the three control factors. Once the models have been established, numerical methods will be used to find the optimal settings. It has to be realised that a unique solution does not necessarily exist.

The design of the CCD is selected such that a quadratic function in the three factors can be fitted. The full quadratic model (which is known to provide a good approximation to many more complicated functions) may be written as equation 5 below.

$$R = \beta_0 + \sum_{i=1}^{3} \beta_i X_i + \sum_{i,j}^{3} \beta_{ij} X_i X_j \tag{5}$$

Where R is the response and X_1, X_2 and X_3 represent the three factors. The regression model that is fitted (using least squares) may be written as equation 6 below.

$$R_{ijk} = \hat{\beta}_0 + \sum_{i=1}^{3} \hat{\beta}_i X_i + \sum_{i,j}^{3} \hat{\beta}_{ij} X_i X_j + e_{ijk} \tag{6}$$

Here the β's are the regression coefficients and e_{ijk} is the error term.

This model contains 9 effects (three linear, three interaction terms and three pure quadratic terms). For any given data set some of these effects may be significant and others may not be significant. The non-significant terms may be omitted from the model and the remaining terms re-fitted. So, for example, the following model (Equation 7) may provide as good a fit as could be found when fitting all the interaction and quadratic effects.

$$R = \beta_0 + \beta_1 X_1 + \beta_2 X_2 + \beta_{12} X_1 X_2 + \beta_{22} X_2^2 \tag{7}$$

In order to find the best, but simplest model, the process is started with a full quadratic model and a stepwise backward regression is applied. Effects are eliminated one at a time until an unsatisfactory fit is encountered. As stated earlier all computations are done with the Design Expert 9 software.

The best model is determined for each response and the results of the analysis contains the following parts:

➢ An analysis of variance (ANOVA) table. This shows the significance of each effect in the model. If the p-value of the F-test is small, the effect may be declared significant at the level of the p-value. For example, if $p \leq 0.05$ the effect may be declared significant at the 5% level of significance.

➢ Basic statistics for the variable, typically the mean value, standard deviation, R-square and coefficient of variation. The most important statistic in that section is the adjusted R-square statistic. An Adj. $R^2 = 0.526$ is interpreted by saying that the regression model explains 52.6% of the variability in the raw response. A high value of Adj. R^2 is good and confirms a good fit of the model. Small values confirm that the factors have little influence on the outcome of the response. This means that there may be unknown factors that drive the response.

➢ The third section shows the model that was fitted in terms of coded factors. The coding is done by identifying points on the vertices of the CCD cube as having coordinates -1 or +1, the centre point of the cube as zero and the star points as -1.68179 and +1.68179. Coding is useful in that all factors are expressed on the same scale and thus the effects of all factors, including interaction between variables are comparable. This section is used to display the significance or insignificance of each one of the effects by reporting a 95% confidence interval (CI) for each effect. If the CI includes zero, the effect is not significant and if zero falls outside of the CI the effect is significantly different from zero (at the 5% significance level or with 95% confidence).

➢ Section four of each set of results shows the equations describing the fitted model (both in coded and engineering units). The engineering units have the advantage of being more readily interpreted by the user. As an example, the equation fitted for Burr Formation in engineering units can be seen in equation 8 below.

$$\text{Burr Formation} = 5.8908 - 0.0008 \times A + 0.3208 \times B - 0.0278 \times C + 0.000004 \times A \times C - 0.0017 \times B \times C \qquad (8)$$

Where A = Spindle Speed [rev/min]; B = Feed rate per Tooth [µm] & C = Depth of Cut [µm]. Note that the neither the AB interaction nor any of the quadratic terms were included into the model by the backward stepwise regression.

For some of the responses (i.e. Resultant Cutting Force and Chip formation) none of the factors had any effect and thus the best model that could be fitted was a constant, irrespective of the values of factors A, B or C. For example as shown in equation 9 below.

$$Resultant\ Cutting\ Force = 84.52 \qquad (9)$$

➢ In some cases the assumptions for the validity of the F-tests in the ANOVA table may not be valid. Sometimes a transformation of the data to a new scale will correct that in a way such that the conclusions reached in the transformed scale remain valid in the original scale. The method applied to establish if a transformation is needed, and if so, to determine the best transformation, is done by the method of Box and Cox. In the analyses of the data a transformation was required for three of the variables, namely, tool wear (R1) and surface roughness (R6) for which a natural log transformation was applied and for chip formation (R4) square root transformation was applied. The log formation is specifically Log(R6 + 0.002). The constant was applied for the benefit of cases with a value of zero.

To optimise the settings required for the best results is the next step. The specification for an optimal outcome is that a set (or sets) of values of the three control factors must be found such that tool life (R2), is maximised whereas all other responses should be as small as possible. For any values of the factors for which the model for the response approaches its desired criterion (for example its maximum that is possible for the model), a desirability function is set up. For response "R_i" (i = 1, … , 6) the desirability is d_i. It is defined in a very simple way for example increasing linearly from 0 to 1 as the best settings moves the response closer to the target. For example, the target tool life in Figure 19 is 425.
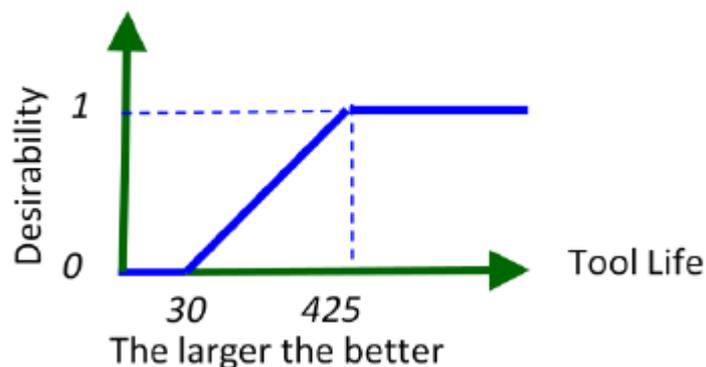
Figure 19: Desirability of tool life

Values of the process factors that will increase the value of one of the responses may decrease the value of another. Therefore the desirability for each response has to be combined to provide an overall

desirability. To achieve this, the combined (overall) desirability is defined as the geometric mean of the individual desirability's shown in equation 10 below.

$$D = \left(\prod_{j=1}^{6} d_j \right)^{\frac{1}{6}} \tag{10}$$

Thus if only one individual desirability is low, the product will be low. All desirability's have to be reasonably large to ensure an overall high desirability. Note that if a response is not affected by the factors (i.e. if the model is R = constant) the factor settings play no role in establishing the desirability of the response.

CHAPTER 4
Experimental Results and Discussion
4.1. Tool Wear and Tool Life

SEM images of the tungsten carbide cutting tools were taken before and after each experiment. Figure 20 below shows the results of a tool before machining (a) and after machining (b).
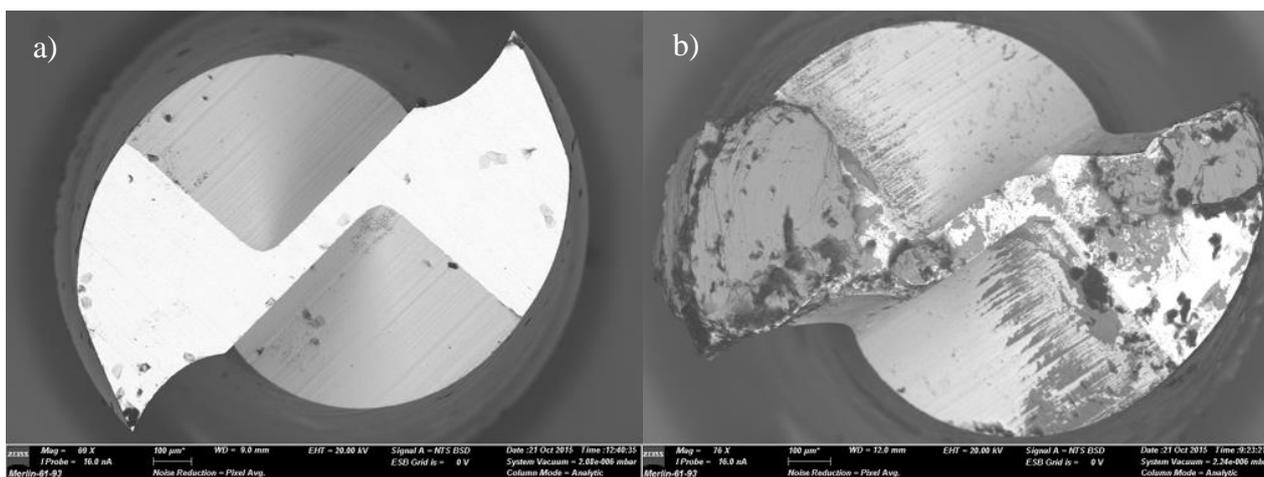

Figure 20: SEM Image of experimental tool 15 before (a) and after (b) machining with parameters v_c = 75.40 [m/min], v_f = 768 [mm/min] and a_p = 125 [μm]

From the image it can clearly be seen that tool cutting edge experienced a reduction in sharpness and that adhesion took place between the Ti-6Al-4V workpiece material and the tungsten carbide tool. This adhesion occurred on all of the tools in varying degrees and their images can be seen in Appendix A. Note that tools 3, 5, 6, 7, 10, 12, 13, 14, 17 and 20 might not show this due to the tool tip breaking off during the experimental run after it experienced 200 μm reduction in diameter.

An EDS analysis was done on the tools before and after the experiments to show their elemental composition and to prove that it is indeed Ti-6Al-4V that adhered to the tool. From the EDS of the tools before the experiments it was learned that the elemental weight percentage of the tungsten carbide tools consisted of approximately 86% Tungsten, 4% Carbon and 10% Cobalt. EDS on the welded parts showed 90% titanium, 6 % aluminium and 4% vanadium and thus proves that the workpiece material adhered to the tools during cutting.

The reduction in diameter of the tool tips was used as a method of assessing tool wear and tool life. However, since the tool diameter cannot be measured during the cutting process the widths of the milled slots was used in this work as a method to measure tool wear and tool life.

For the purpose of this study tool life was defined as the distance cut to where the tool experienced 200 μm wear. This wear was measured by measuring the width of the slots of each experiment on the Ti-6Al-4V plates. Each Ti-6Al-4V plate contained 6-8 experiments with between 1 and 6, 70 mm slots each. The width of the slots were measured in 20 mm increments across all experiments. These measurements were fitted with a mathematical model and the distance cut in millimetres from where the slot width was 1300 μm was calculated and recorded as the tool life result. For the purpose of this study tool wear was defined as the rate at which the tungsten carbide tool tips reduce in diameter per millimetre cut. These values were also calculated from the width measurements of the slots over distance cut. Figure 21 shows a graph of experiment 15 with the equation used to calculate the exact distance where the reduction in tool diameter equals 200 μm. This value was used to calculate the rate of tool wear over each mm of the cutting process. For the remaining experimental graphs, please view appendix B.

$$y = -0.0000000000233535853094111x^5 + 0.00000030897801671890 5x^4 - 0.000156319222739842x^3 + 0.0364852200706309x^2 - 3.98621659991841x + 1\,494.4490514471$$

$$R^2 = 0.98$$
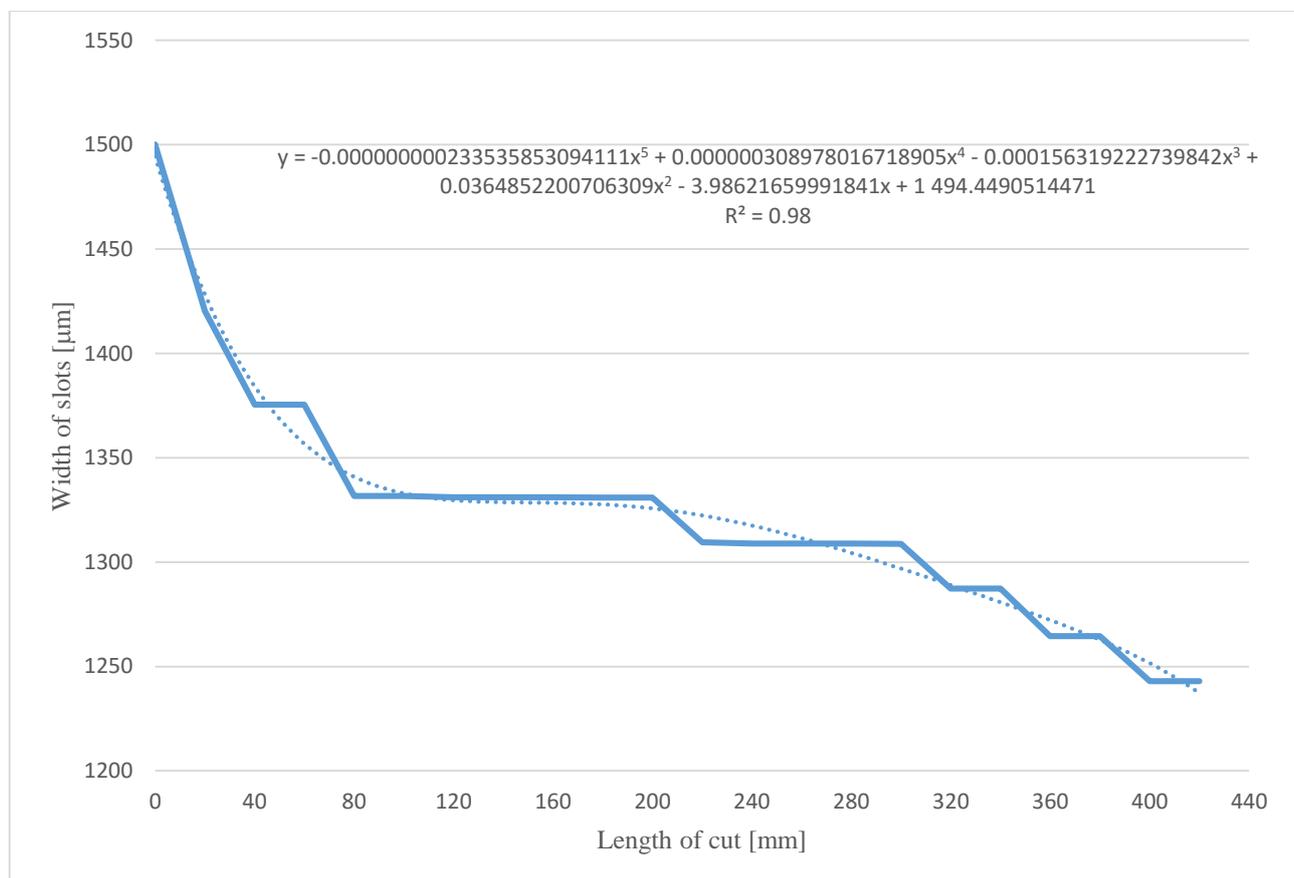
Figure 21: Graph of experiment 15 showing the equation used to calculate distance cut to 1300 μm wear

The results of tool wear and tool life is summarised in Table 11 below. From the experimental results the lowest tool wear of 0.49 μm/mm and highest tool life of 410 mm was measured after machining with parameters 16000 RPM spindle speed, 960 mm/min feed rate and 125 μm depth of cut.

Table 11: Experimental results of tool wear and tool life

Run Order	Effect Label	Spindle Speed [rev/min]	Feed Rate [mm/min]	Depth of Cut [μm]	Tool Wear [μm/mm]	Tool life [μm cut to 200mm wear]
1	Axial	14000	672	125.00	1.42	140
2	Axial	16000	768	93.75	2.60	77
3	Centre	16000	768	125.00	2.44	82
4	Factorial	17000	937	143.58	0.57	351
5	Factorial	17000	695	143.58	2.20	87
6	Factorial	17000	695	106.42	0.99	203
7	Axial	16000	576	125.00	4.17	42
8	Factorial	15000	613	106.42	0.65	308
9	Axial	16000	960	125.00	0.49	410
10	Factorial	15000	827	106.42	3.74	29
11	Factorial	15000	613	143.58	0.71	281
12	Centre	16000	768	125.00	2.63	67
13	Axial	18000	864	125.00	2.35	72
14	Factorial	17000	937	106.42	1.80	111
15	Centre	16000	768	125.00	0.69	292
16	Centre	16000	768	125.00	0.62	324
17	Centre	16000	768	125.00	0.94	186
18	Factorial	15000	827	143.58	0.88	226
19	Centre	16000	768	125.00	0.76	264
20	Axial	16000	768	156.25	3.30	61

Using the analysis method as described in Section 3.3 the results for tool wear is described in the following section. A natural log transformation was applied to the tool wear data and a constant of 0.002 was added for the benefit of cases with a value of zero. The results for the ANOVA for tool wear is summarised in Table 12 below.

Table 12: ANOVA results for tool wear

			LOG(TOOL WEAR)		
		ANOVA for Response Surface Mean model			
	Analysis of variance table [Partial sum of squares - Type III]				
Source	Sum of Squares	df	Mean Square	F-Value	p-value (Prob > F)
Model	2.060476	3	0.686825472	1.481344	0.257326
B-Feed Rate	0.418042	1	0.418041684	0.901632	0.356468
C-Depth of Cut	0.125479	1	0.125479454	0.270634	0.61003
BC	1.516955	1	1.516955279	3.271767	0.089311
Residual	7.418402	16	0.463650131		
Lack of Fit	5.317949	11	0.483449939	1.150823	0.468259
Pure Error	2.100453	5	0.420090553		
Cor Total	9.478879	19			

The Model F-value of 1.48 implies the model is not significant relative to the noise. There is a 25.74% chance that an F-value this large could occur due to noise. Values of "Prob > F" less than 0.0500 indicate model terms are significant. In this case there are no significant model terms. Values greater than 0.1000 indicate the model terms are not significant.

The "Lack of Fit F-value" of 1.15 implies the Lack of Fit is not significant relative to the pure error. There is a 46.82% chance that a "Lack of Fit F-value" this large could occur due to noise. Non-significant lack of fit is good because we want the model to fit.

The basic statistics for tool wear is summarised in Table 13 below.

Table 13: Basic statistics for tool wear

Std. Dev.	0.680919	R-Squared	0.217376
Mean	0.298235	Adj R-Squared	0.070633
C.V. %	228.3163	Pred R-Squared	-0.3079
PRESS	12.39746	Adeq Precision	4.009059

A negative "Pred R-Squared" implies that the overall mean is a better predictor of the response than the current model. "Adeq Precision" measures the signal to noise ratio. A ratio greater than 4 is desirable. The ratio of 4.009 indicates an adequate signal. This model can thus be used to navigate the design space.

The next section (summarised in Table 14) shows the model that was fitted in terms of coded factors. The coding is done by identifying points on the vertices of the CCD cube as having coordinates -1 or +1, the centre point of the cube as zero and the star points as -1.6818 and +1.6818. Coding is useful in that all factors are expressed on the same scale and thus the effects of all factors, including interaction between variables are comparable. This section is also used to display the significance (or not) of each one of the effects by reporting a 95% confidence interval (CI) for each effect. If the CI includes zero, the effect is not significant and if zero falls outside of the CI the effect is significantly different from zero (at the 5% significance level or with 95% confidence).

Table 14: Tool wear results of coded factors and CI

Factor	Coefficient Estimate	df	Standard Error	95% CI Low	95% CI High
Intercept	0.300078	1	0.152020427	-0.02219	0.622347
B-Feed Rate per tooth	-0.19578	1	0.206263721	-0.63304	0.241479
C-Depth of Cut	-0.1609	1	0.309408858	-0.81682	0.495018
BC	-0.81986	1	0.45327055	-1.78075	0.141028

The final equation for tool wear in terms of coded factors therefore is displayed in equation 11 below.

$$\text{Ln(Tool Wear} + 0.00) = 0.300078 - 0.19578 \times B - 0.1609 \times C - 0.81986 \times BC \qquad (11)$$

The equation (11) in terms of coded factors can be used to make predictions about the response for given levels of each factor. By default, the high levels of the factors are coded as +1 and the low levels of the factors are coded as -1. The coded equation is useful for identifying the relative impact of the factors by comparing the factor coefficients.

The final equation for tool wear in terms of actual factors can thus be written as displayed in equation 12 below.

$$\text{Ln(Tool Wear} + 0.00) = -17.55835 + 0.77092 \times f_z + 0.15226 \times a_p - 0.0065589 \times f_z \times a_p \qquad (12)$$

Where a_p = depth of cut [μm] and f_z = feed per tooth [μm]. The equation in terms of actual factors can be used to make predictions about the response for given levels of each factor. Here, the levels should be specified in the original units for each factor. This equation should not be used to determine the relative impact of each factor because the coefficients are scaled to accommodate the units of each factor and the intercept is not at the centre of the design space.

Diagnostic plots provide a valuable tool for visual assessment of the ANOVA findings. Most of the plots display residuals, which indicates the difference between the actual and predicted values for each point and shows how well the model satisfies the residual assumptions of the ANOVA. These plots are shown in Figure 22 – 25 below. The normal plot of residuals show that there is almost no deviation from normality. The residuals vs. predicted plot show that the data is within limits and that there is no constant error. The residuals vs. run plot also shows that the data is within limits and that there are two possible outliers and the predicted vs. actual plot shows relatively good performance of the model, especially on points that are on or close to the line.
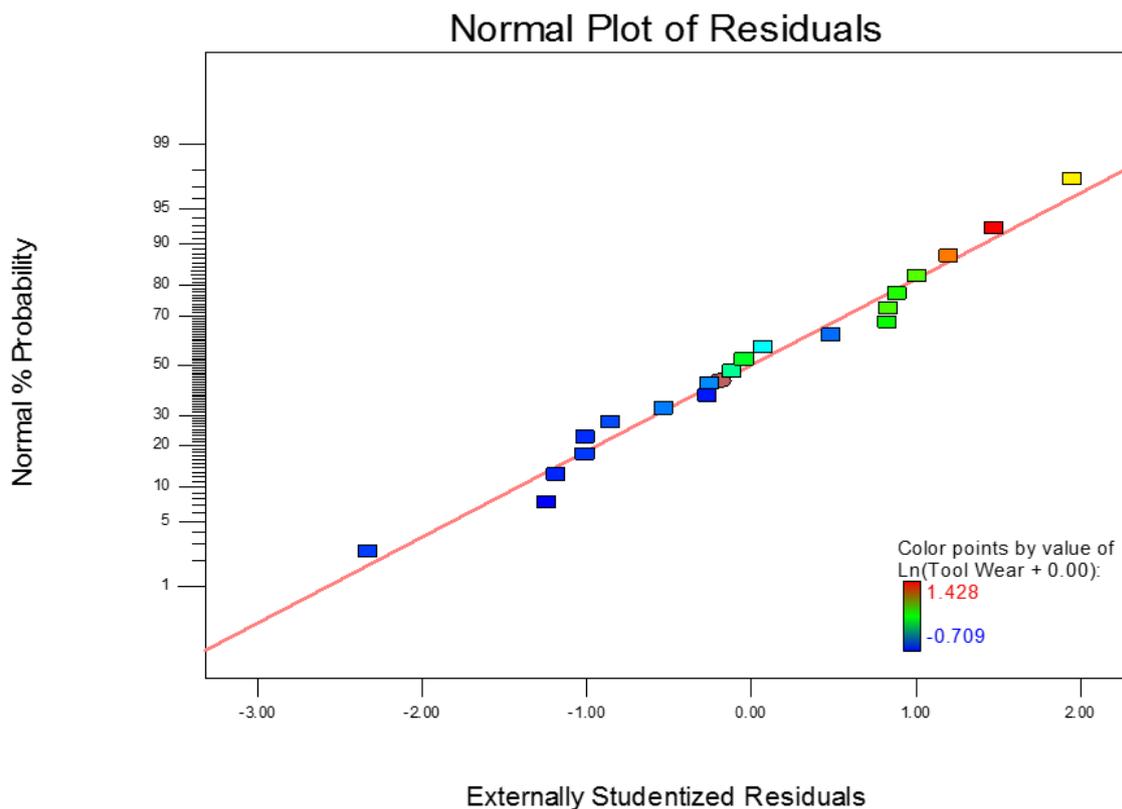
**Figure 22:** Normal plot of residuals for tool wear
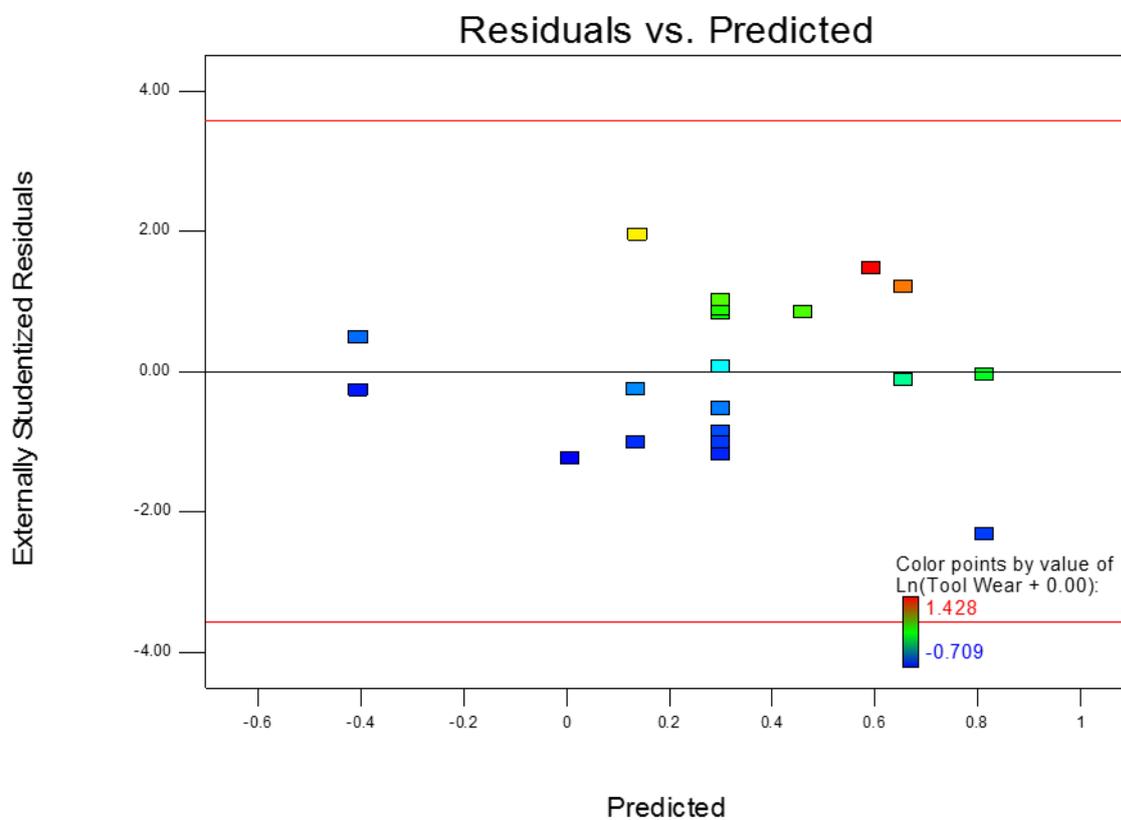
**Figure 23:** Residual vs. predicted plot for tool wear
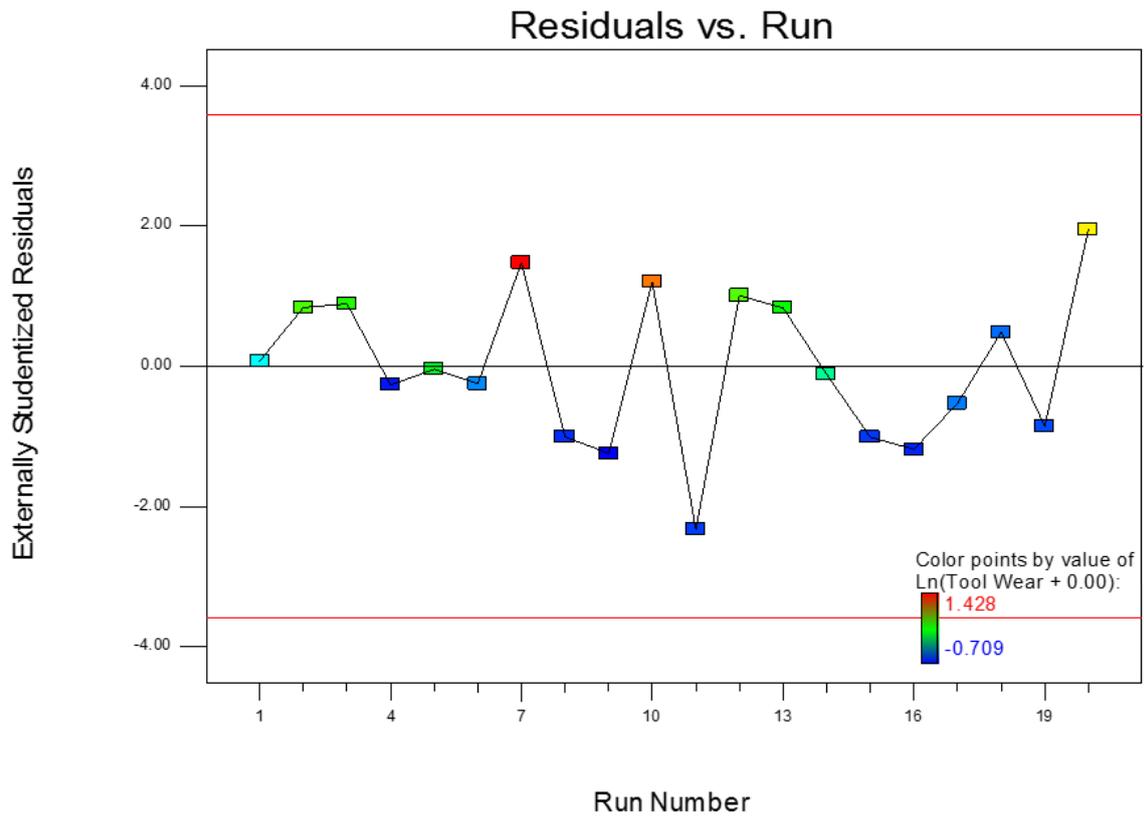
Figure 24: Residual vs. run plot for tool wear
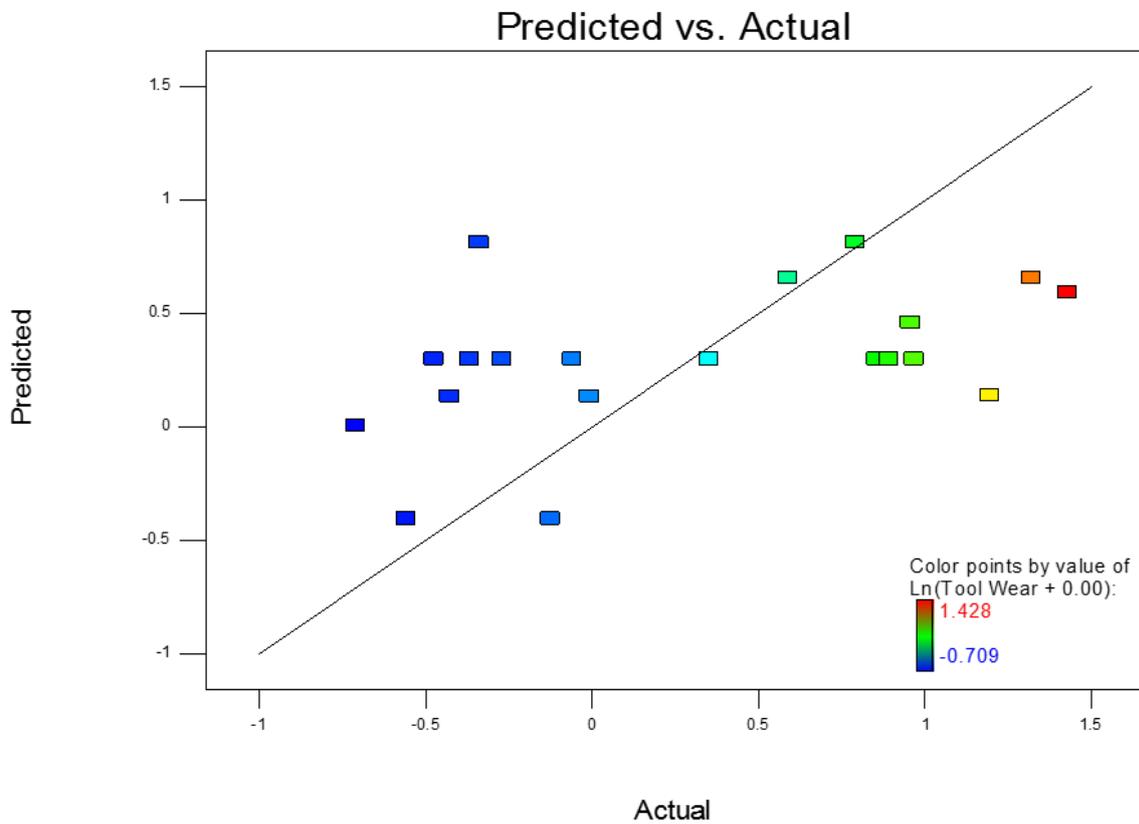

Figure 25: Predicted vs. actual plot for tool wear

The Box-Cox plot for the log transforms that were performed on the primary data before the ANOVA was performed, reveals no further requirements as shown in Figure 26. The ANOVA and diagnostic plots provide satisfactory results of a significant second-order model that fits the design space.

Despite the suboptimal nature of the model, results still provide the opportunity to assess the model within the selected response surface. The model is not fitted to the optimal response surface, therefore significant predictions about any values outside of the experimental area cannot be made at the 95% confidence level.
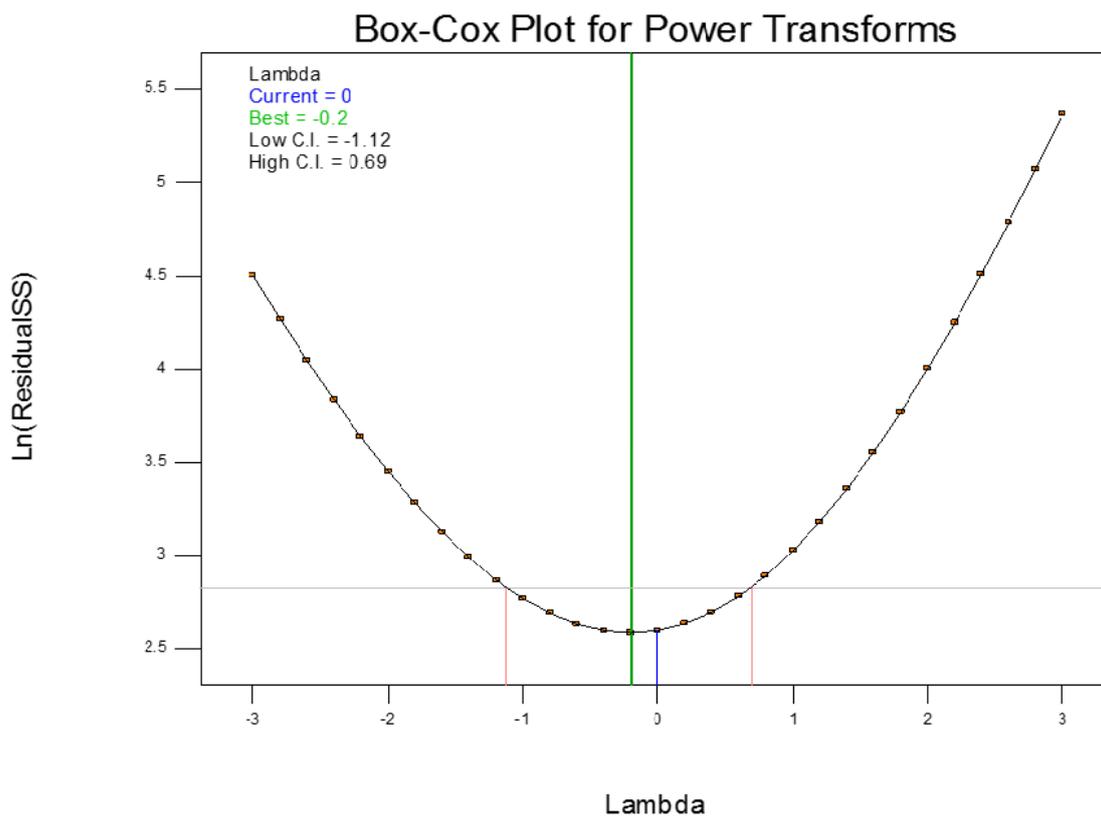

Figure 26: Tool wear Box-Cox plot for power transforms

The results of the second order model that was fitted to the data is shown in Figure 27 below. It shows that the lowest tool wear can be achieved using a depth of cut of 156.25 μm and a feed rate per tooth of 28 μm. Spindle speed had no effect on tool wear.
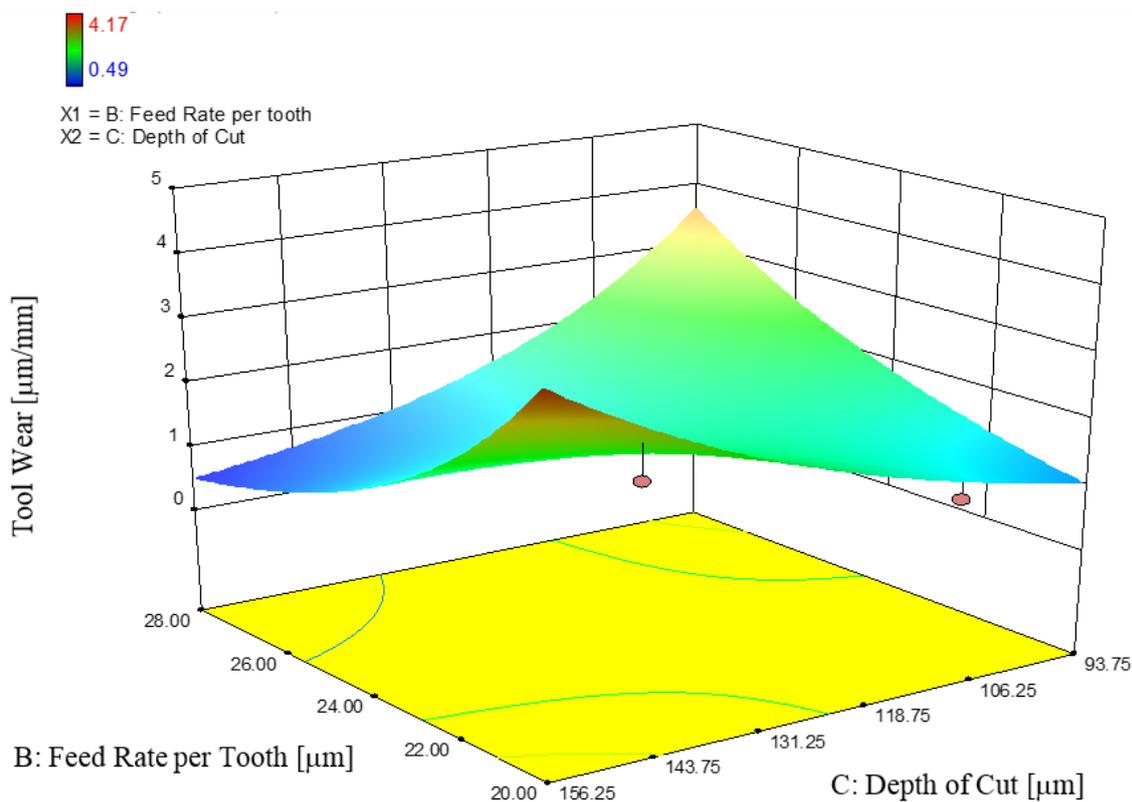
Figure 27: Surface plot for tool wear model

The results for tool life is described in the following section. No transformation was required for this response. The results for the ANOVA for tool life is summarised in Table 15 below.

Table 15: ANOVA results for tool life

Source	Sum of Squares	df	Mean Square	F-Value	p-value (Prob > F)
TOOL LIFE					
ANOVA for Response Surface 2FI model					
Analysis of variance table [Partial sum of squares - Type III]					
Model	62538.95	3	20846.32	1.628819	0.222208
B-Feed Rate	15359.9	1	15359.9	1.20014	0.28951
C-Depth of Cut	5187.026	1	5187.026	0.405286	0.533375
BC	41992.02	1	41992.02	3.281032	0.088898
Residual	204774.7	16	12798.42		
Lack of Fit	145113.4	11	13192.12	1.105583	0.488206
Pure Error	59661.37	5	11932.27		
Cor Total	267313.7	19			

The Model F-value of 1.63 implies the model is not significant relative to the noise. There is a 22.22% chance that an F-value this large could occur due to noise. Values of "Prob > F" less than 0.0500 indicate model terms are significant. In this case there are no significant model terms. Values greater than 0.1000 indicate the model terms are not significant.

The "Lack of Fit F-value" of 1.11 implies the Lack of Fit is not significant relative to the pure error. There is a 48.82% chance that a "Lack of Fit F-value" this large could occur due to noise. Non-significant lack of fit is good because we want the model to fit.

The basic statistics for tool wear is summarised in Table 16 below.

Table 16: Basic statistics for tool life

Std. Dev.	113.1301	R-Squared	0.233953
Mean	180.64	Adj R-Squared	0.09032
C.V. %	62.62738	Pred R-Squared	-0.27395
PRESS	340544.2	Adeq Precision	4.189746

A negative "Pred R-Squared" implies that the overall mean is a better predictor of the response than the current model. "Adeq Precision" measures the signal to noise ratio. A ratio greater than 4 is desirable. The ratio of 4.190 indicates an adequate signal. This model can thus be used to navigate the design space.

The next section (summarised in Table 17) shows the model that was fitted in terms of coded factors. The coding is done by identifying points on the vertices of the CCD cube as having coordinates -1 or +1, the centre point of the cube as zero and the star points as -1.6818 and +1.6818. Coding is useful in that all factors are expressed on the same scale and thus the effects of all factors, including interaction between variables are comparable. This section is also used to display the significance (or not) of each one of the effects by reporting a 95% confidence interval (CI) for each effect. If the CI includes zero, the effect is not significant and if zero falls outside of the CI the effect is significantly different from zero (at the 5% significance level or with 95% confidence).

Table 17: Tool life results of coded factors and CI

Factor	Coefficient Estimate	df	Standard Error	95% CI Low	95% CI High
Intercept	180.64	1	25.29668	127.0134	234.2666
B-Feed Rate per tooth	37.60106	1	34.32294	-35.1603	110.3624
C-Depth of Cut	32.7762	1	51.48662	-76.3706	141.923
BC	136.623	1	75.42567	-23.2722	296.5183

The final equation for tool wear in terms of coded factors therefore is displayed in equation 13 below.

Tool life = 180.64 + 37.60×B + 32.78×C + 136.62×BC (13)

The equation (13) in terms of coded factors can be used to make predictions about the response for given levels of each factor. By default, the high levels of the factors are coded as +1 and the low levels of the factors are coded as -1. The coded equation is useful for identifying the relative impact of the factors by comparing the factor coefficients.

The final equation for tool wear in terms of actual factors can thus be written as displayed in equation 14 below.

Tool life = $3102.88175 - 127.22277 \times f_z - 25.18279 \times a_p + 1.09298 \times f_z \times a_p$ (14)

Where a_p = depth of cut [μm] and f_z = feed per tooth [μm]. The equation in terms of actual factors can be used to make predictions about the response for given levels of each factor. Here, the levels should be specified in the original units for each factor. This equation should not be used to determine the relative impact of each factor because the coefficients are scaled to accommodate the units of each factor and the intercept is not at the centre of the design space.

Diagnostic plots provide a valuable tool for visual assessment of the ANOVA findings. These plots are shown in Figure 28– 31 below. The normal plot of residuals show that there is a slight deviation from normality. The residuals vs. predicted plot show that the data is within limits and that there is no constant error. The residuals vs. run plot also shows that the data is within limits and that there are three possible outliers and the predicted vs. actual plot shows relatively good performance of the model, especially on points on or close to the line.
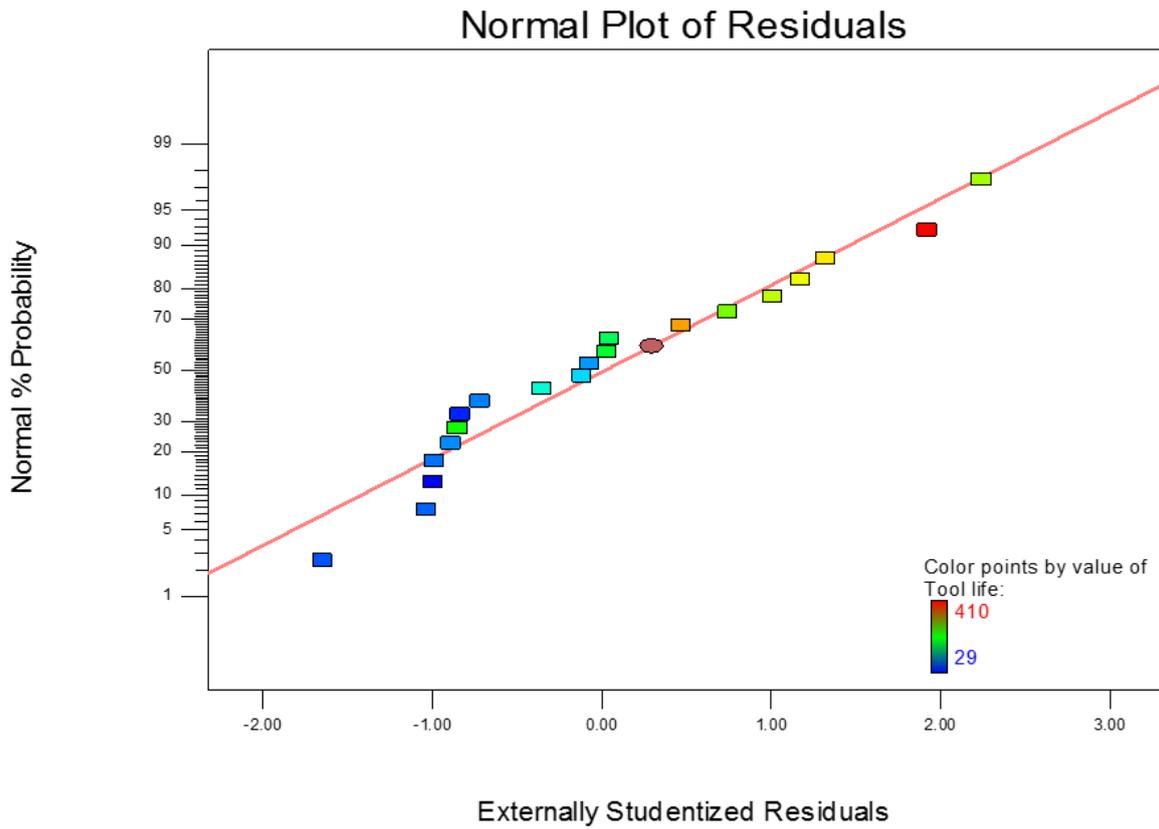
**Figure 28:** Normal plot of residuals for tool life
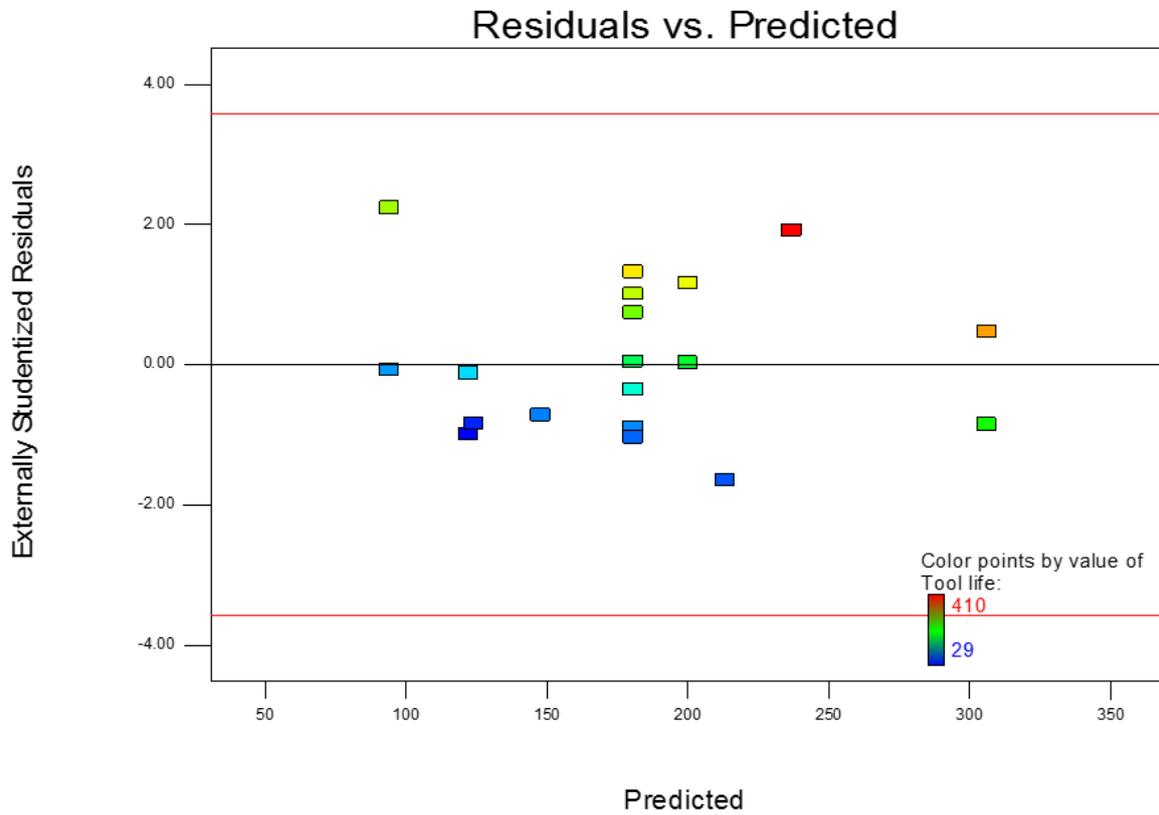
Figure 29: Residual vs. predicted plot for tool life
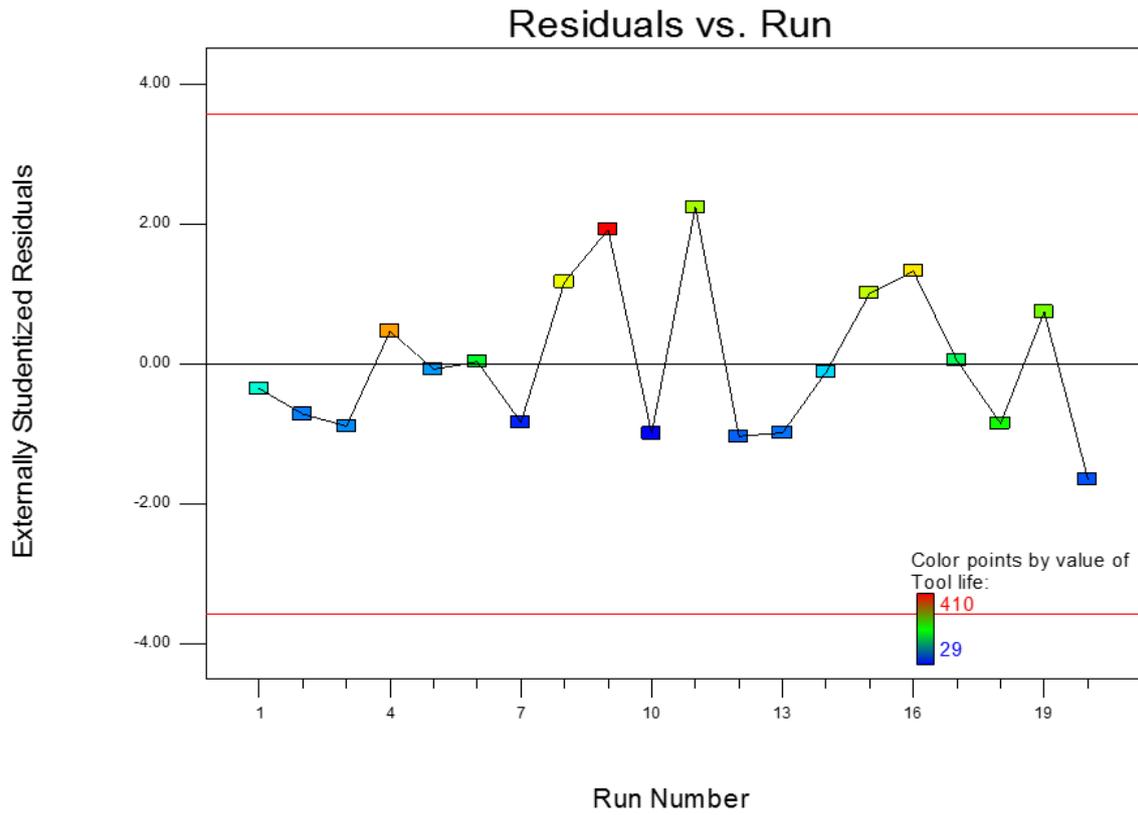
Figure 30: Residual vs. run plot for tool life
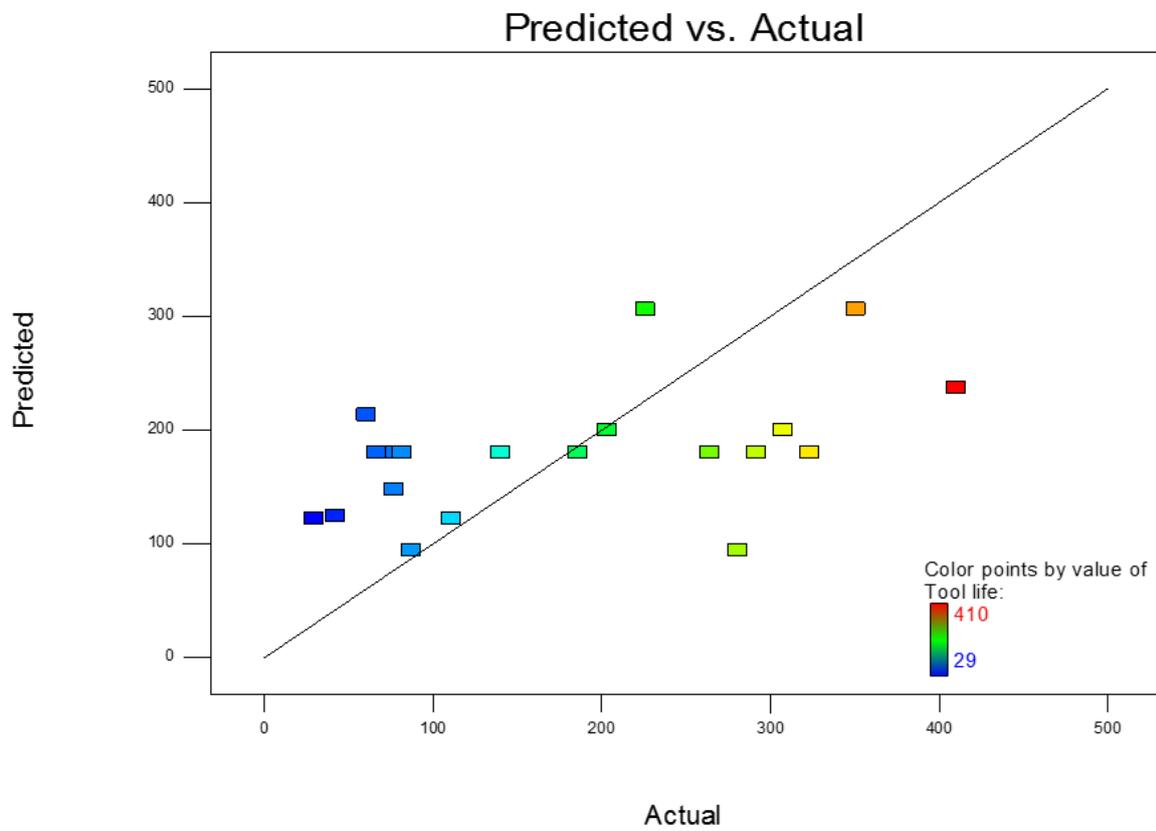

Figure 31: Predicted vs. actual plot for tool life

The Box-Cox plot for the log transforms that were performed on the primary data before the ANOVA was performed, reveals no further requirements as shown in Figure 32. The ANOVA and diagnostic plots provide satisfactory results of a significant second-order model that fits the design space.

Despite the suboptimal nature of the model, results still provide the opportunity to assess the model within the selected response surface. The model is not fitted to the optimal response surface, therefore significant predictions about any values outside of the experimental area cannot be made at the 95% confidence level.
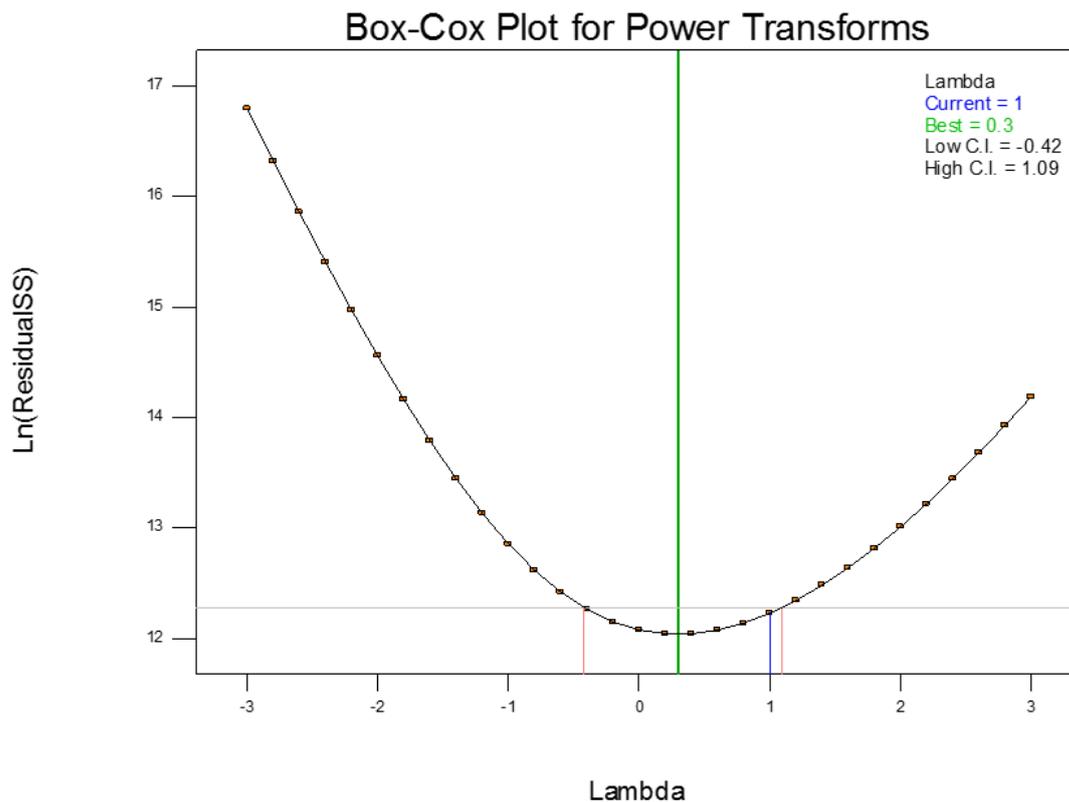

Figure 32: Tool life Box-Cox plot for power transforms

The results of the second order model that was fitted to the data is shown in Figure 33 below. It shows that the highest tool life can be achieved at using a depth of cut of 156.25 μm and a feed rate per tooth of 28 μm. All values of spindle speed yielded the same values thus spindle speed had no effect on tool life.
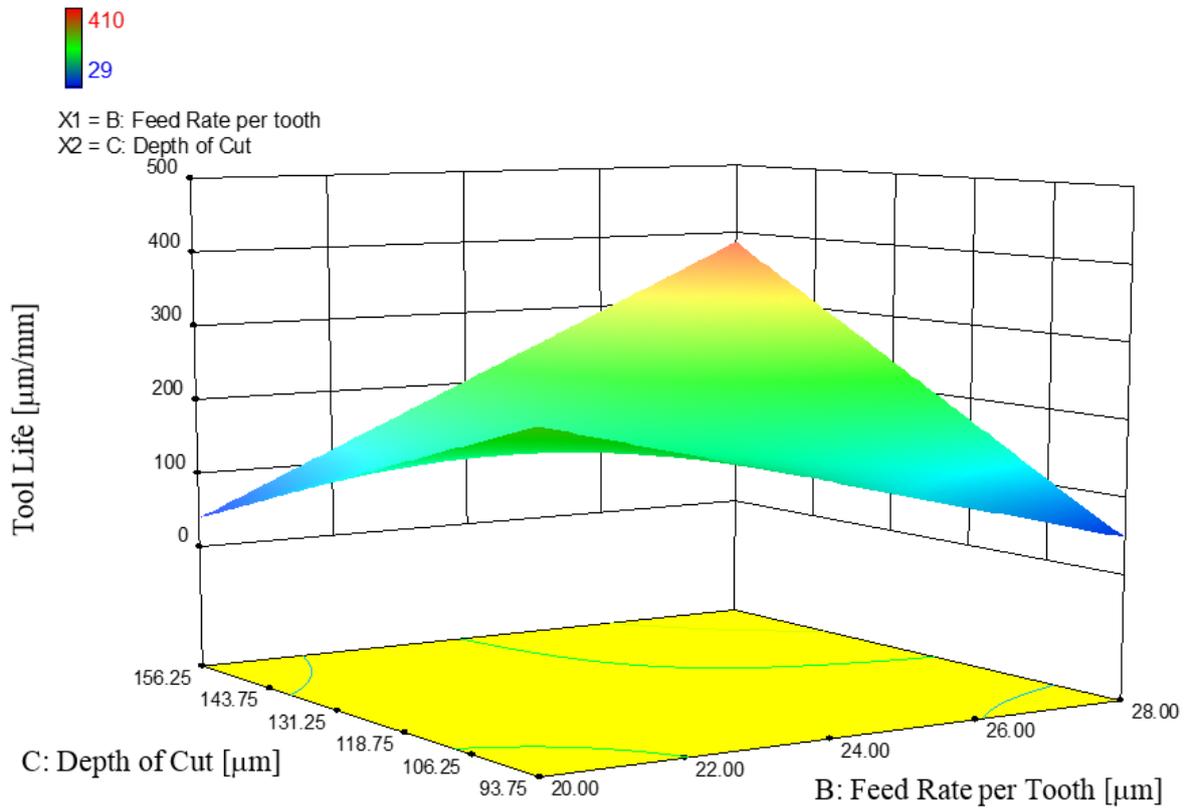
Figure 33: Surface plot for tool life model

4.2. Cutting Force

The X, Y and Z cutting force data was recorded with an ATI Net F/T gamma sensor and the results were plotted in Excel. The plot for experiment 15 is shown in Figure 34. The force pattern corresponds to the spindle speed with two peaks per revolution and a longer pattern between engaging the workpiece and moving on to a next slot.
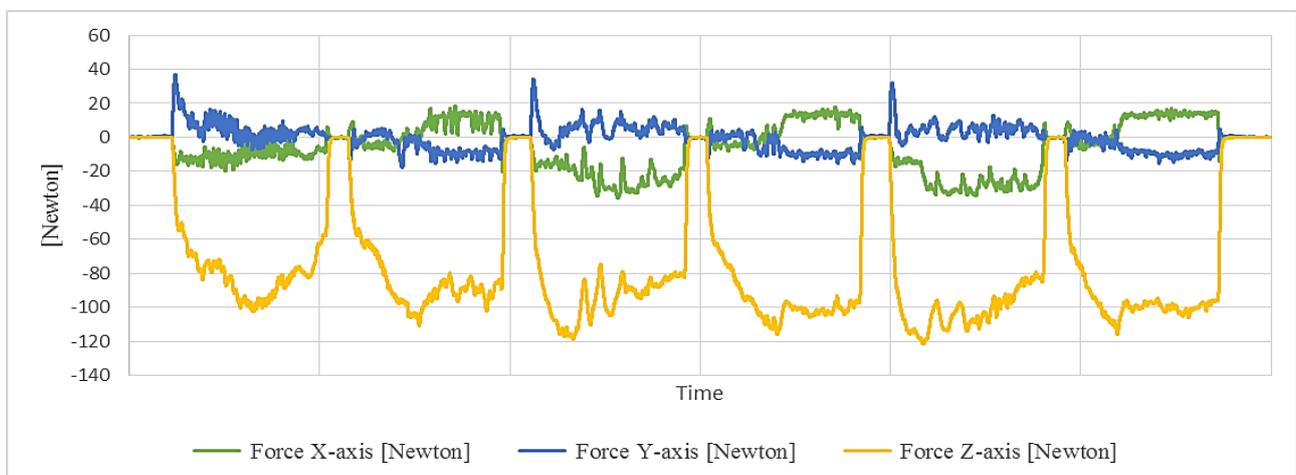

Figure 34: Force data for experiment 15 with force X-axis, Y-axis and Z-axis displayed in Newton

The average of the X, Y and Z forces were calculated for the duration that the tool was engaging the workpiece. These average values were used to calculate the resultant force for each experiment. The data of the resultant forces for the duration of experiment 15 is shown in Figure 35.
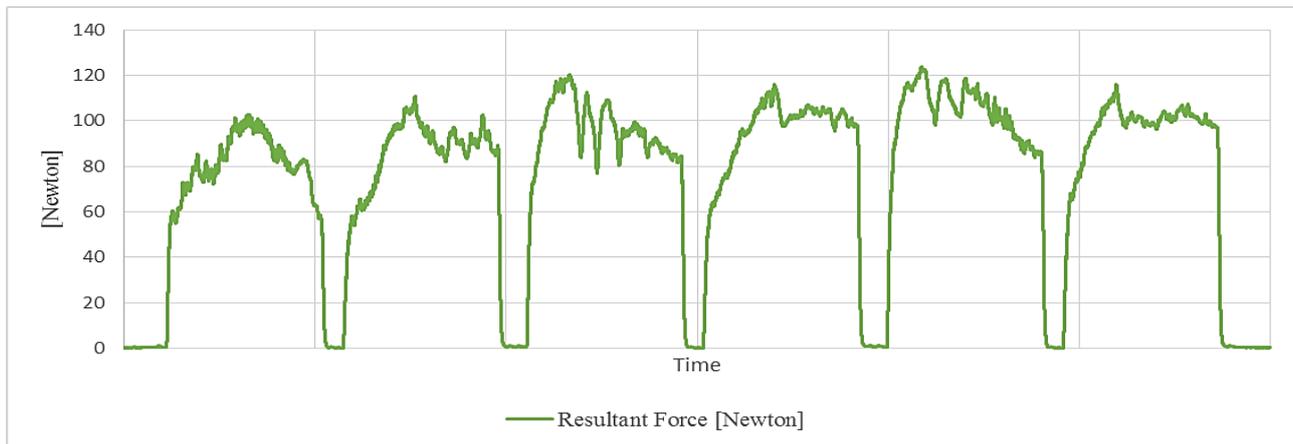

Figure 35: Resultant force data for experiment 15 displayed in Newton

The results of the X, Y, Z and resultant force values calculated for each experiment is summarised in Table 18. From the experimental results the lowest resultant force of 45.97 Newton was measured after machining with parameters 17000 RPM spindle speed, 937 mm/min feed rate and 106.42 µm depth of cut.

Table 18: Experimental results of force measurements

Run Order	Effect Label	Spindle Speed [rev/min]	Feed Rate [mm/min]	Depth of Cut [μm]	Cutting Force X [Newton]	Cutting Force Y [Newton]	Cutting Force Z [Newton]	Resultant Cutting Force [Newton]
1	Axial	14000	672	125.00	6.59	3.82	70.20	70.66
2	Axial	16000	768	93.75	5.82	3.74	78.20	78.16
3	Centre	16000	768	125.00	17.91	5.43	87.69	88.75
4	Factorial	17000	937	143.58	5.33	3.36	72.58	71.54
5	Factorial	17000	695	143.58	15.75	7.15	80.77	82.59
6	Factorial	17000	695	106.42	13.01	5.18	82.87	83.58
7	Axial	16000	576	125.00	16.80	7.43	85.57	85.01
8	Factorial	15000	613	106.42	10.77	4.32	92.81	92.84
9	Axial	16000	960	125.00	15.08	5.25	98.10	97.97
10	Factorial	15000	827	106.42	9.25	5.80	73.34	72.68
11	Factorial	15000	613	143.58	18.14	8.62	104.21	100.05
12	Centre	16000	768	125.00	6.52	5.77	71.72	71.48
13	Axial	18000	864	125.00	15.58	11.01	93.61	93.36
14	Factorial	17000	937	106.42	3.79	3.77	69.85	67.65
15	Centre	16000	768	125.00	14.08	6.90	88.30	88.70
16	Centre	16000	768	125.00	11.27	7.75	97.26	97.26
17	Centre	16000	768	125.00	18.46	7.23	96.93	96.90
18	Factorial	15000	827	143.58	11.33	4.62	94.27	94.24
19	Centre	16000	768	125.00	6.41	3.16	45.67	45.97
20	Axial	16000	768	156.25	15.67	6.56	109.48	110.91

The ANOVA analysis confirmed that the estimated resultant force is a constant value of 84.54 N with a 95% CI between 77.56 and 91.47.

4.3. Chip Formation

After each experiment the chips for that experiment were gathered and microscope images was taken of each set of chips. The chip sets were then categorised from 0 – 2 depending on what they looked like. A score of zero was given to chip sets which were relatively large and well formed. A score of 2 was given to chip sets which were extremely fragmented and broken into very small bits. A score of 1 was given to chip sets which contained elements of both. The score category for each of the experiments is summarised in Table 19. Experimental run 1-4, 12 and 14 provided the best formed chips according to the various experimental parameters used. Images of each of the three categories are shown in Figure 36. All of the experimental chip sets and their corresponding scores can be seen in Appendix C.

Table 19: Experimental results of chip formation

Run Order	Effect Label	Spindle Speed [rev/min]	Feed Rate [mm/min]	Depth of Cut [μm]	Chip Formation [ranked 0-2]
1	Axial	14000	672	125.00	0
2	Axial	16000	768	93.75	0
3	Centre	16000	768	125.00	0
4	Factorial	17000	937	143.58	0
5	Factorial	17000	695	143.58	1
6	Factorial	17000	695	106.42	1
7	Axial	16000	576	125.00	2
8	Factorial	15000	613	106.42	1
9	Axial	16000	960	125.00	2
10	Factorial	15000	827	106.42	1
11	Factorial	15000	613	143.58	2
12	Centre	16000	768	125.00	0
13	Axial	18000	864	125.00	2
14	Factorial	17000	937	106.42	0
15	Centre	16000	768	125.00	2
16	Centre	16000	768	125.00	1
17	Centre	16000	768	125.00	2
18	Factorial	15000	827	143.58	1
19	Centre	16000	768	125.00	1
20	Axial	16000	768	156.25	2

Figure 36: Chip set examples with relevant scores

4.4. Burr Formation

After the experiments the Ti-6Al-4V plates were imaged and the burr formation was measured for each experiment. The burr length measurements were taken along the length of the slots and documented to be able to calculate the length of cut of each experiment where burrs were formed on one or both sides of the machined slot. The total length of the burrs in millimetres were then divided by the total length of cut for each experiment to deduce a percentage of burr formation for each experiment. The results of the burr formation is summarised in Table 20 below. From the

experimental results the lowest percentage burr formation of 5% was measured after machining with parameters 16000 RPM spindle speed, 960 mm/min feed rate and 125 μm depth of cut.

Table 20: Experimental results of burr formation

Run Order	Effect Label	Spindle Speed [rev/min]	Feed Rate [mm/min]	Depth of Cut [μm]	Burr Formation [% of total cut]
1	Axial	14000	672	125.00	37%
2	Axial	16000	768	93.75	9%
3	Centre	16000	768	125.00	30%
4	Factorial	17000	937	143.58	42%
5	Factorial	17000	695	143.58	64%
6	Factorial	17000	695	106.42	8%
7	Axial	16000	576	125.00	81%
8	Factorial	15000	613	106.42	28%
9	Axial	16000	960	125.00	5%
10	Factorial	15000	827	106.42	79%
11	Factorial	15000	613	143.58	45%
12	Centre	16000	768	125.00	41%
13	Axial	18000	864	125.00	64%
14	Factorial	17000	937	106.42	46%
15	Centre	16000	768	125.00	35%
16	Centre	16000	768	125.00	29%
17	Centre	16000	768	125.00	20%
18	Factorial	15000	827	143.58	11%
19	Centre	16000	768	125.00	42%
20	Axial	16000	768	156.25	19%

The results for burr formation is described in the following section. No transformation was required for this response. The results for the ANOVA for burr formation is summarised in Table 21 below.

Table 21: ANOVA results for burr formation

BURR FORMATION					
ANOVA for Response Surface 2FI model					
Analysis of variance table [Partial sum of squares - Type III]					
Source	Sum of Squares	df	Mean Square	F-Value	p-value (Prob > F)
Model	0.478662	5	0.095732	2.851368	0.055826
A-Cutting Speed	0.016397	1	0.016397	0.488367	0.496103
B-Feed Rate	0.06755	1	0.06755	2.011948	0.177941
C-Depth of Cut	0.002056	1	0.002056	0.061225	0.808163
AC	0.13183	1	0.13183	3.926532	0.067518
BC	0.26083	1	0.26083	7.768767	0.014541
Residual	0.470039	14	0.033574		
Lack of Fit	0.436008	9	0.048445	7.118036	0.021839

The Model F-value of 2.85 implies there is a 5.58% chance that an F-value this large could occur due to noise. Values of "Prob > F" less than 0.0500 indicate model terms are significant. In this case BC is a significant model term. Values greater than 0.1000 indicate the model terms are not significant.

The "Lack of Fit F-value" of 7.12 implies the Lack of Fit is significant. There is only a 2.18% chance that a "Lack of Fit F-value" this large could occur due to noise. Significant lack of fit is bad because we want the model to fit.

The basic statistics for burr formation is summarised in Table 22 below.

Table 22: Basic statistics of burr formation

Std. Dev.	0.183233	R-Squared	0.504545
Mean	0.366831	Adj R-Squared	0.327596
C.V. %	49.9501	Pred R-Squared	-0.194
PRESS	1.132746	Adeq Precision	8.195967

A negative "Pred R-Squared" implies that the overall mean is a better predictor of the response than the current model. "Adeq Precision" measures the signal to noise ratio. A ratio greater than 4 is desirable. The ratio of 8.196 indicates an adequate signal. This model can thus be used to navigate the design space.

The next section (summarised in Table 23) shows the model that was fitted in terms of coded factors. The coding is done by identifying points on the vertices of the CCD cube as having coordinates -1 or +1, the centre point of the cube as zero and the star points as -1.6818 and +1.6818. Coding is useful in that all factors are expressed on the same scale and thus the effects of all factors, including interaction between variables are comparable. This section is also used to display the significance (or not) of each one of the effects by reporting a 95% confidence interval (CI) for each effect. If the CI includes zero, the effect is not significant and if zero falls outside of the CI the effect is significantly different from zero (at the 5% significance level or with 95% confidence).

Table 23: Burr formation results of coded factors and CI

Factor	Coefficient Estimate	df	Standard Error	95% CI Low	95% CI High
Intercept	0.366831	1	0.040972	0.278955	0.454708
A-Spindle Speed	0.032012	1	0.045808	-0.06624	0.130261
B-Feed Rate per tooth	-0.07885	1	0.055592	-0.19808	0.040379
C-Depth of Cut	0.020635	1	0.083391	-0.15822	0.19949
AC	0.215907	1	0.108959	-0.01779	0.4496
BC	-0.3405	1	0.122164	-0.60252	-0.07849

The final equation for burr formation wear in terms of coded factors therefore is displayed in equation 15 below.

$$\text{Burr formation} = 0.37 + 0.032 \times A - 0.079 \times B + 0.021 \times C + 0.22 \times AC - 0.34 \times BC \tag{15}$$

The equation (15) in terms of coded factors can be used to make predictions about the response for given levels of each factor. By default, the high levels of the factors are coded as +1 and the low levels of the factors are coded as -1. The coded equation is useful for identifying the relative impact of the factors by comparing the factor coefficients.

The final equation for burr formation in terms of actual factors can thus be written as displayed in equation 16 below.

$$\text{Burr formation life} = 5.89122 - 8.31616 \times 10^{-4} \times \text{RPM} + 0.32079 \times f_z - 0.044508 \times a_p + \tag{16}$$
$$6.90902 \times 10^{-6} \times \text{RPM} \times a_p - 2.72401 \times 10^{-3} \times f_z \times a_p$$

Where a_p = depth of cut [μm], f_z = feed per tooth [μm] and RPM = spindle speed [rev/min]. The equation in terms of actual factors can be used to make predictions about the response for given levels of each factor. Here, the levels should be specified in the original units for each factor. This equation should not be used to determine the relative impact of each factor because the coefficients are scaled to accommodate the units of each factor and the intercept is not at the centre of the design space.

Diagnostic plots provide a valuable tool for visual assessment of the ANOVA findings. These plots are shown in Figure 37– 40 below. The normal plot of residuals show that there is almost not deviation from normality. The residuals vs. predicted plot show that the data is within limits and that there is no constant error. The residuals vs. run plot also shows that the data is within limits and that there are one possible outliers and the predicted vs. actual plot shows relatively good performance of the model, especially on points on or close to the line.
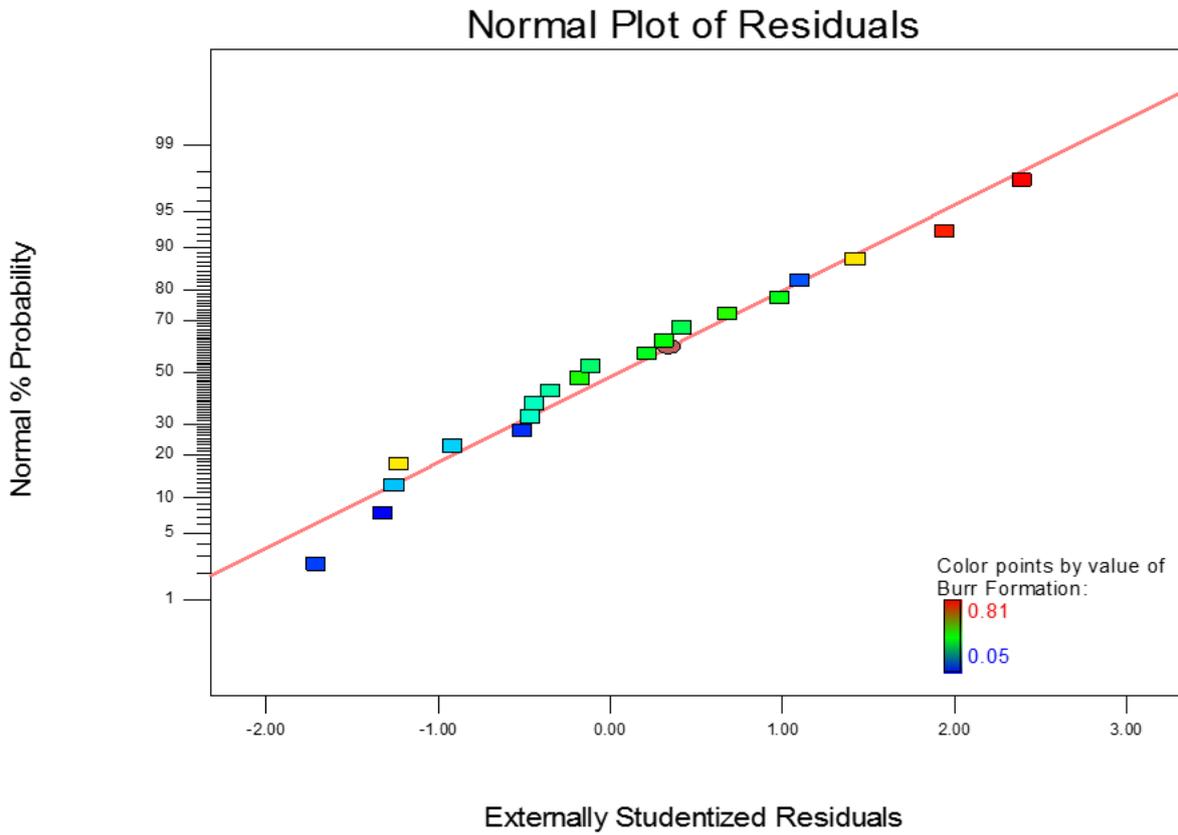
Figure 37: Normal plot of residuals for burr formation
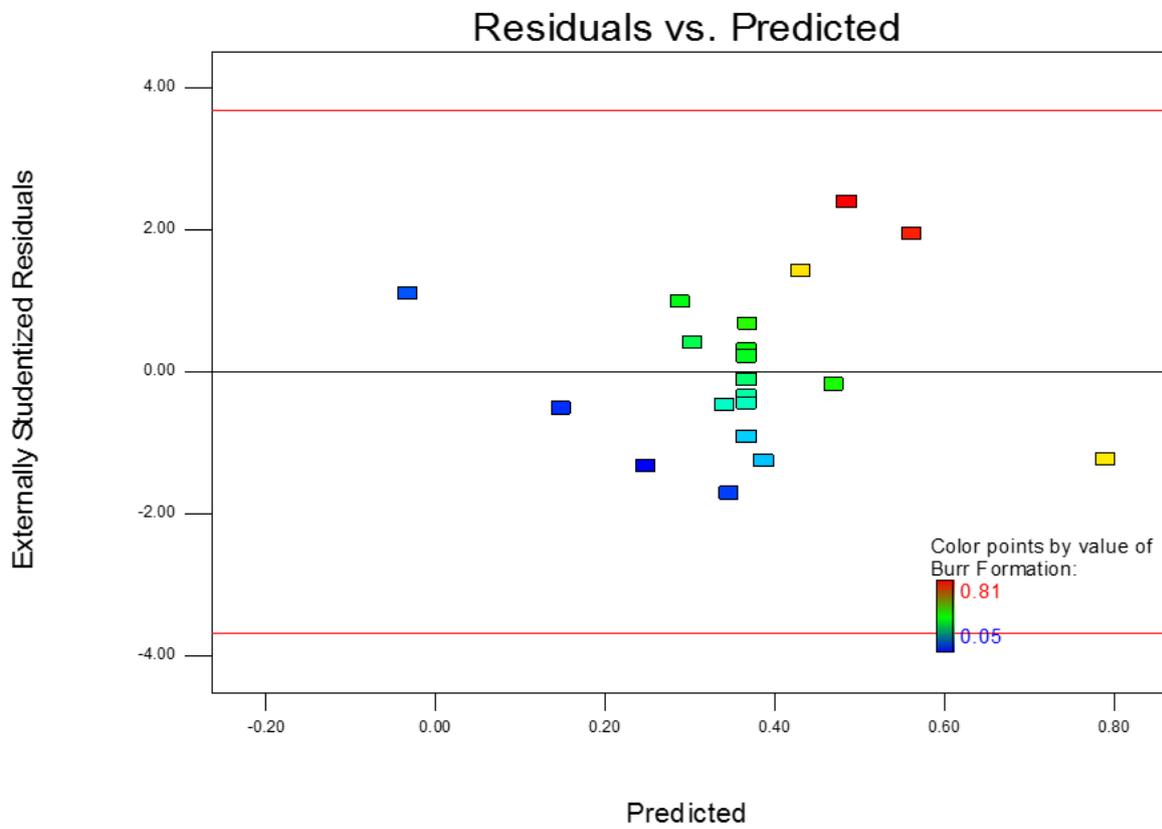
**Figure 38:** Residual vs. predicted plot for burr formation
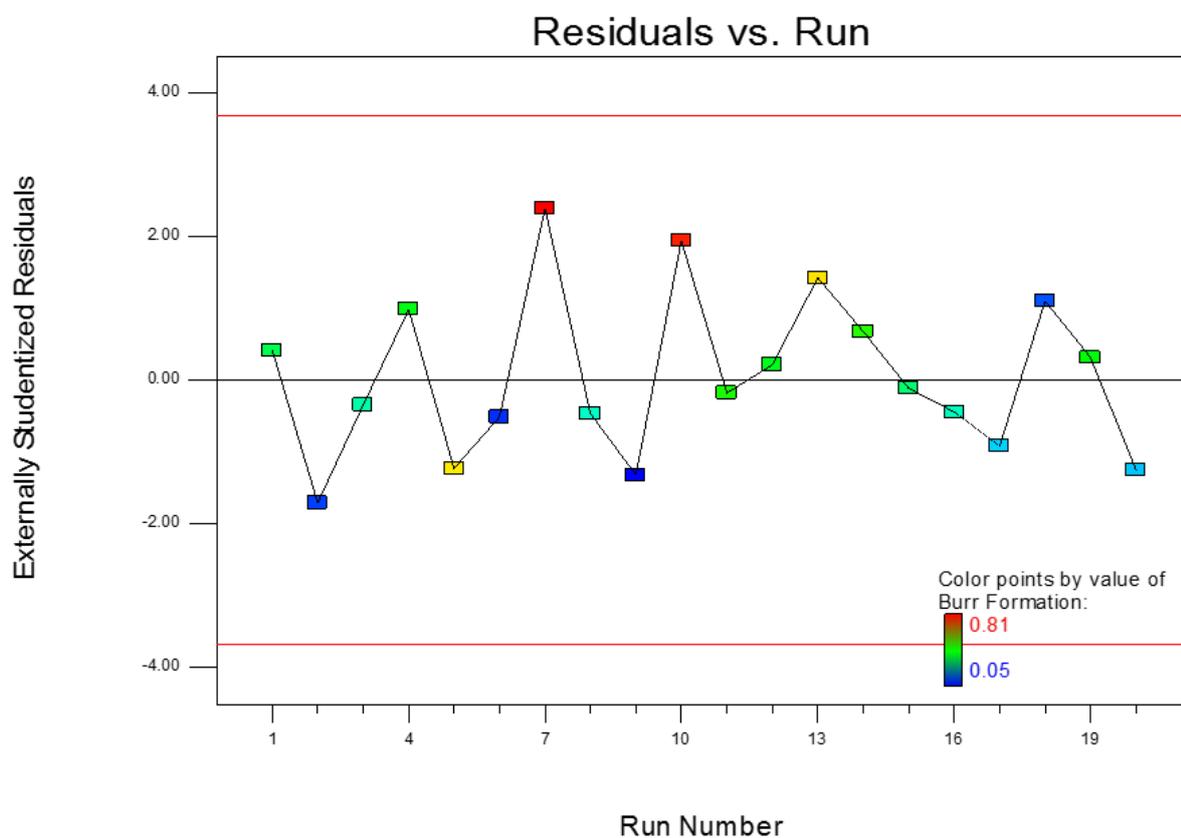
**Figure 39:** Residual vs. run plot for burr formation
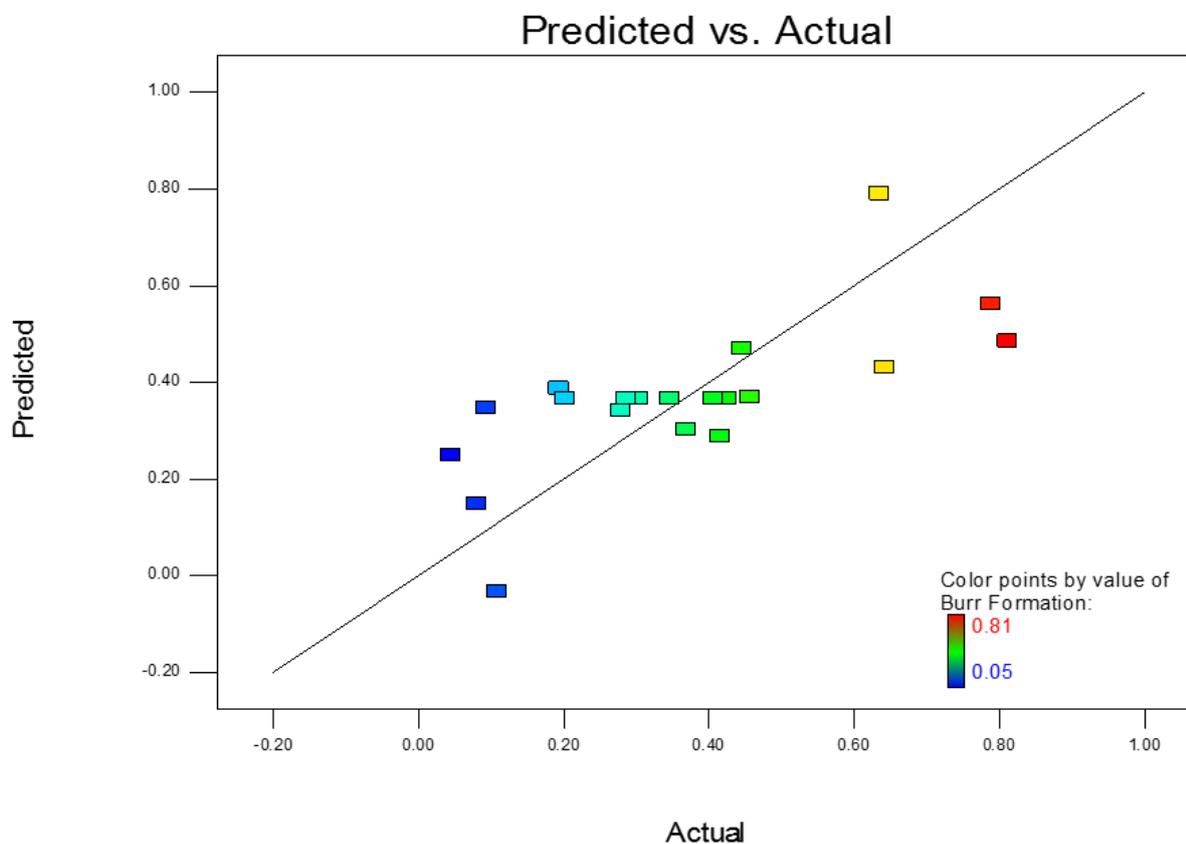
Figure 40: Predicted vs. actual plot for burr formation

The Box-Cox plot for the log transforms that were performed on the primary data before the ANOVA was performed, reveals no further requirements as shown in Figure 41. The ANOVA and diagnostic plots provide satisfactory results of a significant second-order model that fits the design space.
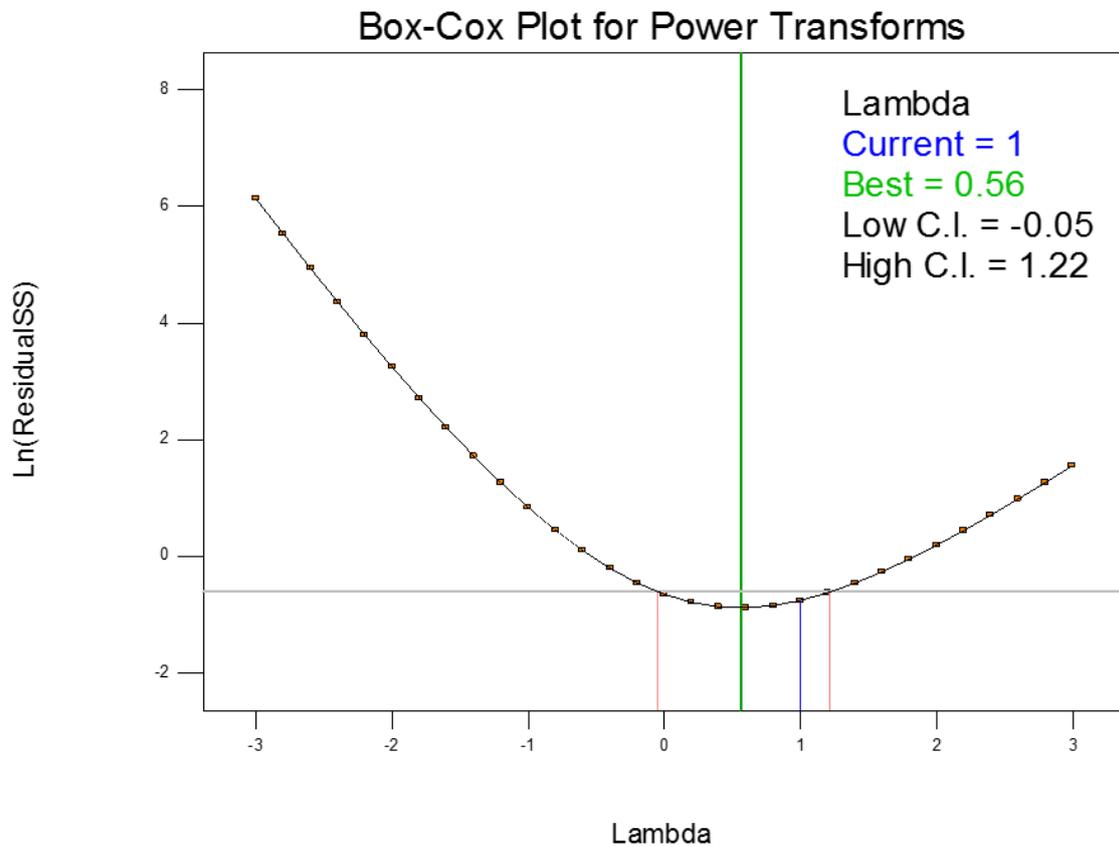
Figure 41: Burr formation Box-Cox plot for power transforms

The results of the second order model that was fitted to the data is shown in Figure 42 below. It shows that the lowest burr formation can be achieved at using a depth of cut of 156.25 μm, spindle speed of 15000 RPM and a feed rate per tooth of 28 μm.
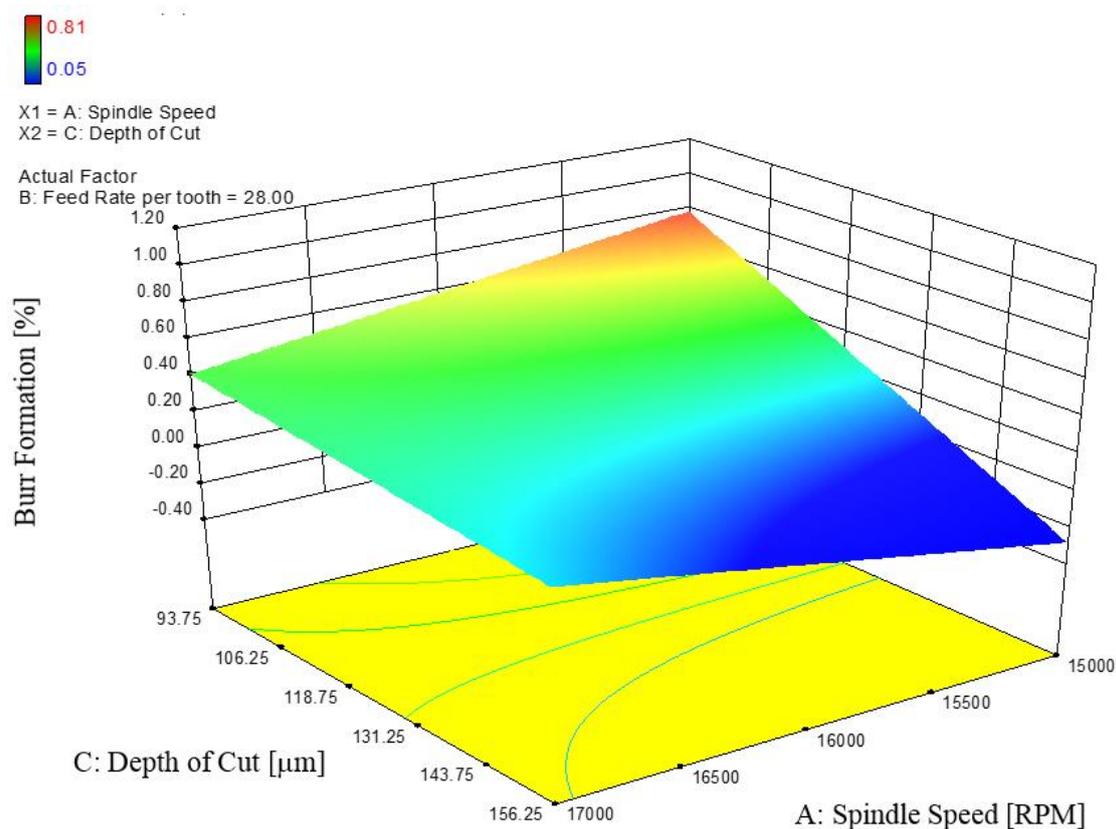
Figure 42: Surface plot for burr formation model

4.5. Surface Finish

After the experiments the Ti-6Al-4V plates underwent atomic force microscopy with a Nanosurf®
Flex AFM instrument to measure the surface roughness, S_a [nm] across various areas in the individual
slots for each experiment. Each experiment was measured on 6 different areas and the average surface
roughness was calculated by the Nanoscan Easyscan 2 software. Figure 43 shows the 6 surface plots
that were generated by the software of experiment 15. The surface roughness results are summarised
in Table 24 below. From the experimental results the lowest surface roughness of 71 nm was
measured after machining with parameters 16000 RPM spindle speed, 768 mm/min feed rate and 125
μm depth of cut.

Table 24: Experimental results for surface roughness

Run Order	Effect Label	Spindle Speed [rev/min]	Feed Rate [mm/min]	Depth of Cut [µm]	Surface Roughness [nm]
1	Axial	14000	672	125.00	377
2	Axial	16000	768	93.75	172
3	Centre	16000	768	125.00	71
4	Factorial	17000	937	143.58	336
5	Factorial	17000	695	143.58	271
6	Factorial	17000	695	106.42	506
7	Axial	16000	576	125.00	138
8	Factorial	15000	613	106.42	94
9	Axial	16000	960	125.00	190
10	Factorial	15000	827	106.42	139
11	Factorial	15000	613	143.58	139
12	Centre	16000	768	125.00	190
13	Axial	18000	864	125.00	242
14	Factorial	17000	937	106.42	331
15	Centre	16000	768	125.00	244
16	Centre	16000	768	125.00	199
17	Centre	16000	768	125.00	182
18	Factorial	15000	827	143.58	295
19	Centre	16000	768	125.00	274
20	Axial	16000	768	156.25	367
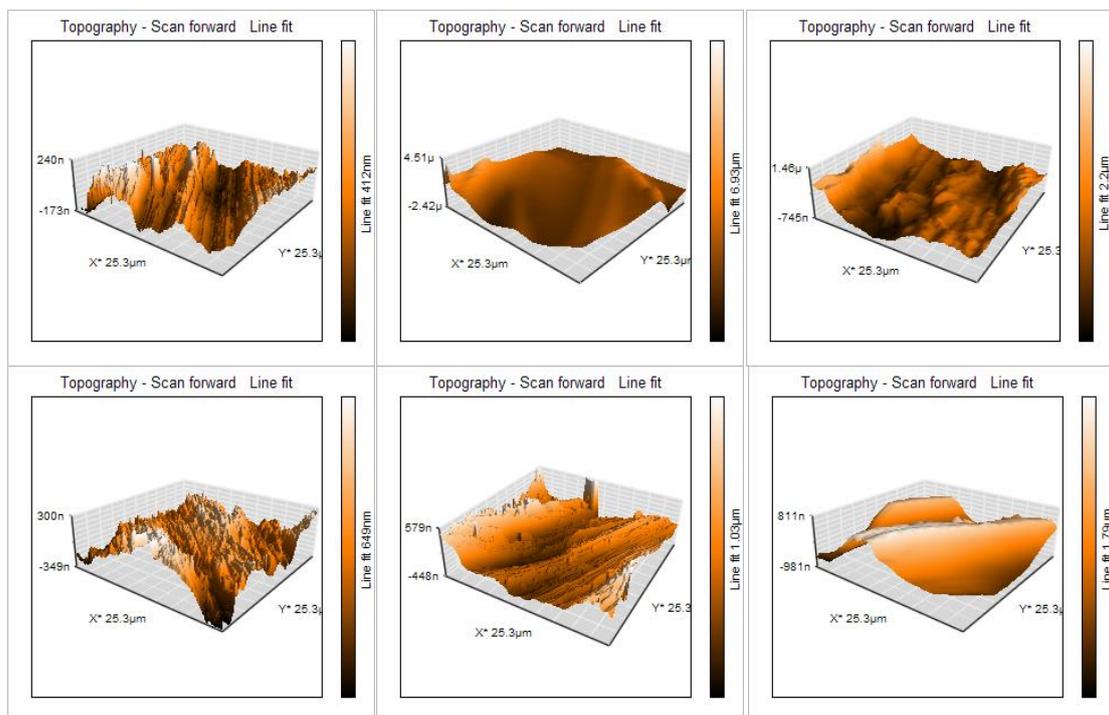
Figure 43: Surface roughness surface plots of experiment 15 machining with parameters $v_c = 65.97$ [m/min], $v_f = 672$ [mm/min] and $a_p = 125$ [µm]

The results for Surface roughness is described in the following section. A natural log transformation was applied to the tool wear data and a constant of 0.002 was added for the benefit of cases with a value of zero. The results for the ANOVA for Surface roughness is summarised in Table 25 below.

Table 25: ANOVA results for surface roughness

	SURFACE ROUGHNESS				
	ANOVA for Response Surface 2FI model				
	Analysis of variance table [Partial sum of squares - Type III]				
Source	Sum of Squares	df	Mean Square	F-Value	p-value (Prob > F)
Model	1.511746353	6	0.251957725	1.072771829	0.42652162
A-Spindle Speed	0.377366246	1	0.377366246	1.606729372	0.227186884
B-Feed Rate per tooth	0.157388607	1	0.157388607	0.670120605	0.42776102
C-Depth of Cut	0.237758717	1	0.237758717	1.012316067	0.332709735
AB	0.228037333	1	0.228037333	0.97092489	0.342434452
AC	0.383468105	1	0.383468105	1.632709535	0.223675091
BC	0.127727345	1	0.127727345	0.543830506	0.473950691
Residual	3.053259175	13	0.23486609		
Lack of Fit	1.905624143	8	0.238203018	1.037799523	0.507573452
Pure Error	1.147635033	5	0.229527007		
Cor Total	4.565005528	19			

The Model F-value of 1.07 implies the model is not significant relative to noise. There is a 42.65% chance that an F-value this large could occur due to noise. Values of "Prob > F" less than 0.0500 indicate model terms are significant. In this case there are no significant model term. Values greater than 0.1000 indicate the model terms are not significant.

The "Lack of Fit F-value" of 1.91 implies the Lack of Fit is not significant. There is a 50.76% chance that a "Lack of Fit F-value" this large could occur due to noise. Non-significant lack of fit is good because we want the model to fit.

The basic statistics for Surface roughness is summarised in Table 26 below.

Table 26: Basic statistics for surface roughness

Std. Dev.	0.484629849	R-Squared	0.331159808
Mean	5.365340917	Adj R-Squared	0.022464334
C.V. %	9.032601215	Pred R-Squared	-0.855388673
PRESS	8.46985955	Adeq Precision	4.374188695

A negative "Pred R-Squared" implies that the overall mean is a better predictor of the response than the current model. "Adeq Precision" measures the signal to noise ratio. A ratio greater than 4 is

desirable. The ratio of 4.374 indicates an adequate signal. This model can thus be used to navigate the design space.

The next section (summarised in Table 27) shows the model that was fitted in terms of coded factors. The coding is done by identifying points on the vertices of the CCD cube as having coordinates -1 or +1, the centre point of the cube as zero and the star points as -1.6818 and +1.6818. Coding is useful in that all factors are expressed on the same scale and thus the effects of all factors, including interaction between variables are comparable. This section is also used to display the significance (or not) of each one of the effects by reporting a 95% confidence interval (CI) for each effect. If the CI includes zero, the effect is not significant and if zero falls outside of the CI the effect is significantly different from zero (at the 5% significance level or with 95% confidence).

Table 27: Surface roughness results of coded factors and CI

Factor	Coefficient Estimate	df	Standard Error	95% CI Low	95% CI High
Intercept	5.365340917	1	0.108366529	5.131229265	5.599452569
A-Spindle Speed	0.153575357	1	0.121157462	-0.108169427	0.415320141
B-Feed Rate per tooth	0.120362873	1	0.14703342	-0.197283519	0.438009266
C-Depth of Cut	0.221913652	1	0.220559595	-0.254576384	0.698403687
AB	-0.189295034	1	0.192108421	-0.604320046	0.225729978
AC	-0.368234048	1	0.288183743	-0.990817174	0.254349078
BC	0.238277206	1	0.323110235	-0.459760019	0.936314431

The final equation for surface roughness wear in terms of coded factors therefore is displayed in equation 17 below.

$$\text{Surface roughness} = 5.37 + 0.15 \times A + 0.12 \times B + 0.22 \times C - 0.19 \times AB - 0.37AC + 0.24 \times BC \qquad (17)$$

The equation (17) in terms of coded factors can be used to make predictions about the response for given levels of each factor. By default, the high levels of the factors are coded as +1 and the low levels of the factors are coded as -1. The coded equation is useful for identifying the relative impact of the factors by comparing the factor coefficients.

The final equation for Surface roughness in terms of actual factors can thus be written as displayed in equation 18 below.

$$\text{Surface roughness life} = -34.72236 + 2.76228 \times 10^{-3} \times \text{RPM} + 0.54899 \times f_z + 0.14989 \times a_p - \qquad (18)$$
$$4.73238 \times 10^{-5} \times \text{RPM} \times f_z - 1.17835 \times 10^{-5} \times \text{RPM} \times a_p + 1.90622 \times 10^{-3} \times f_z \times a_p$$

Where a_p = depth of cut [μm], f_z = feed per tooth [μm] and RPM = spindle speed [rev/min]. The equation in terms of actual factors can be used to make predictions about the response for given levels of each factor. Here, the levels should be specified in the original units for each factor. This equation should not be used to determine the relative impact of each factor because the coefficients are scaled to accommodate the units of each factor and the intercept is not at the centre of the design space.

Diagnostic plots provide a valuable tool for visual assessment of the ANOVA findings. These plots are shown in

Figure 44– 47 below. The normal plot of residuals show that there is almost not deviation from normality. The residuals vs. predicted plot show that the data is within limits and that there is no constant error. The residuals vs. run plot also shows that the data is within limits and that there are one possible outliers and the predicted vs. actual plot shows relatively good performance of the model, especially on points on or close to the line.
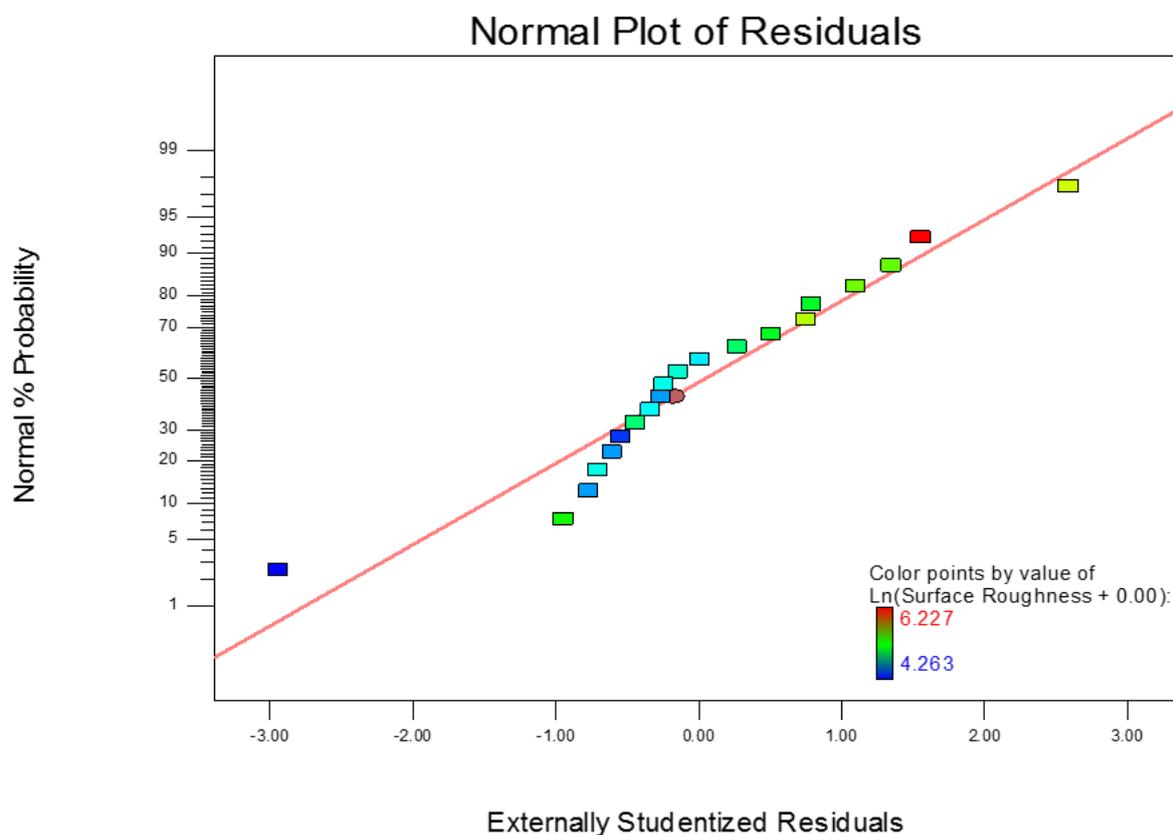
Figure 44: Normal plot of residuals for surface roughness
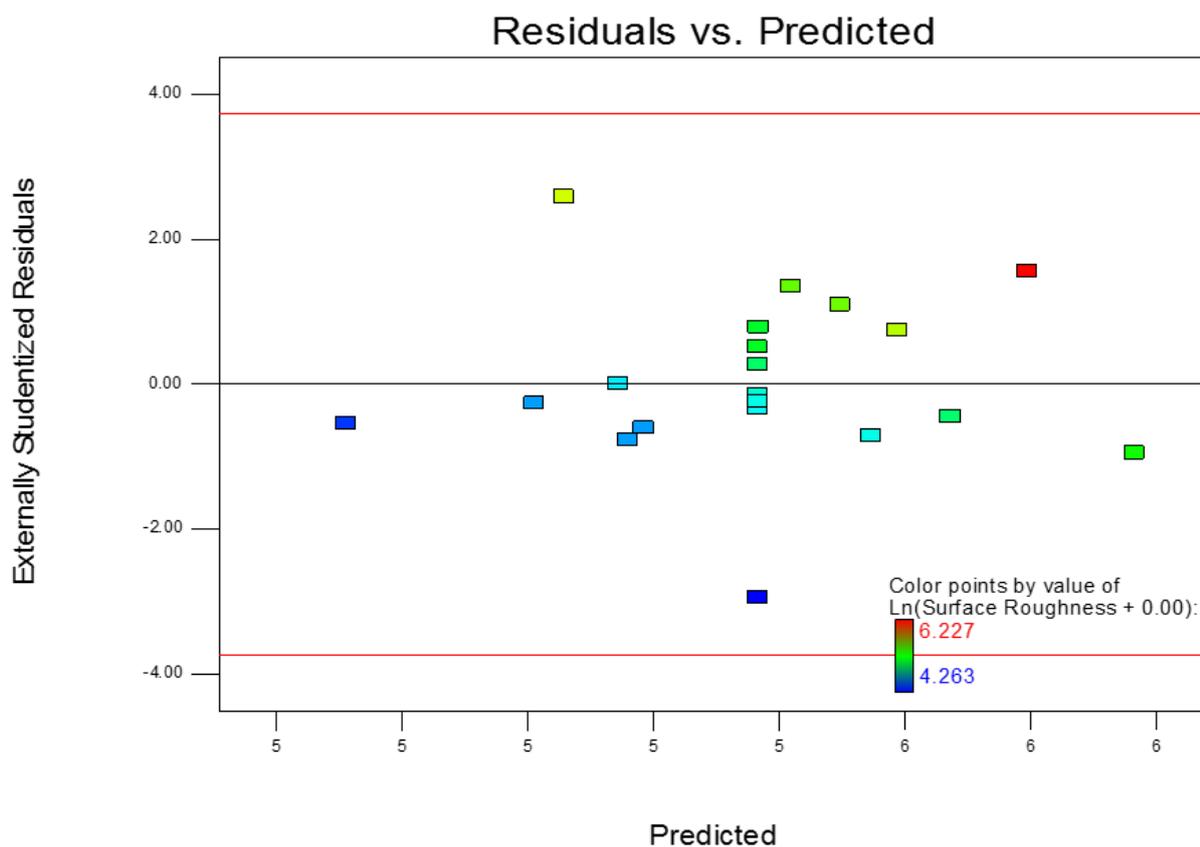
Figure 45: Residual vs. predicted plot for surface roughness
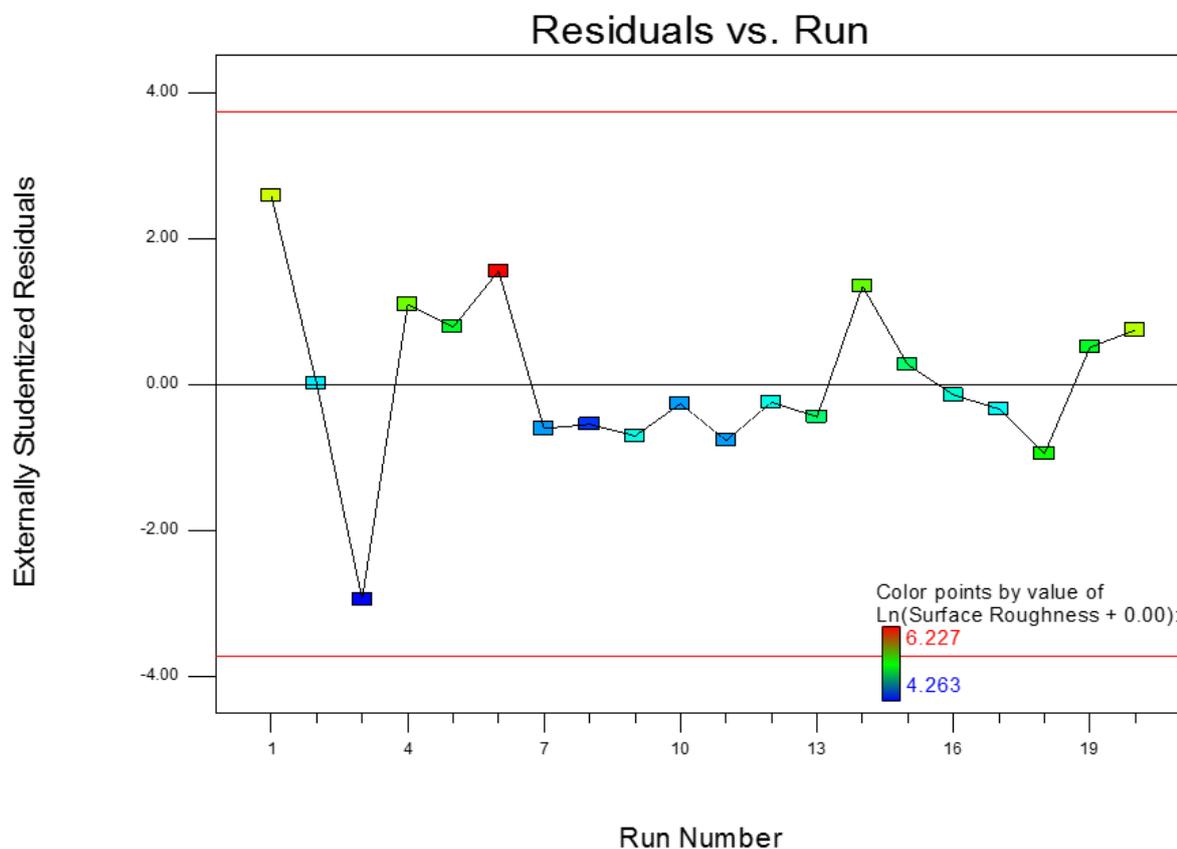
Figure 46: Residual vs. run plot for Surface roughness
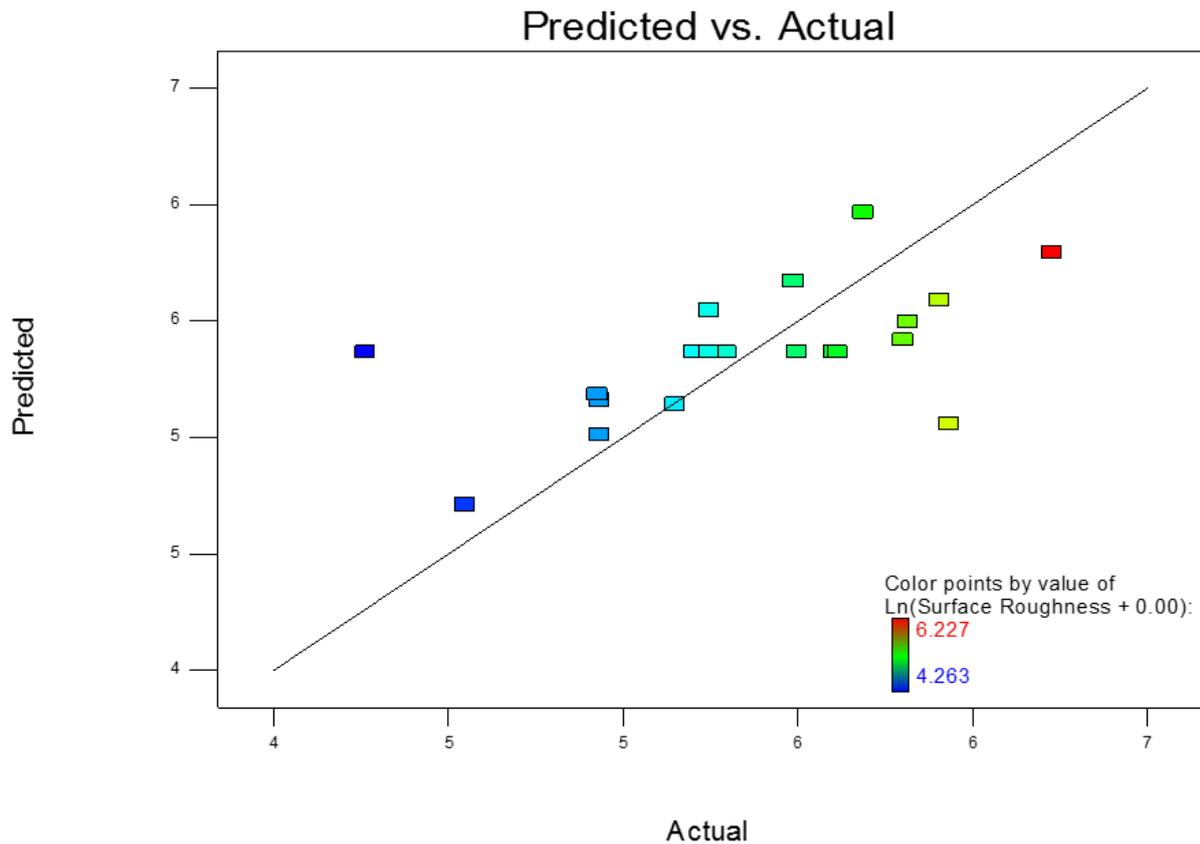
Figure 47: Predicted vs. actual plot for surface roughness

The Box-Cox plot for the log transforms that were performed on the primary data before the ANOVA was performed, reveals no further requirements as shown in Figure 48. The ANOVA and diagnostic plots provide satisfactory results of a significant second-order model that fits the design space. Despite the suboptimal nature of the model, results still provide the opportunity to assess the model within the selected response surface. The model is not fitted to the optimal response surface, therefore significant predictions about any values outside of the experimental area cannot be made at the 95% confidence level.

Box-Cox Plot for Power Transforms

Lambda
Current = 0
Best = 0.38
Low C.I. = -0.58
High C.I. = 1.45
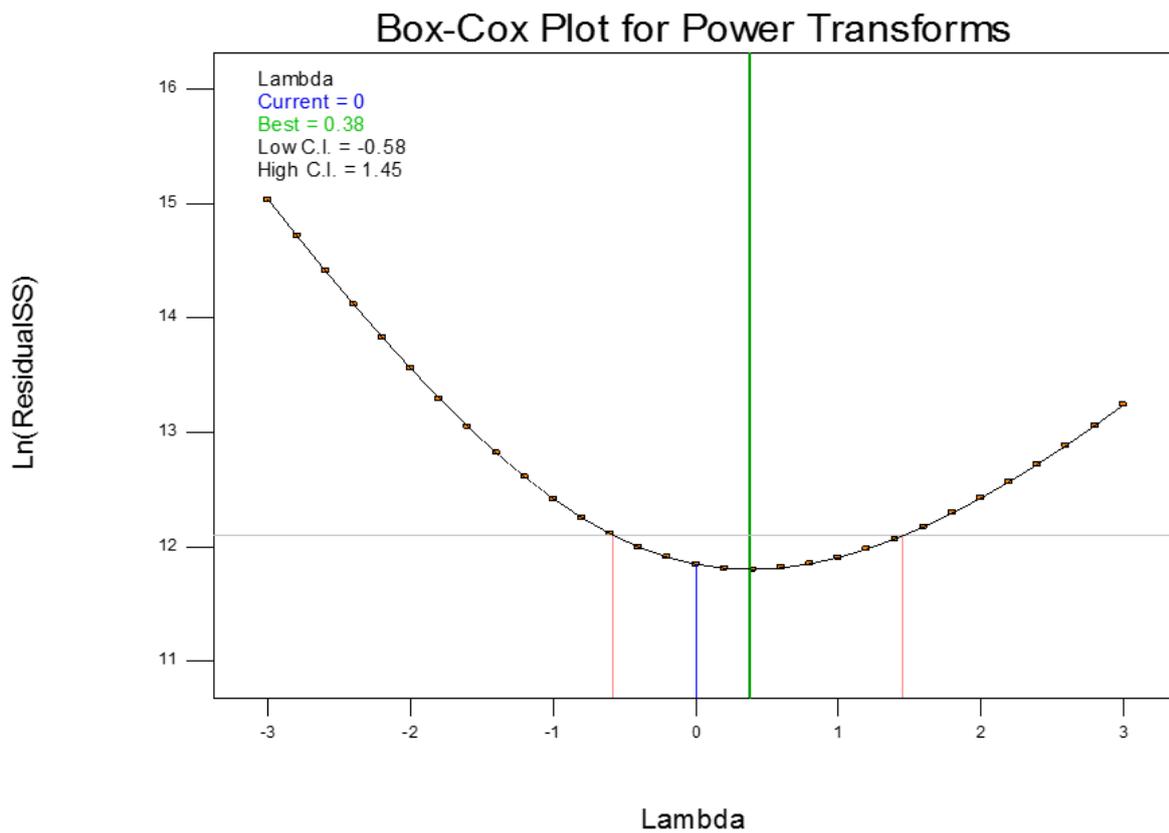
Figure 48: Box-Cox plot for surface roughness

The results of the second order model that was fitted to the data is shown in Figure 49 below. It shows that the lowest surface roughness can be achieved at using a depth of cut of 93.75 μm and spindle speed of 15000 RPM. Feed rate per tooth had no effect on the model.
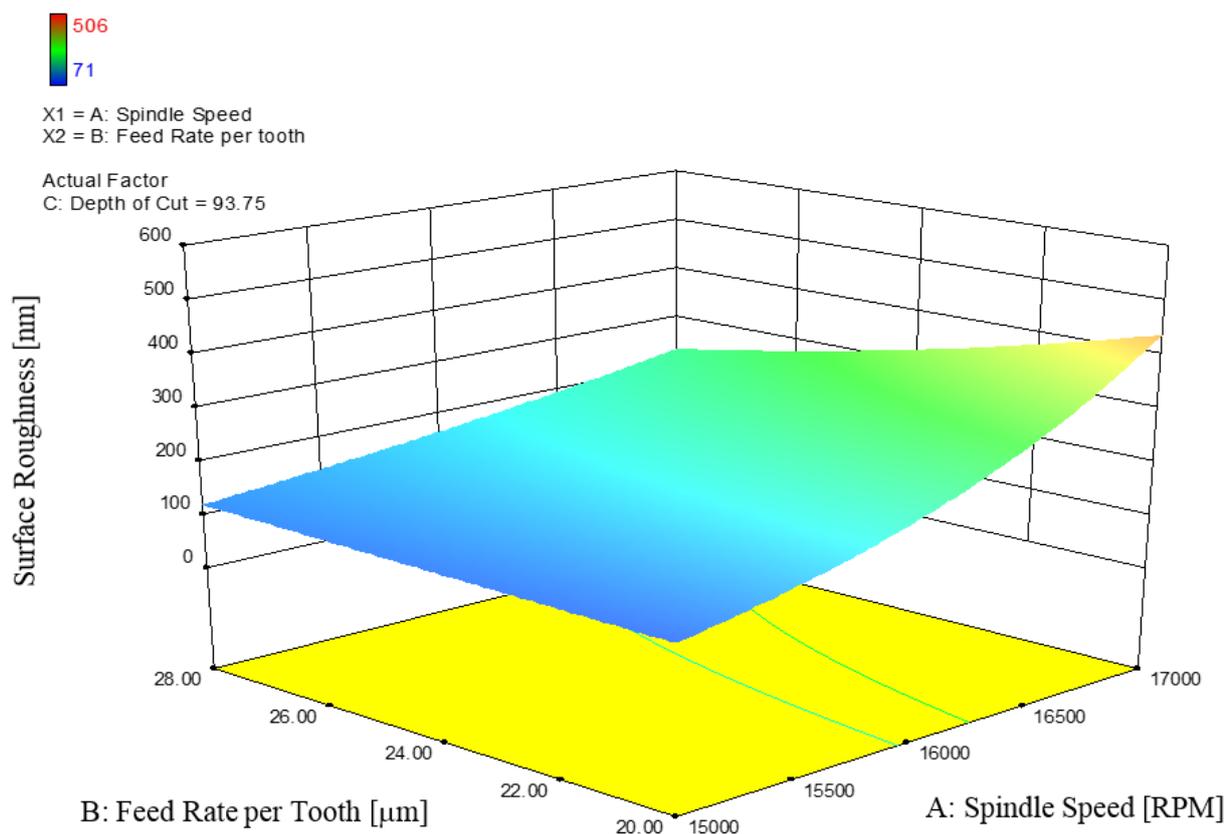
Figure 49: Results of surface roughness model

4.6. Optimisation

From all the results it is now possible to optimise the model to find the specific set of input variables that will yield the best results. The specification for an optimal outcome is that a set of values of the three control factors must be found such that tool life (R2), is maximised whereas all other responses should be as small as possible. For any values of the factors for which the model for the response approaches its desired criterion (for example its maximum that is possible for the model), a desirability function is set up. This desirability should be as close to one as possible. For spindle speed (15000 – 17000 RPM), feed rate per tooth (20 – 28 μm) and depth of cut (93.75 – 156.25 μm) the solution graphs in Figure 50 were generated. This specific solution produced the highest desirability value of 0.780. The surface plot of the optimal solution is shown in Figure 51.

.
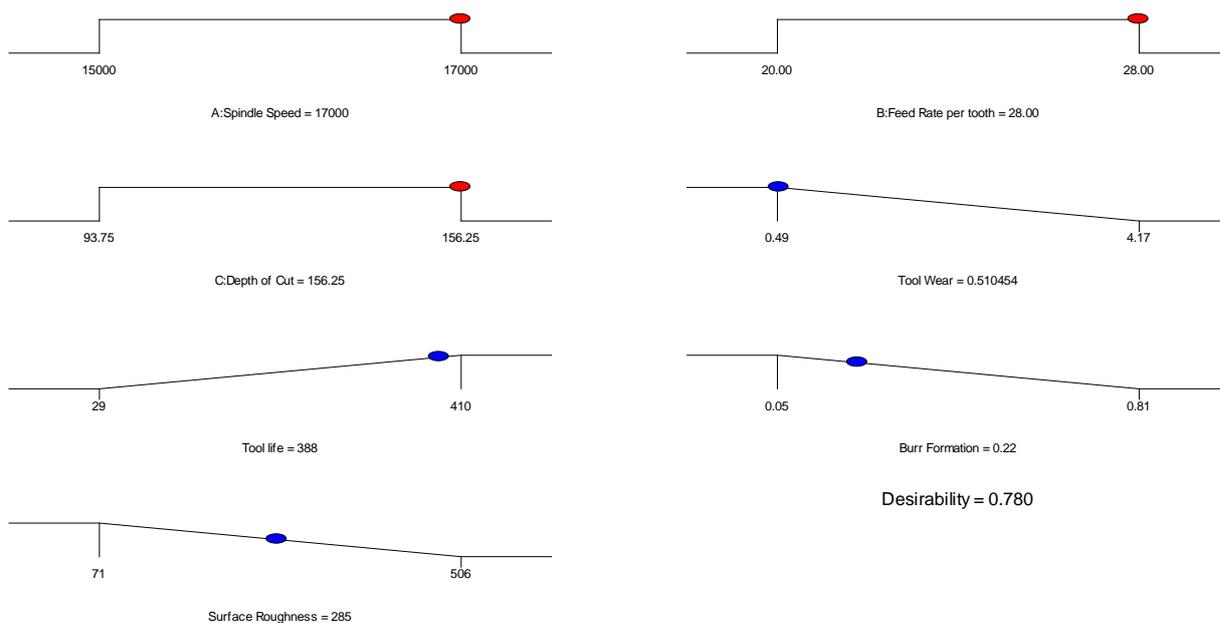
**Figure 50:** Model solution graphs of where the optimal solution lies within limits
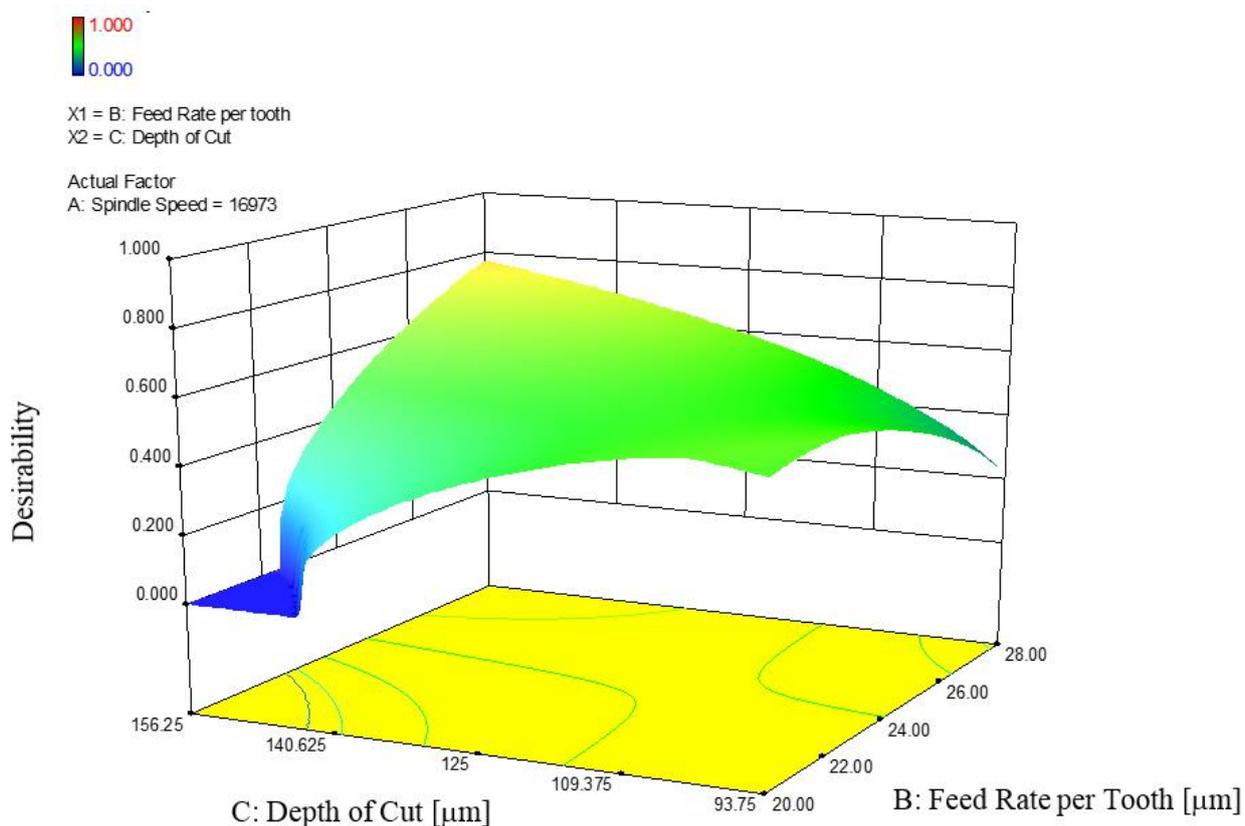
Figure 51: Surface plot of the model's optimal solution

From these graphs, to produce the best tool life of 388 mm, the values of the three factors should be 17000 RPM for spindle speed, 156.25 μm for depth of cut and 28 μm for feed per tooth.

Due to these values all being close to or at their limits that were used in the CCD, it is to be believed that an even better optimal solution should exist. By increasing the limits of the three factors to outside the experimental space the model can predict a solution using the results. For spindle speed (15000 – 20000 RPM), feed rate per tooth (20 – 35 μm) and depth of cut (93.75 – 250 μm) the solution graphs of the new optimal solution are shown in Figure 52. This specific solution produced the highest desirability value of 1.000. The surface plot of the new optimal solution with relaxed limits is shown in Figure 53.
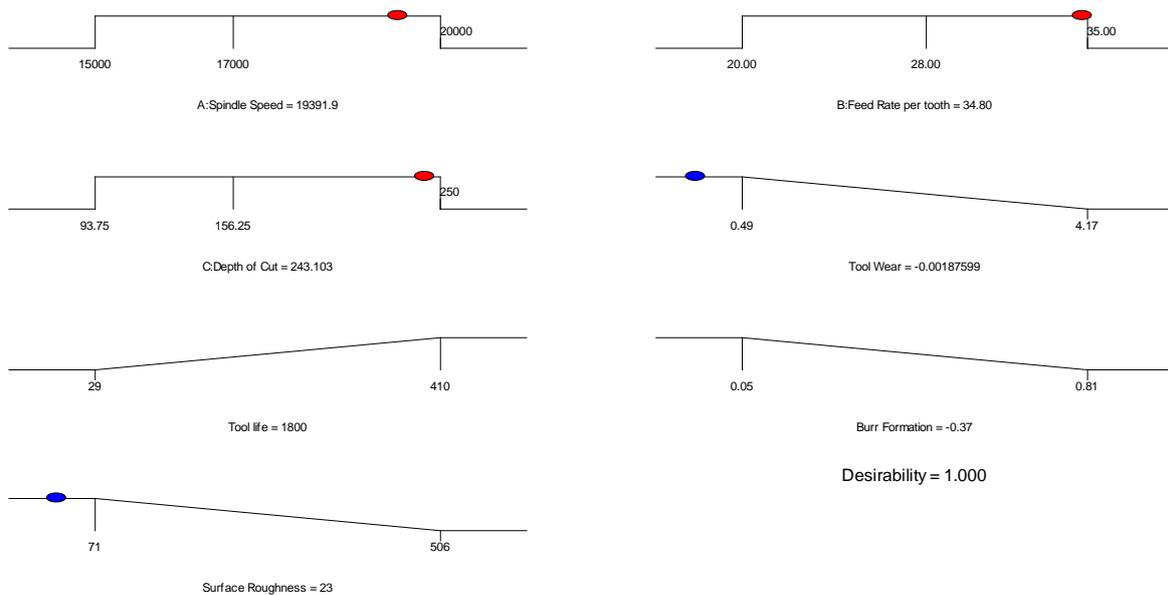
Figure 52: Model solution graphs of where the optimal solution lies outside of the initial limits
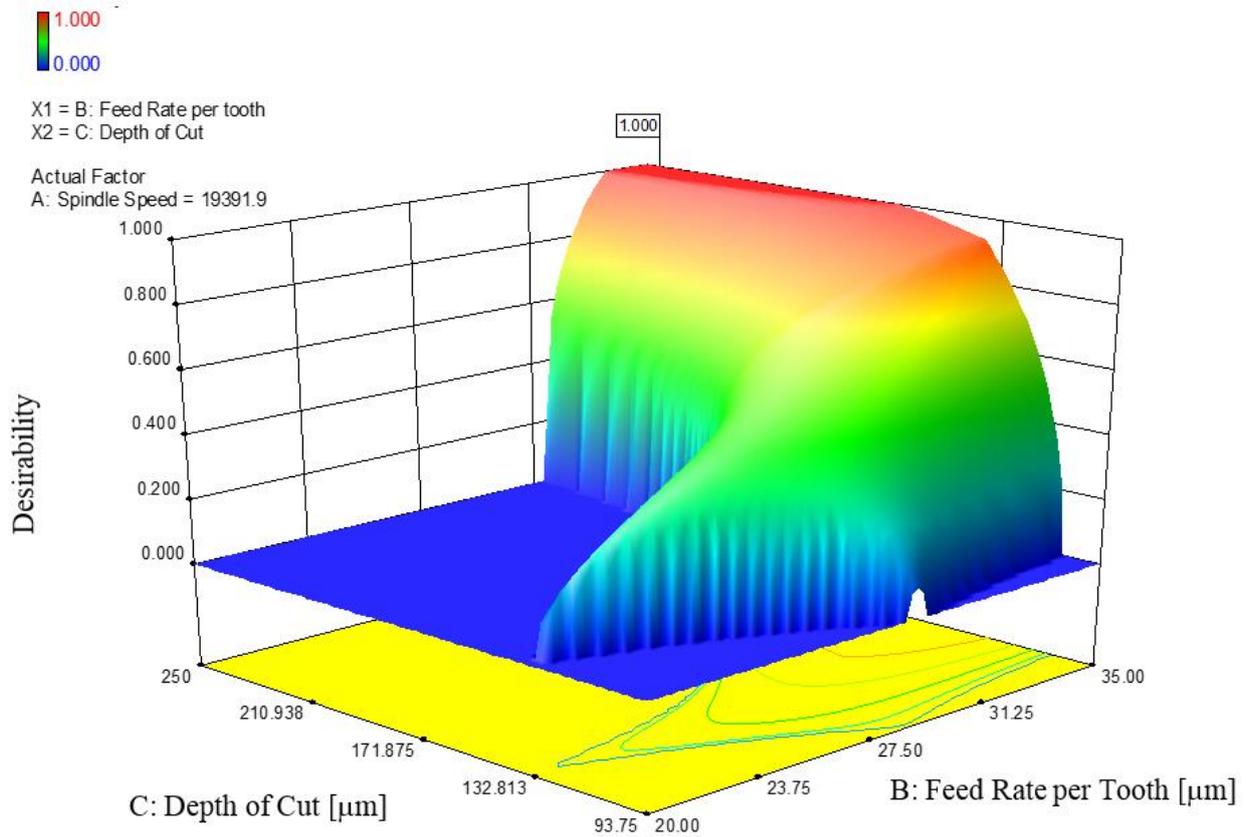
Figure 53: Surface plot of the model's optimal solution with relaxed limits

From these graphs, to produce the best tool life of 1800 mm, the values of the three factors should be 19000 RPM for spindle speed (machine can only set in increments of 1000), 243.10 μm for depth of cut and 34.80 μm for feed per tooth. Since the predicted optimal parameters lie outside of the experimental space it is suggested that future studies should explore this region.

CHAPTER 5
Conclusion

A strong demand exists from various industries to fabricate miniature devices and components with complex microscale features from a wide range of materials including Ti-6Al-4V. Miniature devices within the medical field include implantable devices that are used to replace damaged or diseased tissues, to perform targeted drug delivery, to monitor and correct functional abnormalities as well as performing tissue-tissue connections. These devices are required to be miniature in size and manufactured from biocompatible materials such as Ti-6Al-4V due to their functional needs together with their biological compatibility considerations. The use of straight tungsten carbide cutting tools is superior in almost all machining processes of titanium alloys and it is the preferred material for machining titanium and its alloys. The need exists to improve the micro-machining process of using tungsten carbide end-mills to micro-mill Ti-6Al-4V.

In this research, the performance of tungsten carbide end-mills was investigated when micro-milling Ti-6Al-4V under nitrogen gas cooling. The purpose of the experiments were to find settings for the three control factors that will maximise tool life and simultaneously minimise all the other responses. In order to achieve this, a mathematical model was fitted for each of the responses in terms of the three control factors. Once the models were established, numerical methods were used to find the optimal settings. For the ranges spindle speed (15000 – 17000 RPM), feed rate per tooth (20 – 28 μm) and depth of cut (93.75 – 156.25 μm), the results of the models showed that an optimal solution can be predicted. To produce the best tool life of 388 mm, the values of the three factors should be 17000 RPM for spindle speed, 156.25 μm for depth of cut and 28 μm for feed per tooth. This yielded an overall desirability of 0.780. However, by increasing the limits of the three factors slightly to outside the experimental space the model can predict an even better solution using the results. For the ranges spindle speed (15000 – 20000 RPM), feed rate per tooth (20 – 35 μm) and depth of cut (93.75 – 250 μm) the best tool life of 1800 mm was found at 19000 RPM for spindle speed, 243.10 μm for depth of cut and 34.80 μm for feed per tooth. This yielded a desirability of 1.000. This prediction should be verified experimentally in a future study.

In machining Ti-6Al-4V, tungsten carbide tools can experience high rates of wear and experience catastrophic failure due to machining parameters not set appropriately. From the experimental results the lowest tool wear of 0.49 μm/mm and highest tool life of 410 mm was measured after machining with parameters 16000 RPM spindle speed, 960 mm/min feed rate and 125 μm depth of cut. The results of the second order model that was fitted to the data shows that the lowest tool wear can be achieved using a depth of cut of 156.25 μm and a feed rate per tooth of 28 μm. For tool life the model

shows that the highest tool life can be achieved at using a depth of cut of 156.25 μm and a feed rate per tooth of 28 μm. Spindle speed had no effect on tool wear or tool life.

For resultant cutting force, the experimental results showed that the lowest resultant force of 67.65 Newton was measured after machining with parameters 17000 RPM spindle speed, 937 mm/min feed rate and 106.42 μm depth of cut. The ANOVA analysis confirmed that the estimated resultant force is a constant value of 84.54 N with a 95% CI between 77.56 and 91.47.

For chip formation, experimental run 1-4, 12 and 14 provided the best formed chips according to the various experimental parameters used.

For burr formation, the experimental results showed that the lowest percentage burr formation of 5% was measured after machining with parameters 16000 RPM spindle speed, 960 mm/min feed rate and 125 μm depth of cut. The results of the second order model that was fitted to the data shows that the lowest burr formation can be achieved at using a depth of cut of 156.25 μm, spindle speed of 15000 RPM and a feed rate per tooth of 28 μm.

For surface roughness, the experimental results showed that the lowest surface roughness of 71 nm was measured after machining with parameters 16000 RPM spindle speed, 768 mm/min feed rate and 125 μm depth of cut. The results of the second order model that was fitted to the data shows that the lowest surface roughness can be achieved at using a depth of cut of 93.75 μm and spindle speed of 15000 RPM. Feed rate per tooth had no effect on the model.

The more micro-milling with tungsten carbide on biocompatible metals can be studied, the greater the contribution will be to specifically the medical field. There are numerous other improved, biocompatible titanium alloys that have been developed, however they are even harder to machine. Thus advancing understanding regarding the micro-machining process of cutting hard to cut metals will be a valuable contribution to the scientific world.

Future work should include optimising tungsten carbide micro-tool geometry for cutting specifically hard to cut metals such as Ti-6Al-4V and other newly developed titanium alloys. Together with developing new geometries, studies should also be done on how to improve the production of the tools in terms of cost. Each tool currently costs approximately R143.00 and when you consider how little volume of material you can actually remove with each tool, you can see that the micro-milling process is extremely expensive. Studies have shown that tungsten carbide tools with one tooth performs better than the 2 and 4 tooth variates, however these tools are not readily available yet due to the challenges in production. Significant value can be contributed to the scientific world if time

and effort can be spent into developing such tools with the most efficient geometries for the least amount of production costs.

REFERENCES

Afazov, S., Ratchev, S., Segal, J. & Popov, A., 2012. Chatter modelling in micro-milling by considering process nonlinearities. *International Journal of Machine Tools and Manufacture,* Volume 56, pp. 28-38.

Alting, L., Kimura, F., Hansen, H. N. & Bissacco, G., 2003. Micro engineering. *CIRP Annals-Manufacturing Technology,* 52(2), pp. 635-657.

Aramcharoen, A. et al., 2008. Evaluation and selection of hard coatings for micro milling of hardened tool steel. *International Journal of Machine Tools and Manufacture,* 48(14), pp. 1578-1584.

Armendia, M. et al., 2010. High bandwidth temperature measurement in interrupted cutting of difficult to machine materials. *CIRP Annals-Manufacturing Technology,* 59(1), pp. 97-100.

ATI Industrial Automation, 2013. *Network Force/Torque Sensor System Installation and Operation Manual.* Document: 9620-05-Net FT ed. s.l.:s.n.

Atkins, P. & Shriver, D., 2010. *Shriver and Atkins' Inorganic Chemistry.* s.l.:Oxford University Press.

Attanasio, A. et al., 2013. Influence of Material Microstructures in Micromilling of Ti6Al4V Alloy. *Materials,* 6(9), pp. 4268-4283.

Balazic, M., Kopac, J., Jackson, M. J. & Ahmed, W., 2007. Review: titanium and titanium alloy applications in medicine. *International Journal of Nano and Biomaterials,* 1(1), pp. 3-34.

Bayoumi, A. & Xie, J., 1995. Some metallurgical aspects of chip formation in cutting Ti-6wt.\% Al-4wt.\% V alloy. *Materials Science and Engineering: A,* 190(1), pp. 173-180.

Benavides, G. L., Adams, D. P. & Yang, P., 2001. Meso-machining capabilities. *Sandia National Laboratories, Albuquerque, New Mexico,* Volume 87185.

Bissacco, G., Hansen, H. N. & De Chiffre, L., 2006. Size effects on surface generation in micro milling of hardened tool steel. *CIRP Annals-Manufacturing Technology,* 55(1), pp. 593-596.

Boyer, R., 1996. An overview on the use of titanium in the aerospace industry. *Materials Science and Engineering: A,* 213(1), pp. 103-114.

Byrne, G., Dornfeld, D. & Denkena, B., 2003. Advancing cutting technology. *CIRP Annals-Manufacturing Technology,* 52(2), pp. 483-507.

Byrne, G. & Scholta, E., 1993. Environmentally clean machining processes—a strategic approach. *CIRP Annals-Manufacturing Technology,* 42(1), pp. 471-474.

Cakir, O., Kiyak, M. & Altan, E., 2004. Comparison of gases applications to wet and dry cuttings in turning. *Journal of Materials Processing Technology,* Volume 153, pp. 35-41.

Camara, M., Rubio, J. C., Abrao, A. & Davim, J., 2012. State of the art on micromilling of materials, a review. *Journal of Materials Science \& Technology,* 28(8), pp. 673-685.

Cardarelli, F., 2008. *Materials handbook: A concise desktop reference.* s.l.:Springer Science & Business Media.

Cardoso, P. & Davim, J. P., 2012. A brief review on micromachining of materials. *Reviews on advanced materials science,* Volume 30, pp. 98-102.

Chae, J., Park, S. & Freiheit, T., 2006. Investigation of micro-cutting operations. *International Journal of Machine Tools and Manufacture,* 46(3), pp. 313-332.

Che-Haron, C., 2001. Tool life and surface integrity in turning titanium alloy. *Journal of Materials Processing Technology,* 118(1), pp. 231-237.

Coetzee, R., 2012. *Micromanufacturing: The factories of the future,* s.l.: s.n.

Damazo, B., Davies, M., Dutterer, B. & Kennedy, M., 1999. *A summary of micro-milling studies.* s.l., s.n., pp. 322-325.

Davis, J. R., 2003. *Handbook of materials for medical devices.* s.l.:ASM international.

Dhanorker, A. & Ozel, T., 2008. Meso/micro scale milling for micro-manufacturing. *International Journal of Mechatronics and Manufacturing Systems,* 1(1), pp. 23-42.

Ding, H., Shen, N. & Shin, Y. C., 2012. Thermal and mechanical modeling analysis of laser-assisted micro-milling of difficult-to-machine alloys. *Journal of Materials Processing Technology,* 212(3), pp. 601-613.

Diniz, A. E. & Micaroni, R., 2002. Cutting conditions for finish turning process aiming: the use of dry cutting. *International Journal of Machine Tools and Manufacture,* 42(8), pp. 899-904.

Disegi, J., 2000. Titanium alloys for fracture fixation implants. *Injury,* Volume 31, pp. D14--D17.

Dornfeld, D., Min, S. & Takeuchi, Y., 2006. Recent advances in mechanical micromachining. *CIRP Annals-Manufacturing Technology,* 55(2), pp. 745-768.

Dow, T. A., Miller, E. L. & Garrard, K., 2004. Tool force and deflection compensation for small milling tools. *Precision Engineering,* 28(1), pp. 31-45.

Ducobu, F., Riviere-Lorphevre, E. & Filippi, E., 2012. *Dynamic simulation of the micro-milling process including minimum chip thickness and size effect.* s.l., s.n., pp. 1269-1274.

Ducobu, F., Riviere-Lorphevre, E. & Filippi, E., 2013. Chip formation in Micro-cutting. *J Mech Eng Autom,* Volume 3, pp. 441-448.

Ehmann, K. F. et al., 2005. *International assessment of research and development in micromanufacturing,* s.l.: s.n.

El Baradie, M., 1996. Cutting fluids: Part I. characterisation. *Journal of materials processing technology,* 56(1), pp. 786-797.

Elias, C., Lima, J., Valiev, R. & Meyers, M., 2008. Biomedical Applications of Titanium and its Alloys. *JOM,* Volume 1, pp. 46-49.

REFERENCES   **97**

Essman, E., 2012. *A cost model for the manufacture of bipolar plates using micro milling,* Stellenbosch: Stellenbosch University.

Ezugwu, E., 2004. High speed machining of aero-engine alloys. *Journal of the Brazilian society of mechanical sciences and engineering,* 26(1), pp. 1-11.

Ezugwu, E., Bonney, J. & Yamane, Y., 2003. An overview of the machinability of aeroengine alloys. *Journal of materials processing technology,* 134(2), pp. 233-253.

Ezugwu, E. & Wang, Z., 1997. Titanium alloys and their machinability—a review. *Journal of Materials Processing Technology,* 68(3), pp. 262-274.

Ferrero, J., 2005. Candidate materials for high-strength fastener applications in both the aerospace and automotive industries. *Journal of materials engineering and performance,* 14(6), pp. 691-696.

Filiz, S., Conley, C. M., Wasserman, M. B. & Ozdoganlar, O. B., 2007. An experimental investigation of micro-machinability of copper 101 using tungsten carbide micro-endmills. *International Journal of Machine Tools and Manufacture,* 47(7), pp. 1088-1100.

Filiz, S., Xie, L., Weiss, L. E. & Ozdoganlar, O., 2008. Micromilling of microbarbs for medical implants. *International Journal of Machine Tools and Manufacture,* 48(3), pp. 459-472.

Gafford, J., Panas, R., Cullinan, M. & Culpepper, M., 2010. *Design principles and practices for rapid prototyping of meso-and micro-scale flexures via micromilling,* s.l.: s.n.

Geetha, M., Singh, A., Asokamani, R. & Gogia, A., 2009. Ti based biomaterials, the ultimate choice for orthopaedic implants--A review. *Progress in Materials Science,* 54(3), pp. 397-425.

Geetha, M., Singh, A., Asokamani, R. & Gogia, A., 2009. Ti based biomaterials, the ultimate choice for orthopaedic implants--A review. *Progress in Materials Science,* 54(3), pp. 397-425.

Ghani, J. A. et al., 2012. Failure mode analysis of carbide cutting tools used for machining titanium alloy. *Ceramics International,* Volume 39, pp. 4449-4456.

Gietzelt, T. & Eichhorn, L., 2012. *Mechanical micromachining by drilling, milling and slotting.* s.l.:INTECH Open Access Publisher.

Gove, P. B. & others, 1963. *Webster's seventh new collegiate dictionary.* s.l.:Allen.

Groover, M. P., 2007. *Automation, production systems, and computer-integrated manufacturing.* s.l.:Prentice Hall Press.

Groover, M. P., 2013. *Fundamentals of modern manufacturing: materials processes, and systems.* s.l.:John Wiley & Sons.

Guillemot, F., 2005. Recent advances in the design of titanium alloys for orthopedic applications. *Expert Review of Medical Devices,* 2(6), pp. 741-748.

Heamawatanachai, S. & Bamberg, E., 2010. Cutting force model of orbital single-point micromachining tool. *International Journal of Machine Tools and Manufacture,* 50(9), pp. 815-823.

He, G. & Hagiwara, M., 2006. Ti alloy design strategy for biomedical applications. *Materials Science and Engineering: C,* 26(1), pp. 14-19.

Hong, S. Y., Ding, Y. & Jeong, W.-c., 2001. Friction and cutting forces in cryogenic machining of Ti--6Al--4V. *International Journal of Machine Tools and Manufacture,* 41(15), pp. 2271-2285.

Jun, M., 2005. *Modeling and analysis of micro-end milling dynamics,* s.l.: s.n.

Kahles, J., Field, M., Eylon, D. & Froes, F., 1985. Machining of titanium alloys. *JOM,* 37(4), pp. 27-35.

Kalpakjian, S. & Schmid, S., 2006. *Manufacturing engineering and technology.* s.l.:Pearson Education India.

Katti, K. S., 2004. Biomaterials in total joint replacement. *Colloids and Surfaces B: Biointerfaces,* 39(3), pp. 133-142.

Ke, Y.-L., Dong, H.-Y., Gang, L. & Zhang, M., 2009. Use of nitrogen gas in high-speed milling of Ti-6Al-4V. *Transactions of Nonferrous Metals Society of China,* 19(3), pp. 530-534.

Kim, B., Schmittdiel, M. C., Degertekin, F. L. & Kurfess, T. R., 2004. Scanning grating microinterferometer for MEMS metrology. *Journal of manufacturing science and engineering,* 126(4), pp. 807-812.

Kim, D. H., Lee, P.-H. & Lee, S. W., 2014. *Experimental Study on Machinability of Ti-6Al-4V in Micro End-Milling.* s.l., s.n.

Klocke, F. & Eisenblatter, G., 1997. Dry cutting. *CIRP Annals-Manufacturing Technology,* 46(2), pp. 519-526.

Komanduri, R. & Brown, R., 1981. On the mechanics of chip segmentation in machining. *Journal of Engineering for Industry,* Volume 103, pp. 33-21.

Komanduri, R. & Reed, W., 1983. Evaluation of carbide grades and a new cutting geometry for machining titanium alloys. *Wear,* 92(1), pp. 113-123.

Komanduri, R., Schroeder, T., HAZRA, J. & BANDHOPADHYAY, D., 1982. Titanium- A model material for analysis of the high speed machining process. *Advanced processing methods for titanium,* pp. 241-256.

Kumabe, J., Fuchizawa, K., Soutome, T. & Nishimoto, Y., 1989. Ultrasonic superposition vibration cutting of ceramics. *Precision Engineering,* 11(2), pp. 71-77.

Kumar, M. & Melkote, S. N., 2012. Process capability study of laser assisted micro milling of a hard-to-machine material. *Journal of Manufacturing Processes,* 14(1), pp. 41-51.

Kurlov, A. S. & Gusev, A. I., 2013. *Tungsten carbides: structure, properties and application in hardmetals.* s.l.:Springer Science & Business Media.

Lavan, D. A., McGuire, T. & Langer, R., 2003. Small-scale systems for in vivo drug delivery. *Nature biotechnology,* 21(10), pp. 1184-1191.

Lee, K., Stirn, B. & Essel, I., 2000. *Burr formation in micro-machining,* s.l.: s.n.

Lemaire, J. C. & Backofen, W., 1972. Adiabatic instability in the orthogonal cutting of steel. *Metallurgical Transactions,* 3(2), pp. 481-485.

Leyens, C. & Peters, M., 2003. *Titanium and titanium alloys.* s.l.:Wiley Online Library.

Li, H. et al., 2008. Modelling and experimental analysis of the effects of tool wear, minimum chip thickness and micro tool geometry on the surface roughness in micro-end-milling. *Journal of Micromechanics and Microengineering,* 18(2), p. 025006.

Liu, C. R. & Mittal, S., 1996. Single-step superfinish hard machining: feasibility and feasible cutting conditions. *Robotics and computer-integrated manufacturing,* 12(1), pp. 15-27.

Liu, J. & Chou, Y. K., 2007. On temperatures and tool wear in machining hypereutectic Al--Si alloys with vortex-tube cooling. *International Journal of Machine Tools and Manufacture,* 47(3), pp. 635-645.

Liu, J., Han, R., Zhang, L. & Guo, H., 2007. Study on lubricating characteristic and tool wear with water vapor as coolant and lubricant in green cutting. *Wear,* 262(3), pp. 442-452.

Liu, X., Jun, M. B., DeVor, R. E. & Kapoor, S. G., 2004. *Cutting mechanisms and their influence on dynamic forces, vibrations and stability in micro-endmilling.* s.l., s.n., pp. 583-592.

Li, X., Lin, R. & Leow, K. W., 2000. Performance-enhanced micro-machined resonant systems with two-degrees-of-freedom resonators. *Journal of Micromechanics and Microengineering,* 10(4), p. 534.

Long, M., Rack, H. & others, 1998. Titanium alloys in total joint replacement-a materials science perspective. *Biomaterials,* 19(18), pp. 1621-1639.

Machado, A. & Wallbank, J., 1990. Machining of titanium and its alloys—a review. *Proceedings of the Institution of Mechanical Engineers, Part B: Journal of Engineering Manufacture,* 204(1), pp. 53-60.

Masuzawa, T., 2000. State of the art of micromachining. *CIRP Annals-Manufacturing Technology,* 49(2), pp. 473-488.

Masuzawa, T. & Tönshoff, H., 1997. Three-dimensional micromachining by machine tools. *CIRP Annals-Manufacturing Technology,* 46(2), pp. 621-628.

Mayor, J. & Sodemann, A., 2009. Investigation of the parameter space for enhanced tool life in high aspect-ratio full-slot micromilling of copper. *Atlanta: Georgia Institute of Technology.*

McKeown, P., 1987. The role of precision engineering in manufacturing of the future. *CIRP Annals-Manufacturing Technology,* 36(2), pp. 495-501.

Mian, A., Driver, N. & Mativenga, P., 2011. Identification of factors that dominate size effect in micro-machining. *International Journal of Machine Tools and Manufacture,* 51(5), pp. 383-394.

Micro Manufacturing Portal Project, 2015. *Micro manufacturing.* s.l.:s.n.

Monroy-Vazquez, K. P. et al., 2013. Evaluation of superficial and dimensional quality features in metallic micro-channels manufactured by micro-end-milling. *Materials,* 6(4), pp. 1434-1451.

Montgomery, D. C. & Runger, G. C., 2010. *Applied statistics and probability for engineers.* 4th ed. USA: John Wiley & Sons.

Moriwaki, T. & Shamoto, E., 1991. Ultraprecision diamond turning of stainless steel by applying ultrasonic vibration. *CIRP Annals-Manufacturing Technology,* 40(1), pp. 559-562.

Moriwaki, T. & Shamoto, E., 1995. Ultrasonic elliptical vibration cutting. *CIRP Annals-Manufacturing Technology,* 44(1), pp. 31-34.

Motonishi, S. et al., 1987. Study on machining of titanium and its alloys. *Kobelco technology review,* Issue 2, pp. 28-31.

Myers, R. H., Montgomery, D. C. & Anderson-Cook, C. M., 2009. *Response surface methodology: process and product optimization using designed experiments.* s.l.:John Wiley & Sons.

Niinomi, M., 1998. Mechanical properties of biomedical titanium alloys. *Materials Science and Engineering: A,* 243(1), pp. 231-236.

Niinomi, M., 2002. Recent metallic materials for biomedical applications. *Metallurgical and materials transactions A,* 33(3), pp. 477-486.

Niinomi, M., 2003. Recent research and development in titanium alloys for biomedical applications and healthcare goods. *Science and Technology of Advanced Materials,* 4(5), pp. 445-454.

Oliveira, V., Chaves, R., Bertazzoli, R. & Caram, R., 1998. Preparation and characterization of Ti-Al-Nb alloys for orthopedic implants. *Brazilian Journal of Chemical Engineering,* 15(4), pp. 326-333.

Onikura, H., Ohnishi, O., Take, Y. & Kobayashi, A., 2000. Fabrication of micro carbide tools by ultrasonic vibration grinding. *CIRP Annals-Manufacturing Technology,* 49(1), pp. 257-260.

Ouellette, J., 2001. Biomaterials facilitate medical breakthroughs. *Industrial Physicist,* 7(5), pp. 18-21.

Pahlitzsch, G., 1953. " Gases Are Good Cutting Coolants. *American Machinist,* Volume 97, pp. 196-197.

Perez, H., Vizan, A., Hernandez, J. & Guzman, M., 2007. Estimation of cutting forces in micromilling through the determination of specific cutting pressures. *Journal of Materials Processing Technology,* 190(1), pp. 18-22.

Perez, J., Llorente, J., Sanchez, J. & others, 2000. Advanced cutting conditions for the milling of aeronautical alloys. *Journal of Materials Processing Technology,* 100(1), pp. 1-11.

Piljek, P., Keran, Z. & Math, M., 2014. Micromachining--Review of Literature from 1980 to 2010. *Interdisciplinary Description of Complex Systems,* 12(1), pp. 1-27.

Pohanish, R. P., 2008. *Sittig's handbook of toxic and hazardous chemicals and carcinogens.* s.l.:William Andrew.

Prakash, J., Senthil Kumar, A., Rahman, M. & Lim, S., 2001. A model for predicting tool life for coated micro end mill. *Proc. Fourth International Machining and Grinding Troy,* pp. 149-158.

Rack, H. & Qazi, J., 2006. Titanium alloys for biomedical applications. *Materials Science and Engineering: C,* 26(8), pp. 1269-1277.

Rahman, M., Kumar, A. S. & Prakash, J., 2001. Micro milling of pure copper. *Journal of Materials Processing Technology,* 116(1), pp. 39-43.

Rahman, M., Wang, Z.-G. & Wong, Y.-S., 2006. A review on high-speed machining of titanium alloys. *JSME International Journal Series C,* 49(1), pp. 11-20.

Rahman, M., Wong, Y. S. & Zareena, A. R., 2002. Machinability of Titanium Alloys.. *JSME International Journal Series C,* 46(1), pp. 107-114.

Ratner, B. D. & Bryant, S. J., 2004. Biomaterials: where we have been and where we are going. *Annu. Rev. Biomed. Eng.,* Volume 6, pp. 41-75.

Recht, R., 1964. Catastrophic thermoplastic shear. *J. appl. Mech,* 31(2), pp. 186-193.

Saffar, R. J., Razfar, M., Zarei, O. & Ghassemieh, E., 2008. Simulation of three-dimension cutting force and tool deflection in the end milling operation based on finite element method. *Simulation Modelling Practice and Theory,* 16(10), pp. 1677-1688.

Schaller, T., Bohn, L., Mayer, J. & Schubert, K., 1999. Microstructure grooves with a width of less than 50 mm cut with ground hard metal micro end mills. *Precision Engineering,* 23(4), pp. 229-235.

Settineri, L. & Faga, M. G., 2008. Nanostructured cutting tools coatings for machining titanium. *Machining Science and Technology,* 12(2), pp. 158-169.

SGS Tool Company, 2015. *2 Flute Micro-End Mills.* [Online] Available at: http://www.sgstool.com/product.aspx?groupcode=MINEM [Accessed 2 November 2015].

Shabouk, S. & Nakamoto, T., 2002. Micro machining of single crystal diamond by utilization of tool wear during cutting process of ferrous material. *Journal of Micromechatronics,* 2(1), pp. 13-26.

Shaw, M. C., 2005. *Metal cutting principles.* New York: Oxford university press .

Siekmann, H. J., 1955. How to machine titanium. *The Tool Engineer,* 34(1), pp. 78-82.

Smart, E. & Trent, E., 1975. Temperature distribution in tools used for cutting iron, titanium and nickel. *The International Journal of Production Research,* 13(3), pp. 265-290.

Sokovic, M. & Mijanovic, K., 2001. Ecological aspects of the cutting fluids and its influence on quantifiable parameters of the cutting processes. *Journal of Materials Processing Technology,* 109(1), pp. 181-189.

Sreejith, P. & Ngoi, B., 2000. Dry machining: machining of the future. *Journal of materials processing technology,* 101(1), pp. 287-291.

Sreeram, S., Kumar, A. S., Rahman, M. & Zaman, M., 2006. Optimization of cutting parameters in micro end milling operations in dry cutting condition using genetic algorithms. *The International Journal of Advanced Manufacturing Technology,* 30(11-12), pp. 1030-1039.

Stanford, M., Lister, P., Morgan, C. & Kibble, K., 2009. Investigation into the use of gaseous and liquid nitrogen as a cutting fluid when turning BS 970-80A15 (En32b) plain carbon steel using WC--Co uncoated tooling. *Journal of Materials Processing Technology,* 209(2), pp. 961-972.

Sugawara, A., 1980. *Study on Micro Diameter Drill Working: Effects of Working Conditions on Burr and Cutting Force,* s.l.: Tohoku University.

Sun, S., Brandt, M. & Dargusch, M., 2010. Machining Ti--6Al--4V alloy with cryogenic compressed air cooling. *International Journal of Machine Tools and Manufacture,* 50(11), pp. 933-942.

Sun, X. & Cheng, K., 2010. Micro/Nano-Machining through Mechanical Cutting. *Micromanufacturing Engineering and Technology,* pp. 24-38.

Su, Y. et al., 2007. Refrigerated cooling air cutting of difficult-to-cut materials. *International Journal of Machine Tools and Manufacture,* 47(6), pp. 927-933.

Tansel, I. et al., 2000. Tool wear estimation in micro-machining.: Part I: tool usage--cutting force relationship. *International Journal of Machine Tools and Manufacture,* 40(4), pp. 599-608.

Tansel, I. et al., 2000. Tool wear estimation in micro-machining.: Part II: neural-network-based periodic inspector for non-metals. *International Journal of Machine Tools and Manufacture,* 40(4), pp. 609-620.

Tansel, I., Nedbouyan, A., Trujillo, M. & Tansel, B., 1998. Micro-end-milling—II. Extending tool life with a Smart Workpiece Holder (SWH). *International Journal of Machine Tools and Manufacture,* 38(12), pp. 1437-1448.

Trucks, H., 1987. Machining titanium alloys. *Mach. Tool Blue Book,* 82(1), pp. 39-41.

Ulutan, D. & Ozel, T., 2011. Machining induced surface integrity in titanium and nickel alloys: A review. *International Journal of Machine Tools and Manufacture,* 51(3), pp. 250-280.

Upadhyaya, G., 2001. Materials science of cemented carbides—an overview. *Materials \& Design,* 22(6), pp. 483-489.

Vieira, J., Machado, A. & Ezugwu, E., 2001. Performance of cutting fluids during face milling of steels. *Journal of Materials Processing Technology,* 116(2), pp. 244-251.

REFERENCES **103**

Vogler, M. P., DeVor, R. E. & Kapoor, S. G., 2003. Microstructure-level force prediction model for micro-milling of multi-phase materials. *Journal of Manufacturing Science and Engineering,* 125(2), pp. 202-209.

Vogler, M. P., DeVor, R. E. & Kapoor, S. G., 2004. On the modeling and analysis of machining performance in micro-endmilling, Part I: Surface generation. *Journal of Manufacturing Science and Engineering,* 126(4), pp. 685-694.

Von Turkovich, B., 1970. Shear stress in metal cutting. *Journal of Engineering for Industry,* Volume 92, p. 151.

Wang, K., 1996. The use of titanium for medical applications in the USA. *Materials Science and Engineering: A,* 213(1), pp. 134-137.

Wang, X., Li, Y., Hodgson, P. & Wen, C., 2007. *Nano-and macro-scale characterisation of the mechanical properties of bovine bone.* s.l., s.n., pp. 156-159.

Weinert, K. & Petzoldt, V., 2004. Machining of NiTi based shape memory alloys. *Materials Science and Engineering: A,* 378(1), pp. 180-184.

Weiss, I. & Semiatin, S., 1998. Thermomechanical processing of beta titanium alloys—an overview. *Materials Science and Engineering: A,* 243(1), pp. 46-65.

Weule, H., Huntrup, V. & Tritschler, H., 2001. Micro-cutting of steel to meet new requirements in miniaturization. *CIRP Annals-Manufacturing Technology,* 50(1), pp. 61-64.

Woon, K. & Rahman, M., 2010. Extrusion-like chip formation mechanism and its role in suppressing void nucleation. *CIRP Annals-Manufacturing Technology,* 59(1), pp. 129-132.

Wright, P. & Trent, E., 1973. Metallographic methods of determining temperature gradients in cutting tools. *J. Iron Steel Inst.,* 211(5), pp. 364-368.

Xiao, M., Sato, K., Karube, S. & Soutome, T., 2003. The effect of tool nose radius in ultrasonic vibration cutting of hard metal. *International Journal of Machine Tools and Manufacture,* 43(13), pp. 1375-1382.

Yang, X. & Richard Liu, C., 1999. Machining titanium and its alloys. *Machining Science and Technology,* 3(1), pp. 107-139.

Zaman, M., Rahman, M., Kumar, A. & Sreeram, S., 2004. *Effect of engagement arc of tool life in micro end milling operations.* s.l., s.n.

Zlatin, N. & Field, M., 1973. Procedures and precautions in machining titanium alloys. *Titanium science and technology,* pp. 489-504.

APPENDIX A

This appendix shows the SEM images of the tungsten carbide cutting tools that were taken after each experiment. The experimental parameters used are indicated in the caption of each images. From the images it can clearly be seen that tool cutting edge experienced a reduction in sharpness and that adhesion tool place between the Ti-6Al-4V workpiece material and the tungsten carbide tool. This adhesion occurred on all of the tools in varying degrees. Note that tools 3, 5, 6, 7, 10, 12, 13, 14, 17 and 20 might not show this due to the tool tip breaking off during the experimental run after it experienced 200 μm reduction in diameter.
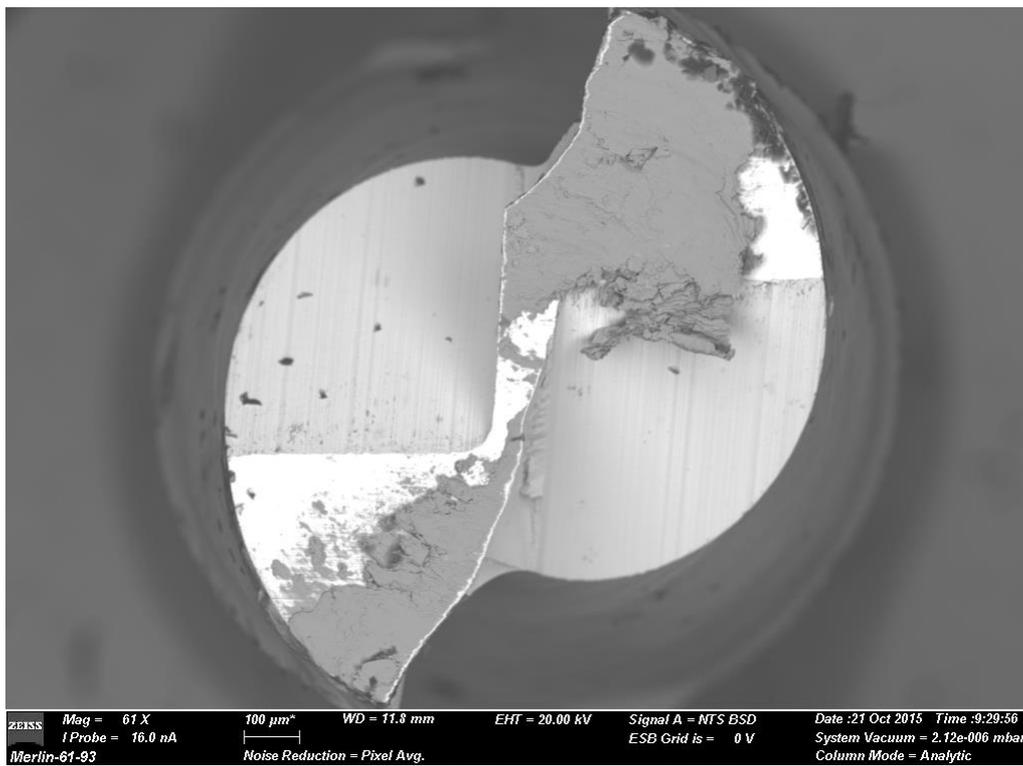
Figure 54: Experimental run 1: Tungsten carbide tool after machining with parameters v_c =65.97 [m/min], v_f =672 [mm/min] and a_p =125 [μm]
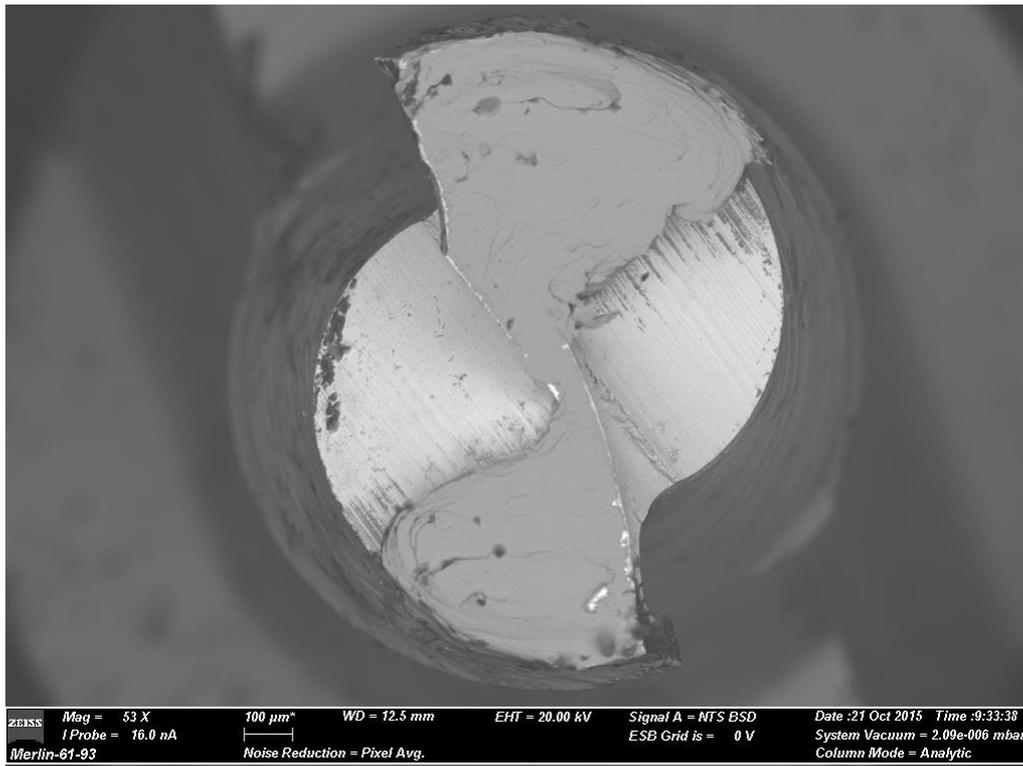
Figure 55: Experimental run 2: Tungsten carbide tool after machining with parameters v_c =75.4 [m/min], v_f =768 [mm/min] and a_p =93.75 [μm]
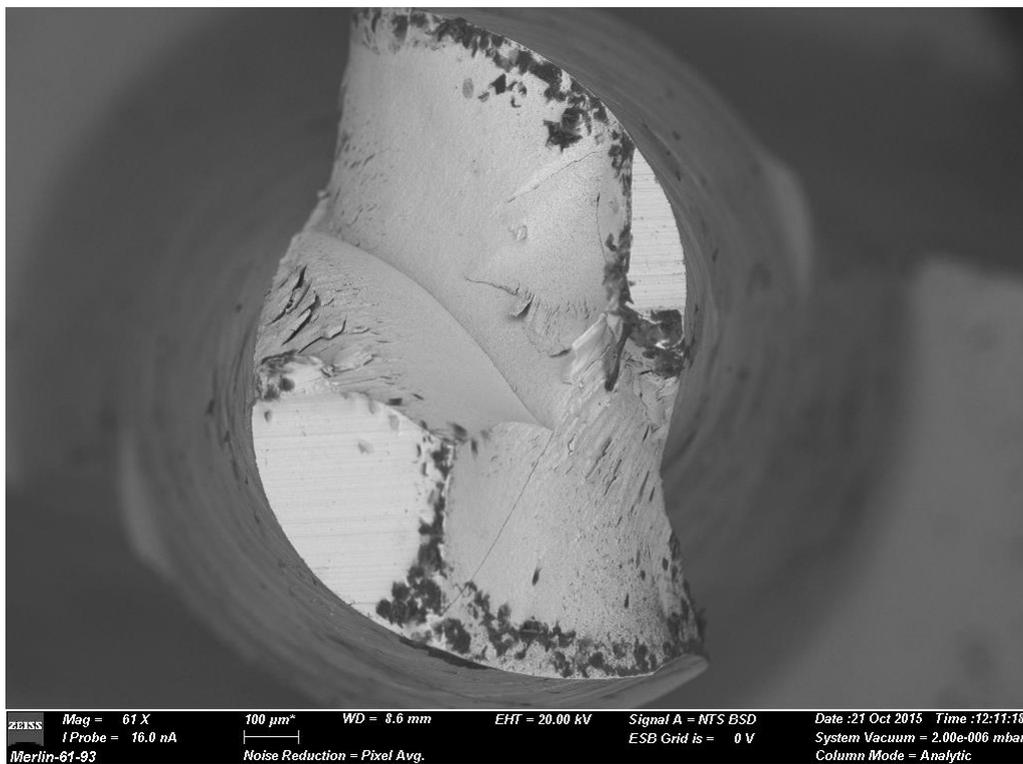

Figure 56: Experimental run 3: Tungsten carbide tool after machining with parameters v_c =75.4 [m/min], v_f =768 [mm/min] and a_p =125 [μm]
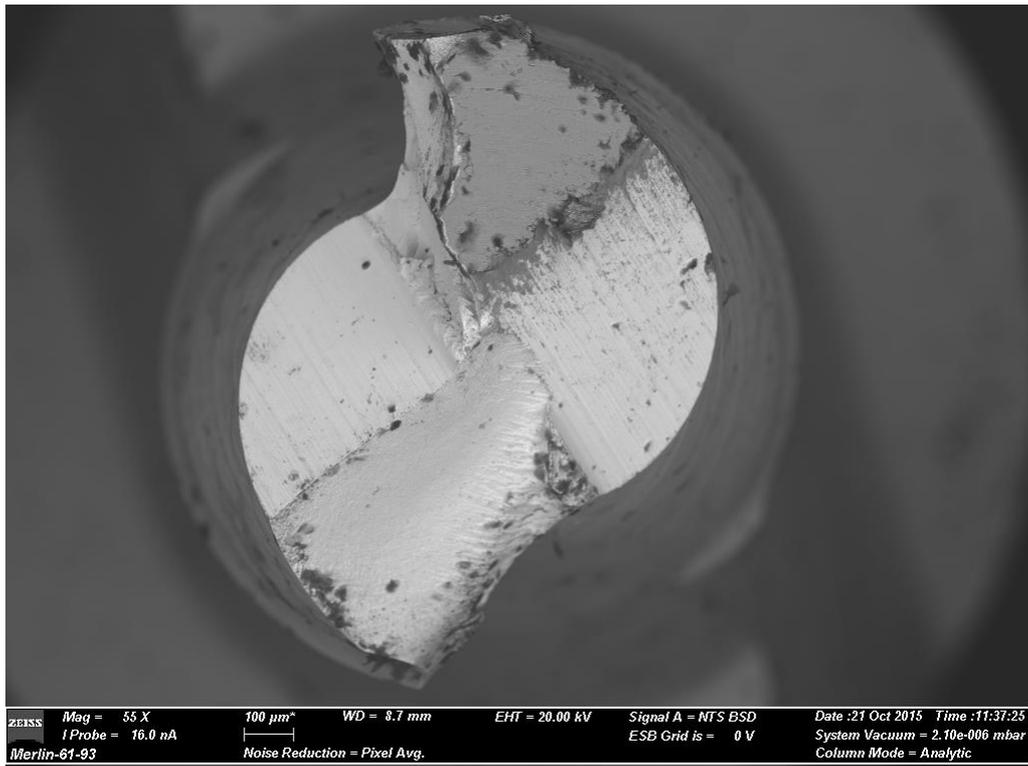
Figure 57: Experimental run 4: Tungsten carbide tool after machining with parameters v_c =80.11 [m/min], v_f =937.3 [mm/min] and a_p =143.58 [μm]
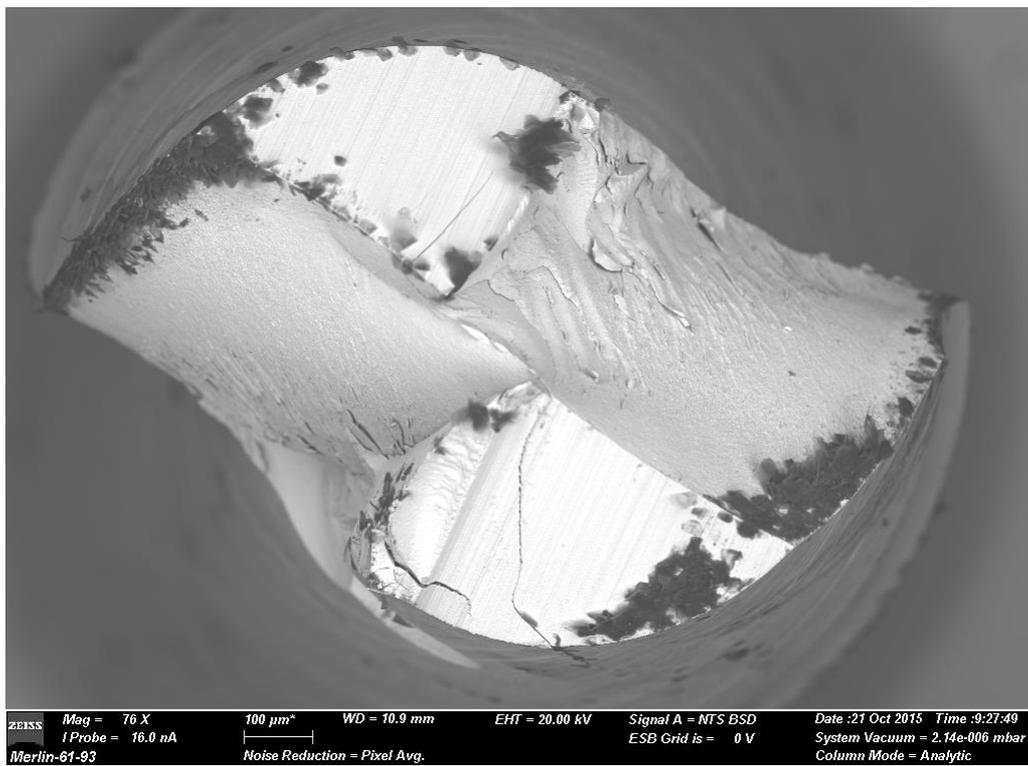
Figure 58: Experimental run 5: Tungsten carbide tool after machining with parameters v_c =80.11 [m/min], v_f =694.7 [mm/min] and a_p =143.58 [μm]
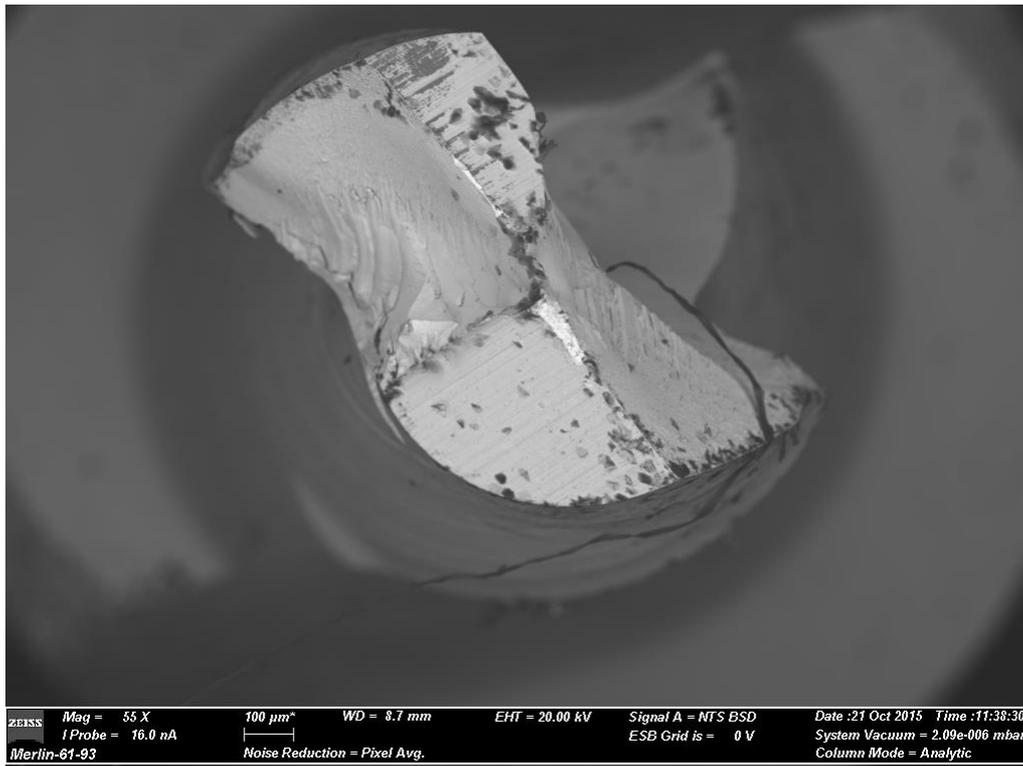
Figure 59: Experimental run 6: Tungsten carbide tool after machining with parameters v_c =80.11 [m/min], v_f =694.7 [mm/min] and a_p =106.42 [μm]
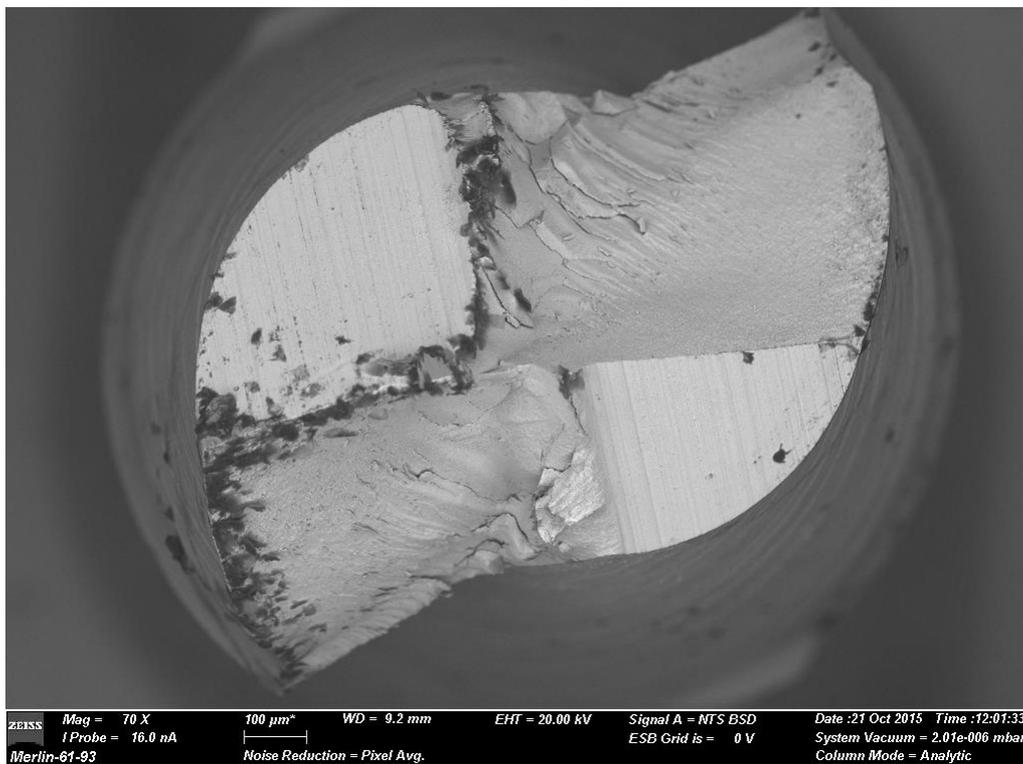
Figure 60: Experimental run 7: Tungsten carbide tool after machining with parameters v_c =75.4 [m/min], v_f =576 [mm/min] and a_p =125 [μm]
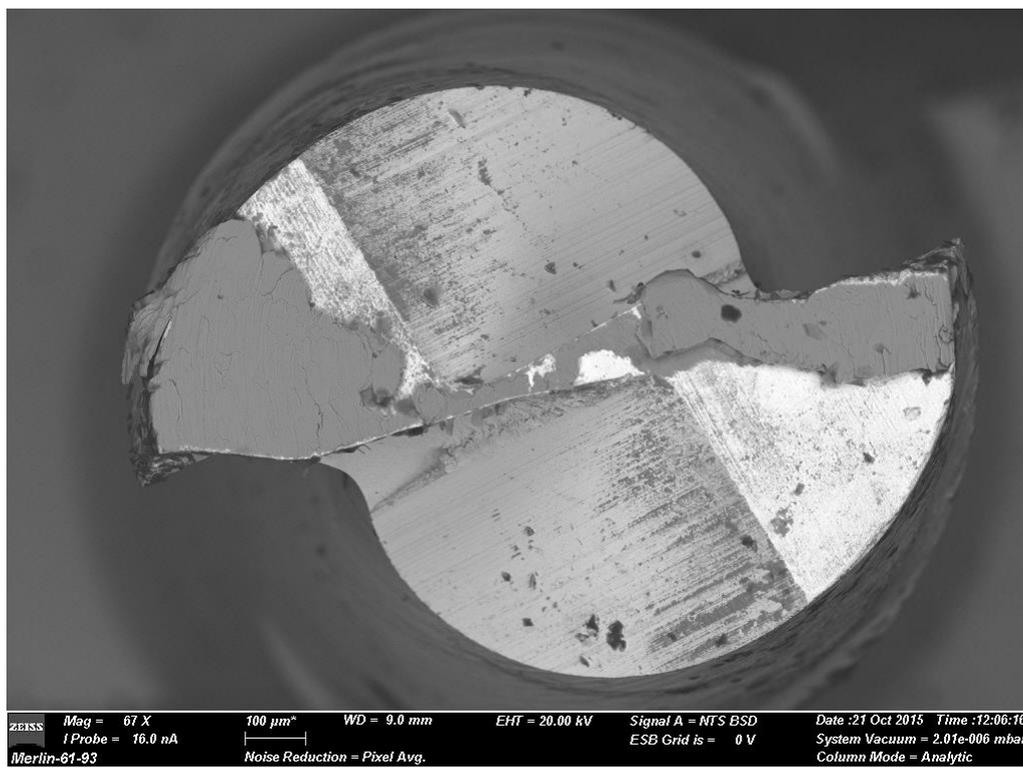
Figure 61: Experimental run 8: Tungsten carbide tool after machining with parameters v_c =70.69 [m/min], v_f =612.97 [mm/min] and a_p =106.42 [μm]
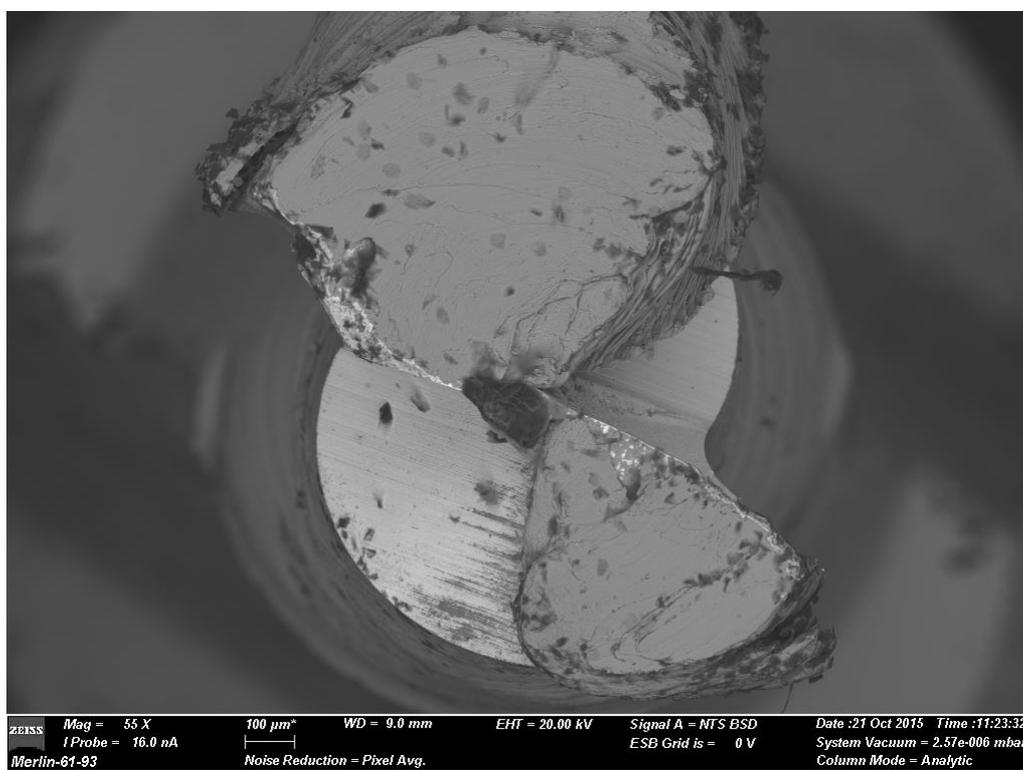
Figure 62: Experimental run 9: Tungsten carbide tool after machining with parameters v_c =75.4 [m/min], v_f =960 [mm/min] and a_p =125 [μm]
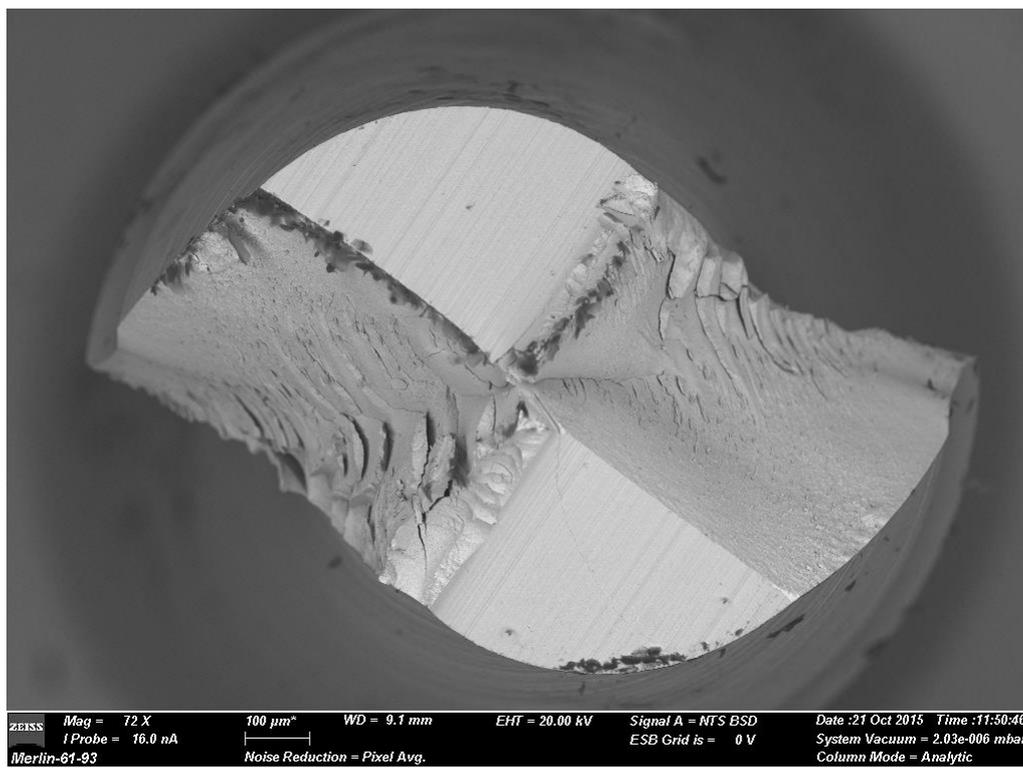
Figure 63: Experimental run 10: Tungsten carbide tool after machining with parameters v_c =70.69 [m/min], v_f =827.03 [mm/min] and a_p =106.42 [μm]
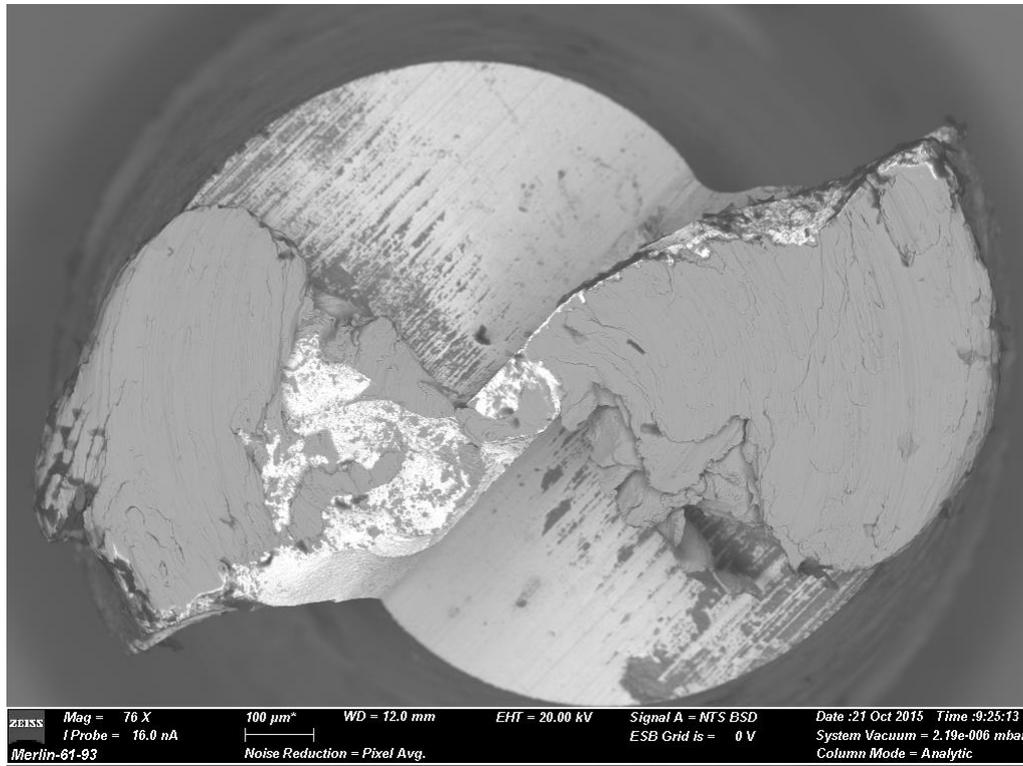
Figure 64: Experimental run 11: Tungsten carbide tool after machining with parameters v_c =70.69 [m/min], v_f =612.97 [mm/min] and a_p =143.58 [μm]
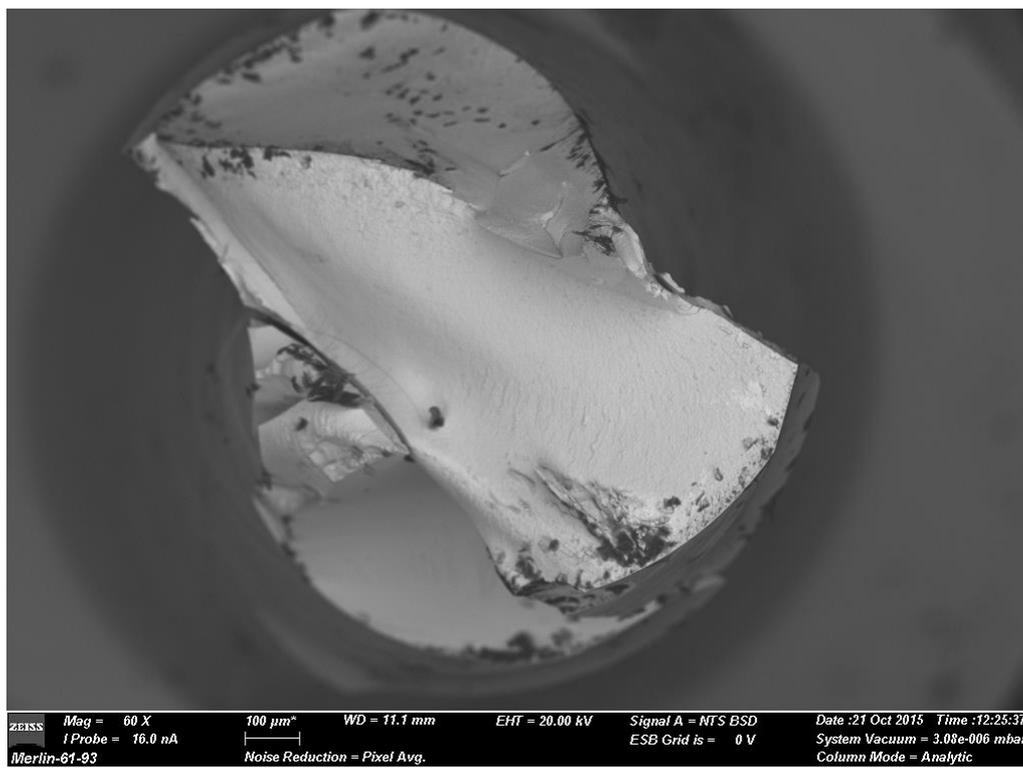
Figure 65: Experimental run 12: Tungsten carbide tool after machining with parameters v_c =75.4 [m/min], v_f =768 [mm/min] and a_p =125 [μm]
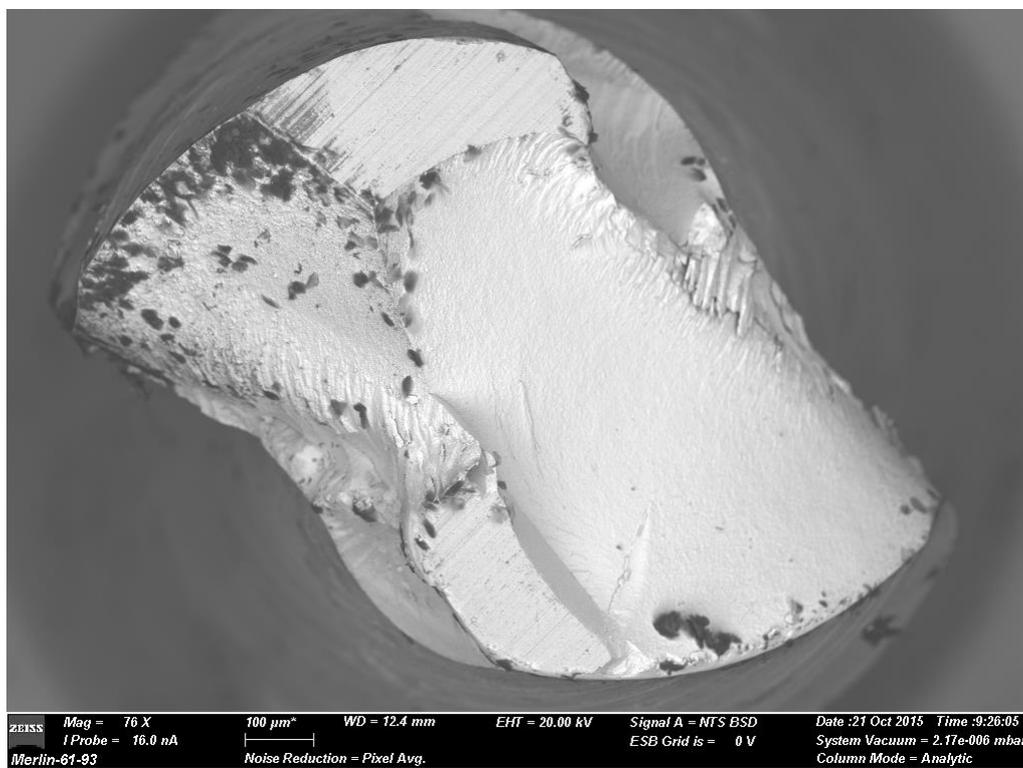
Figure 66: Experimental run 13: Tungsten carbide tool after machining with parameters v_c =84.82 [m/min], v_f =864 [mm/min] and a_p =125 [μm]
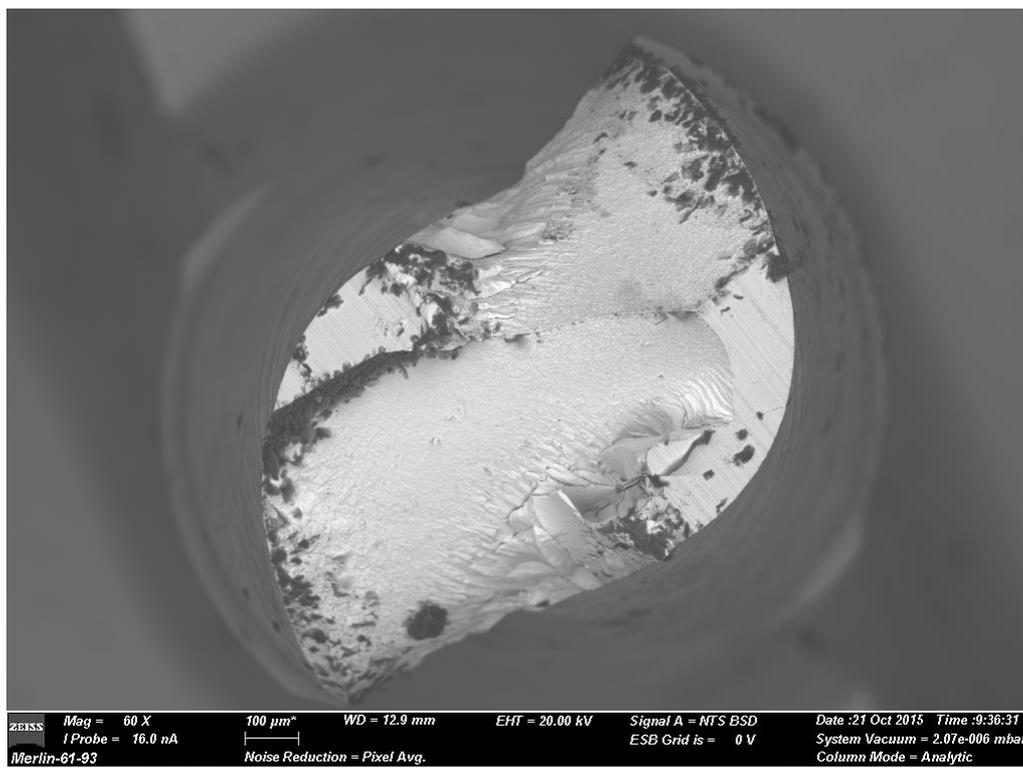
Figure 67: Experimental run 14: Tungsten carbide tool after machining with parameters v_c =80.11 [m/min], v_f =937.3 [mm/min] and a_p =106.42 [µm]
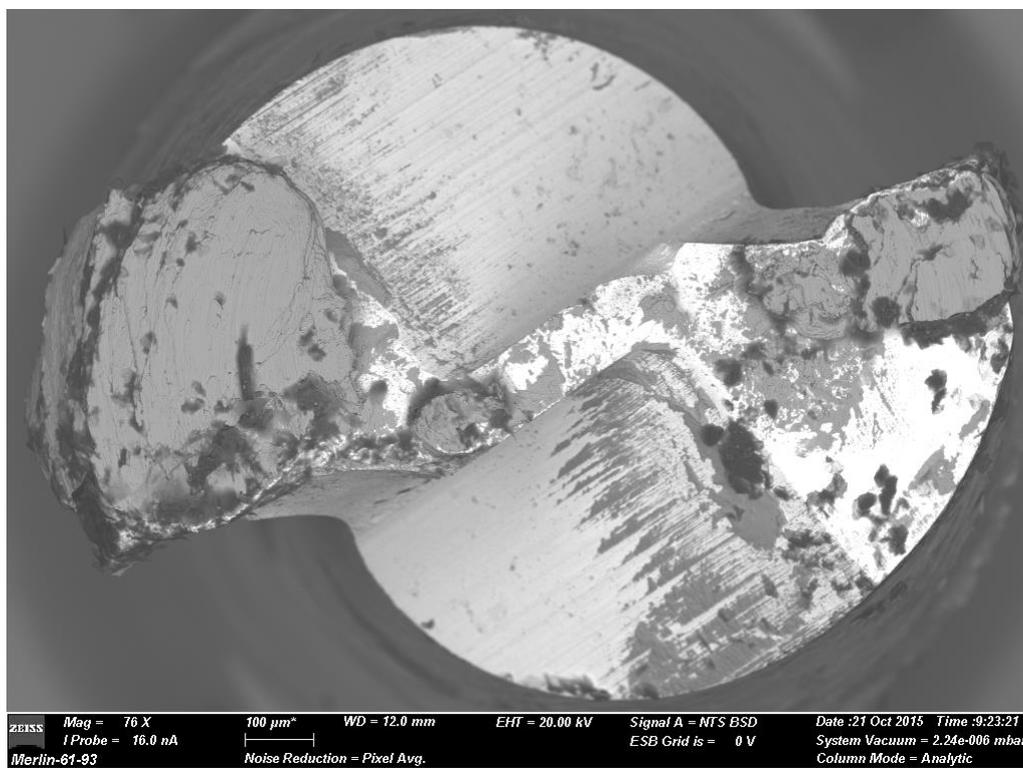
Figure 68: Experimental run 15: Tungsten carbide tool after machining with parameters v_c =75.4 [m/min], v_f =768 [mm/min] and a_p =125 [µm]
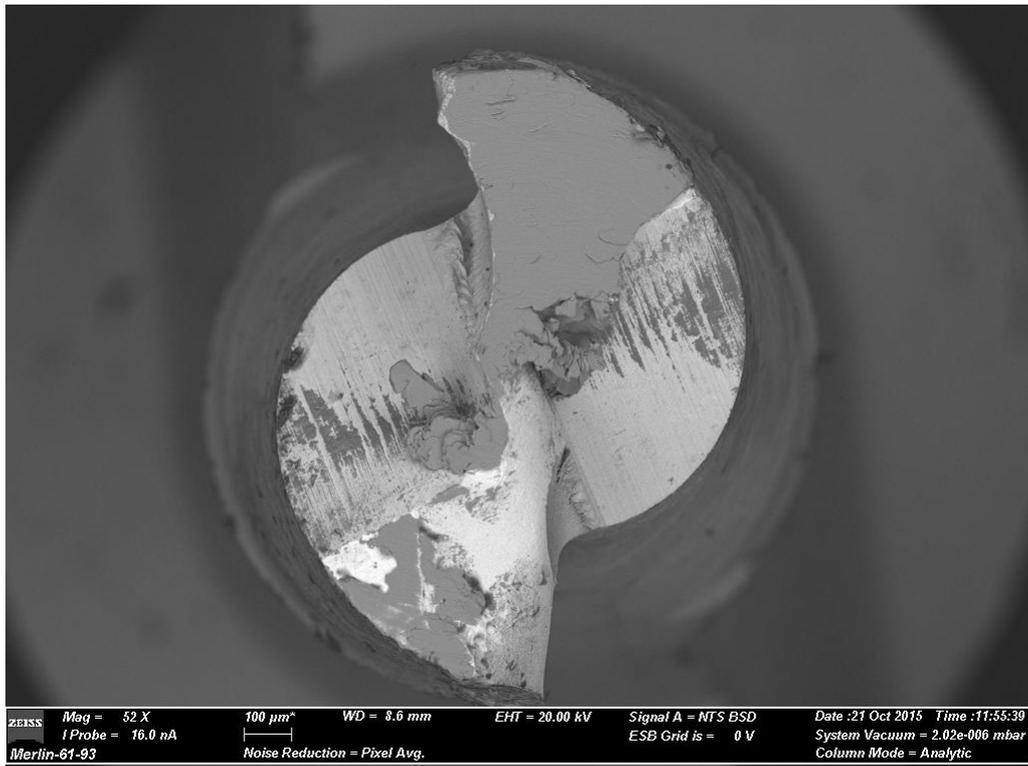
Figure 69: Experimental run 16: Tungsten carbide tool after machining with parameters v_c =75.4 [m/min], v_f =768 [mm/min] and a_p =125 [μm]
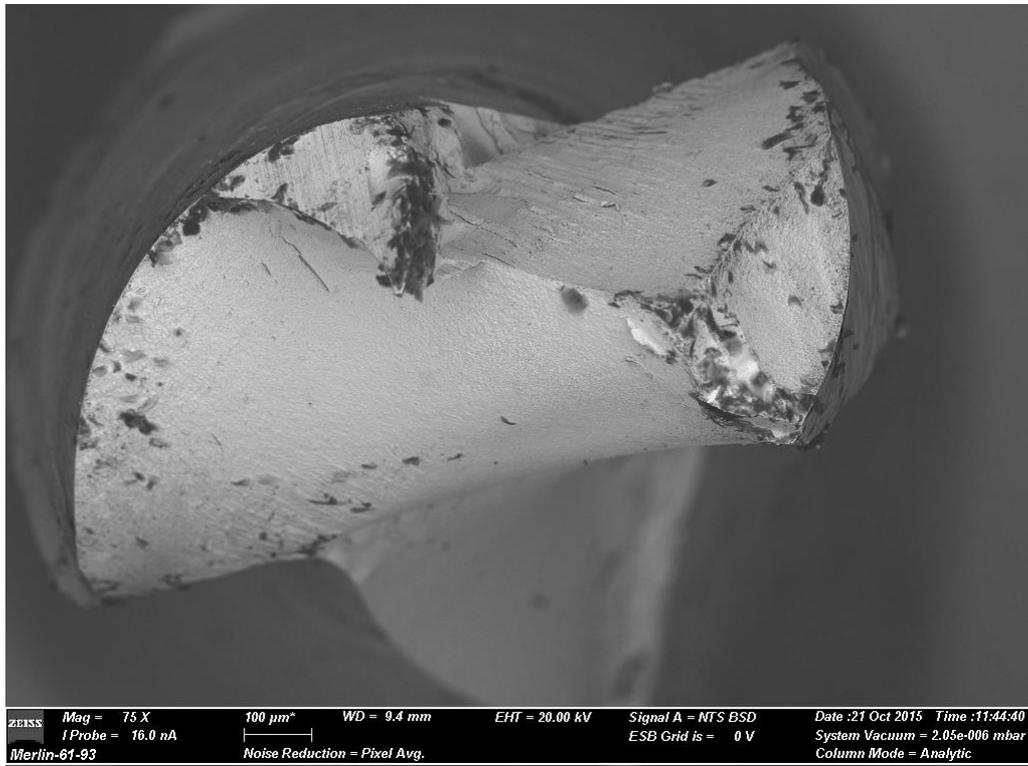
Figure 70: Experimental run 17: Tungsten carbide tool after machining with parameters v_c =75.4 [m/min], v_f =768 [mm/min] and a_p =125 [μm]
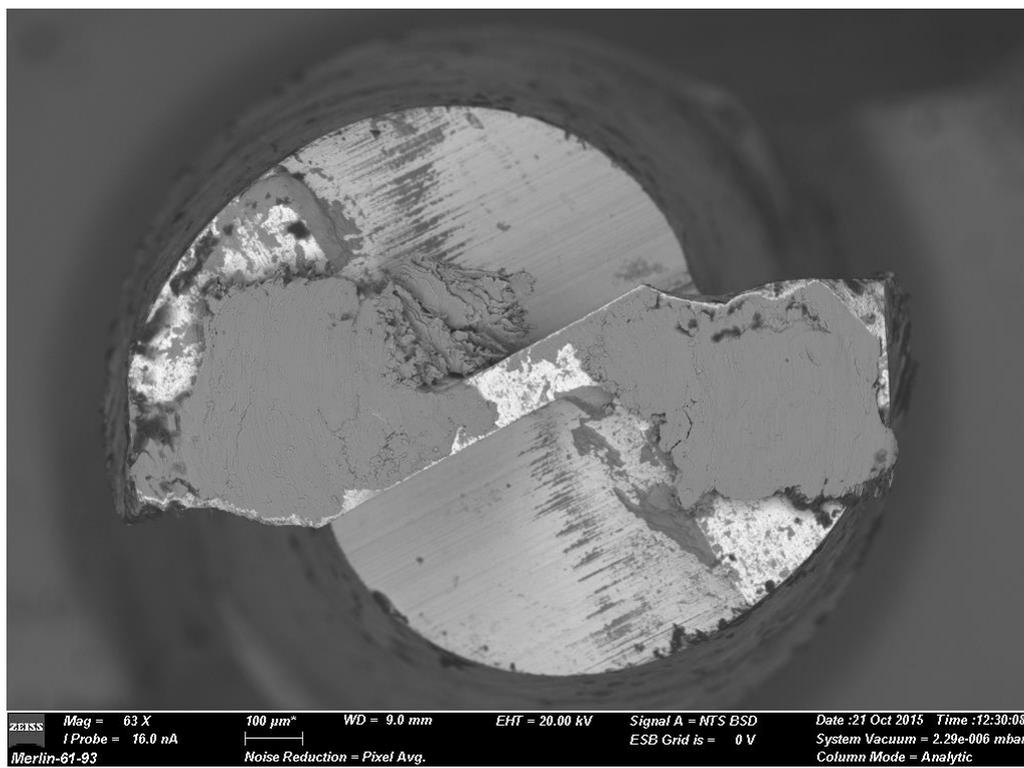
Figure 71: Experimental run 18: Tungsten carbide tool after machining with parameters v_c =70.69 [m/min], v_f =827.03 [mm/min] and a_p =143.58 [μm]
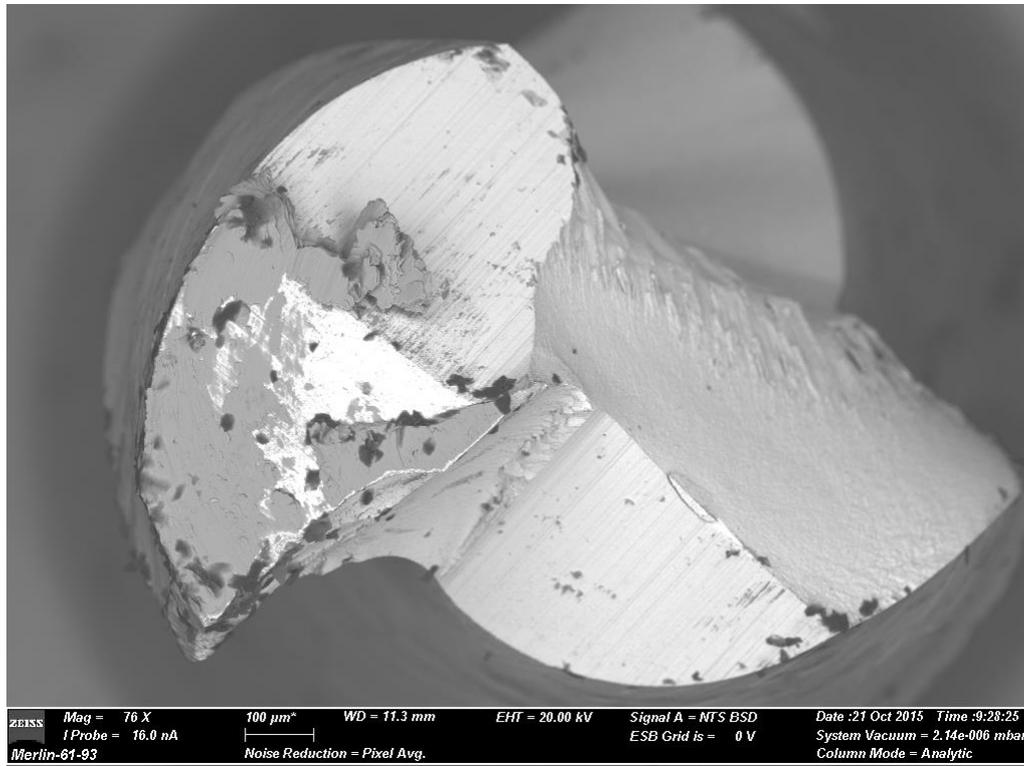
Figure 72: Experimental run 19: Tungsten carbide tool after machining with parameters v_c =75.4 [m/min], v_f =768 [mm/min] and a_p =125 [μm]
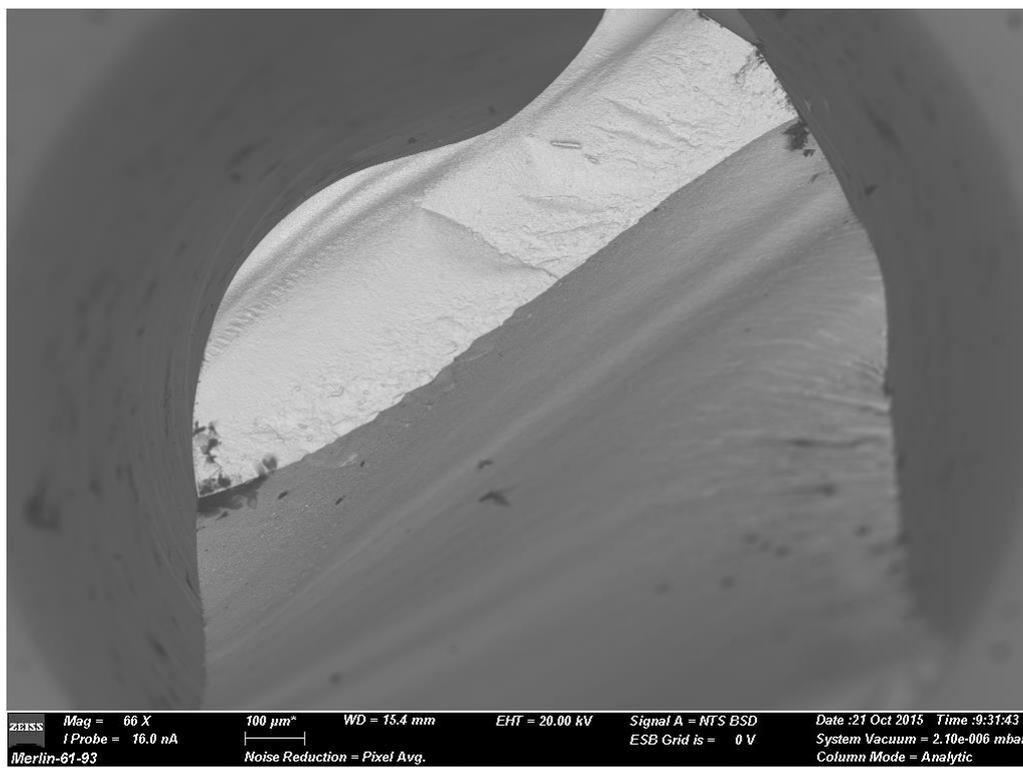
Figure 73: Experimental run 20: Tungsten carbide tool after machining with parameters v_c =75.4 [m/min], v_f =768 [mm/min] and a_p =156.25 [µm]

APPENDIX B

For the purpose of this study tool life was defined as the distance cut to where the tool experienced 200 μm wear. This wear was measured by measuring the width of the slots of each experiment on the Ti-6Al-4V plates. Each Ti-6Al-4V plate contained 6-8 experiments with between 1 and 6, 70 mm slots each. The width of the slots were measured in 20 mm increments across all experiments. These measurements were fitted with a mathematical model and the distance cut in millimetres from where the slot width was 1300 μm was calculated and recorded as the tool life result. For the purpose of this study tool wear was defined as the rate at which the tungsten carbide tool tips reduce in diameter per millimetre cut. These values were also calculated from the width measurements of the slots over distance cut. Appendix B shows the width of the milled slots over time for each tool.
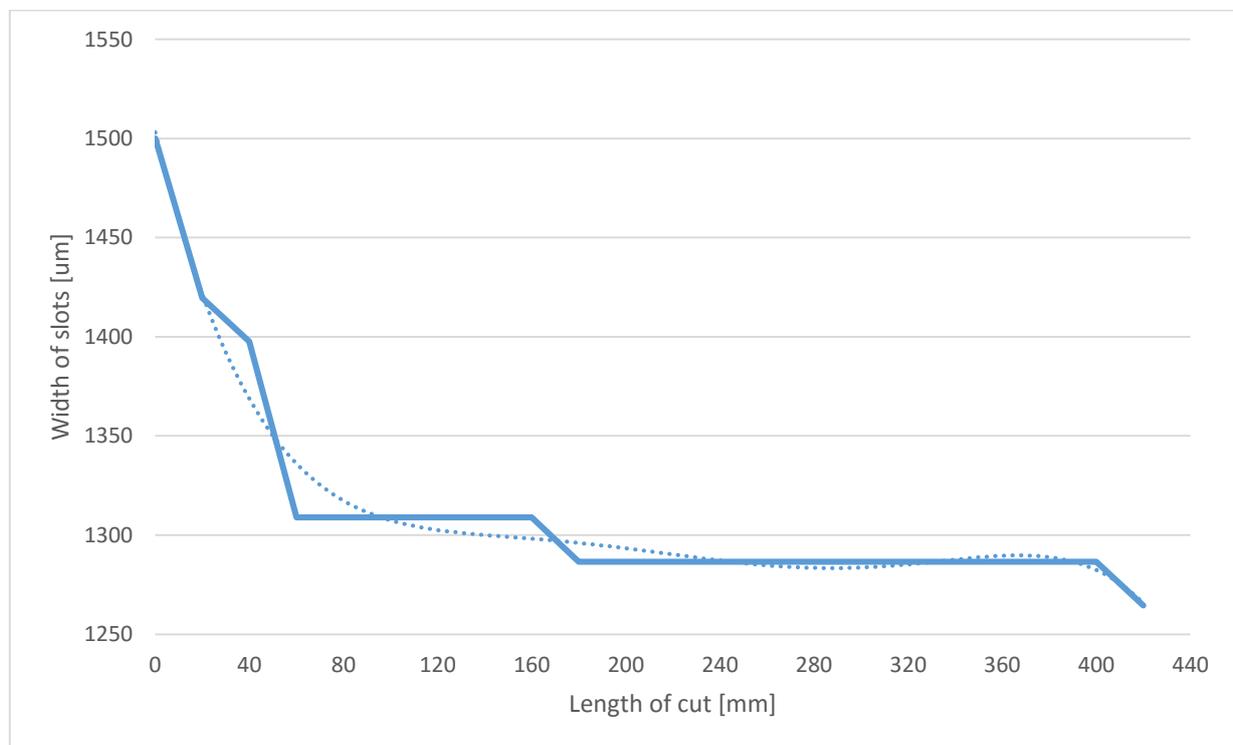

Figure 74: Experimental run 1: Tool wear graph after machining with parameters v_c =65.97 [m/min], v_f =672 [mm/min] and a_p =125 [μm]
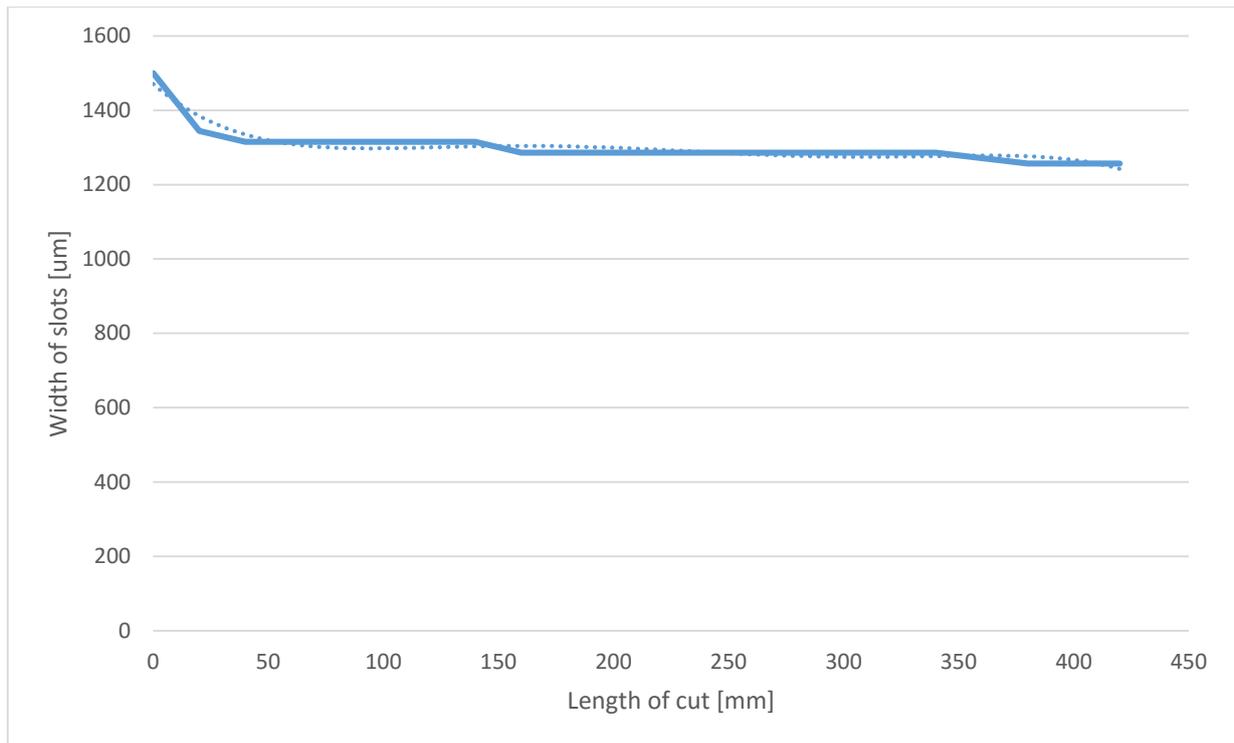
Figure 75: Experimental run 2: Tool wear graph after machining with parameters v_c =75.4 [m/min], v_f =768 [mm/min] and a_p =93.75 [μm]
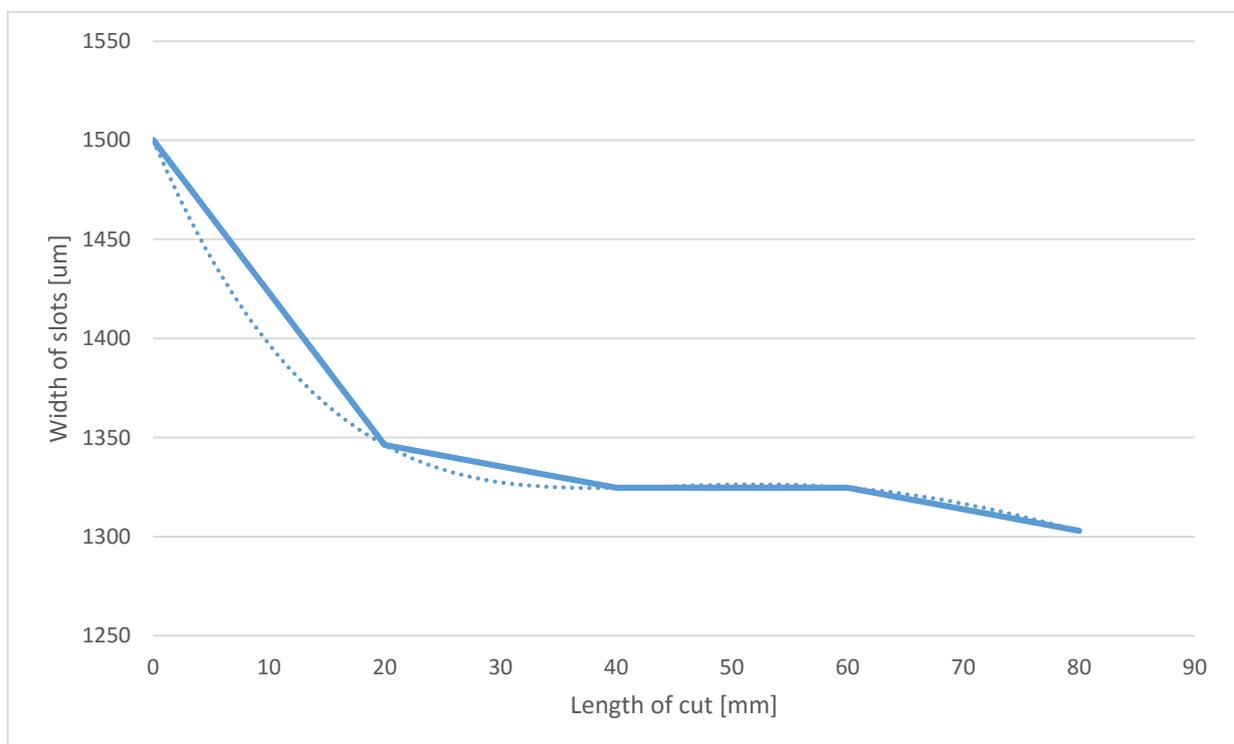
Figure 76: Experimental run 3: Tool wear graph after machining with parameters v_c =75.4 [m/min], v_f =768 [mm/min] and a_p =125 [μm]
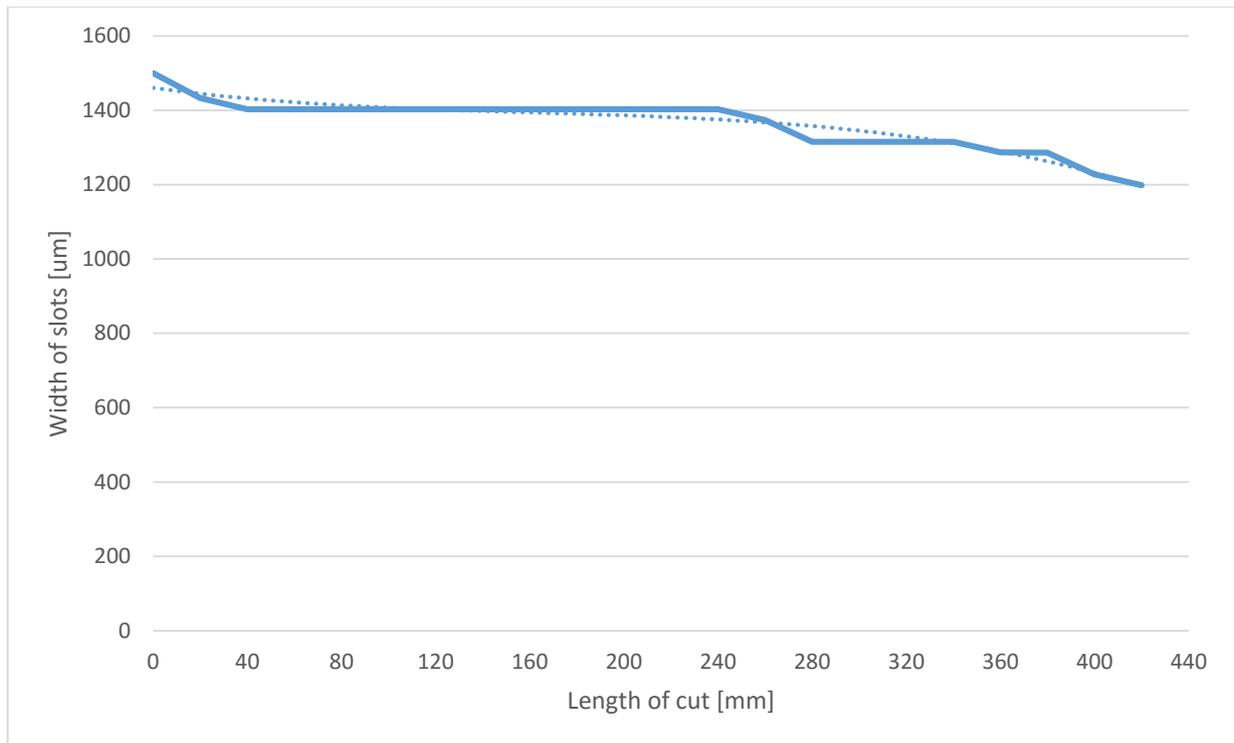
Figure 77: Experimental run 4: Tool wear graph after machining with parameters v_c =80.11 [m/min], v_f =937.3 [mm/min] and a_p =143.58 [μm]
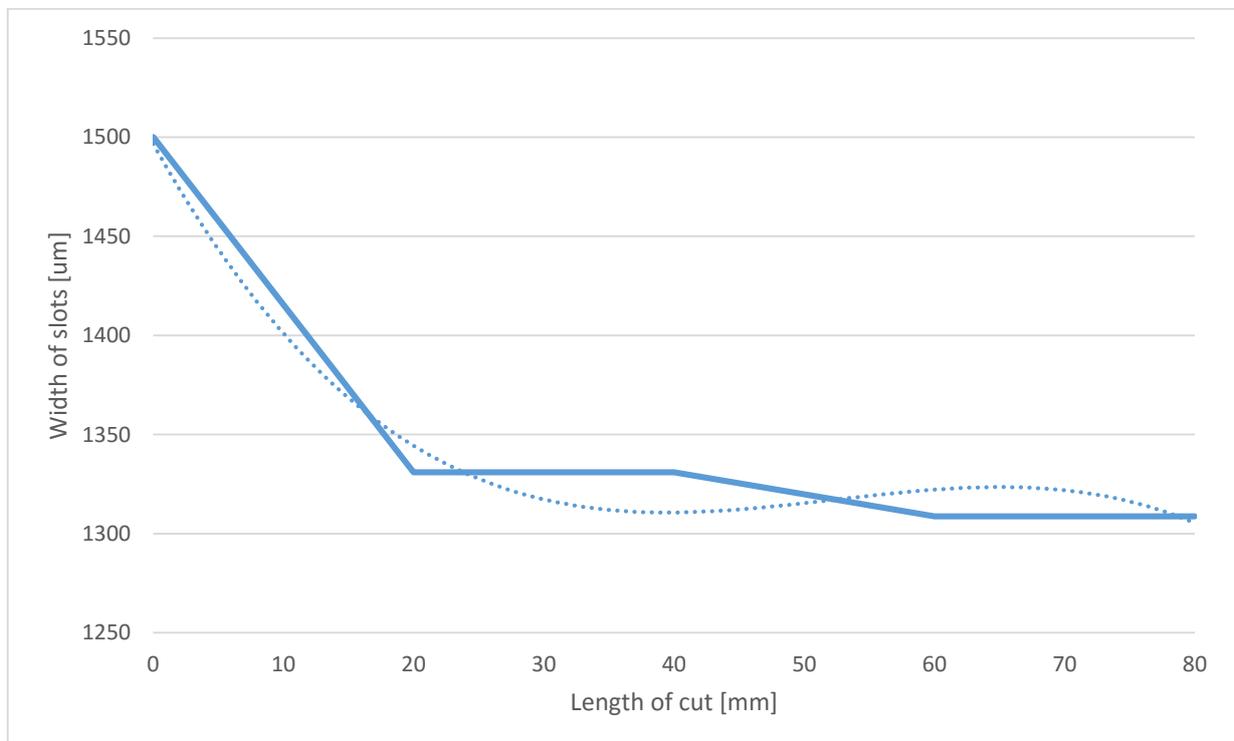

Figure 78: Experimental run 5: Tool wear graph after machining with parameters v_c =80.11 [m/min], v_f =694.7 [mm/min] and a_p =143.58 [μm]
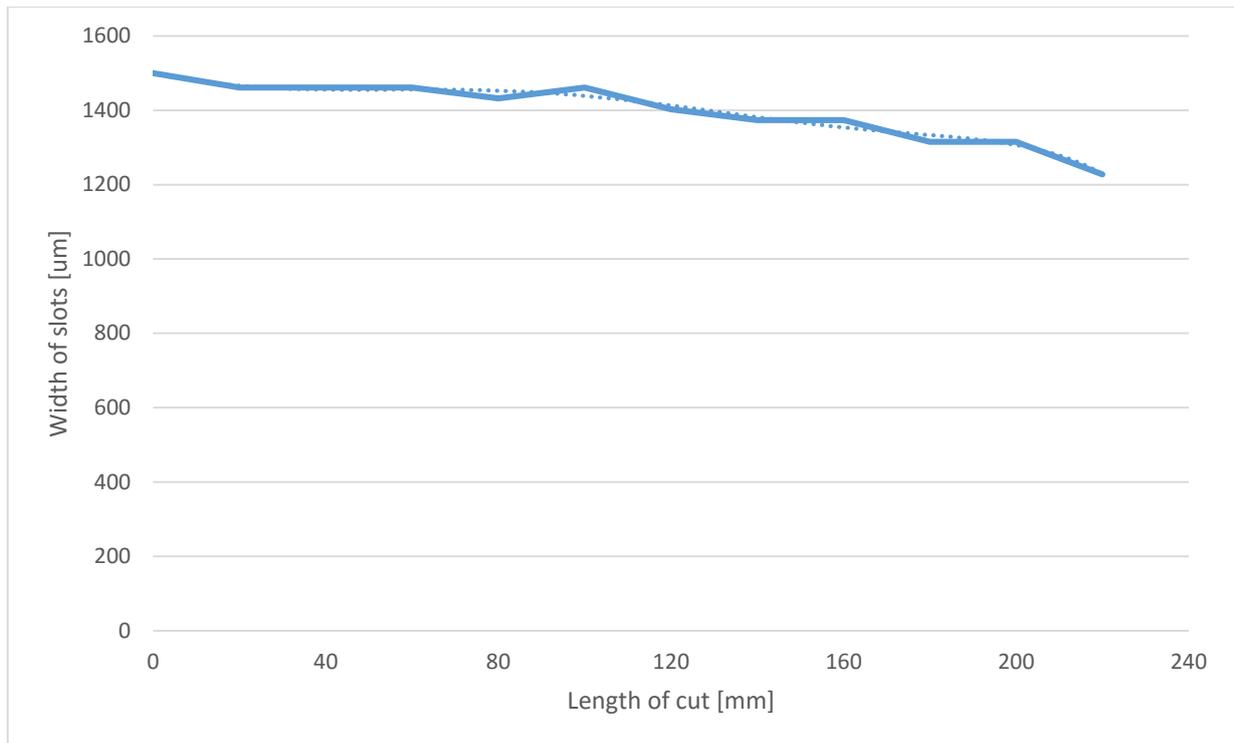
Figure 79: Experimental run 6: Tool wear graph after machining with parameters v_c =80.11 [m/min], v_f =694.7 [mm/min] and a_p =106.42 [μm]
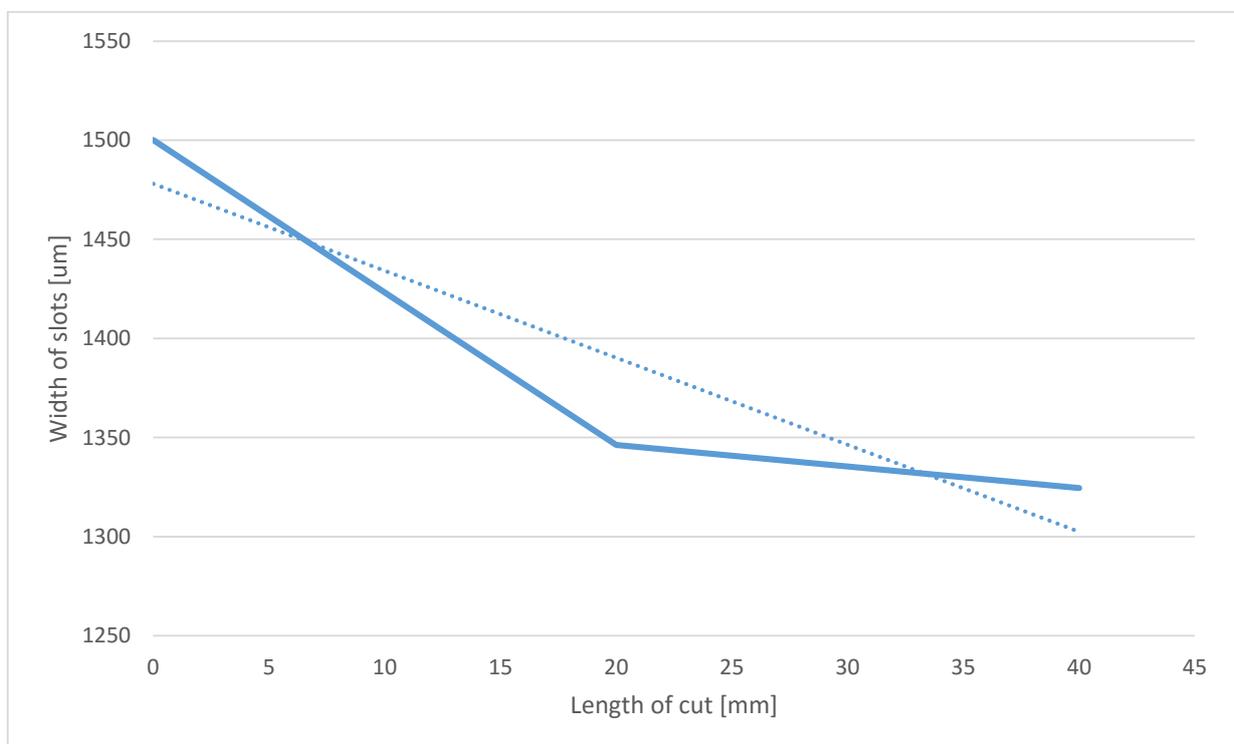

Figure 80: Experimental run 7: Tool wear graph after machining with parameters v_c =75.4 [m/min], v_f =576 [mm/min] and a_p =125 [μm]
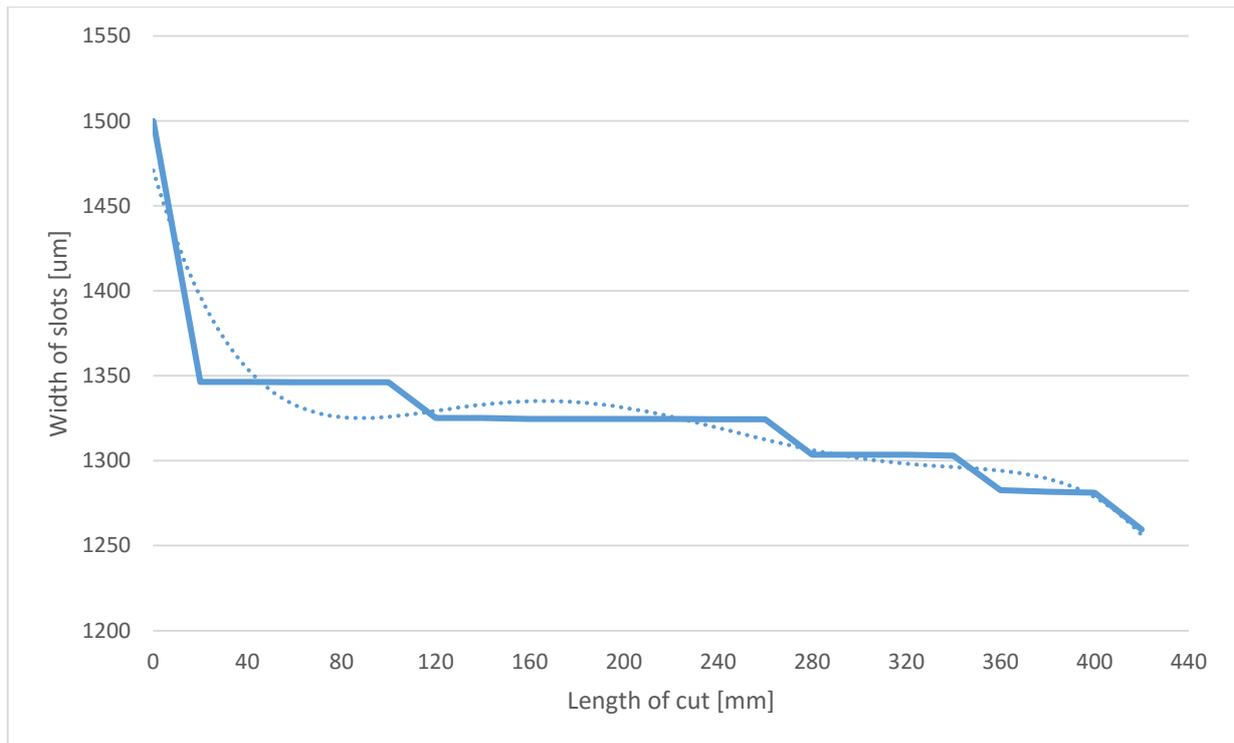
Figure 81: Experimental run 8: Tool wear graph after machining with parameters v_c =70.69 [m/min], v_f =612.97 [mm/min] and a_p =106.42 [μm]
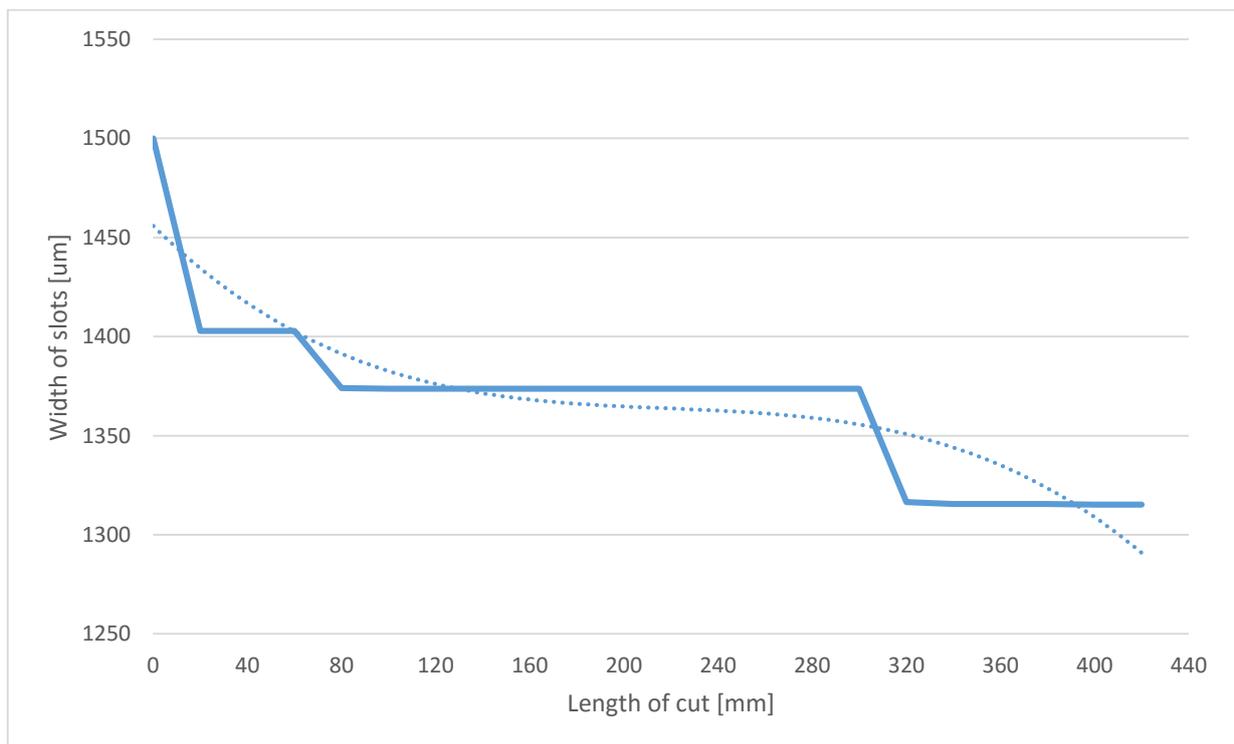
Figure 82: Experimental run 9: Tool wear graph after machining with parameters v_c =75.4 [m/min], v_f =960 [mm/min] and a_p =125 [μm]
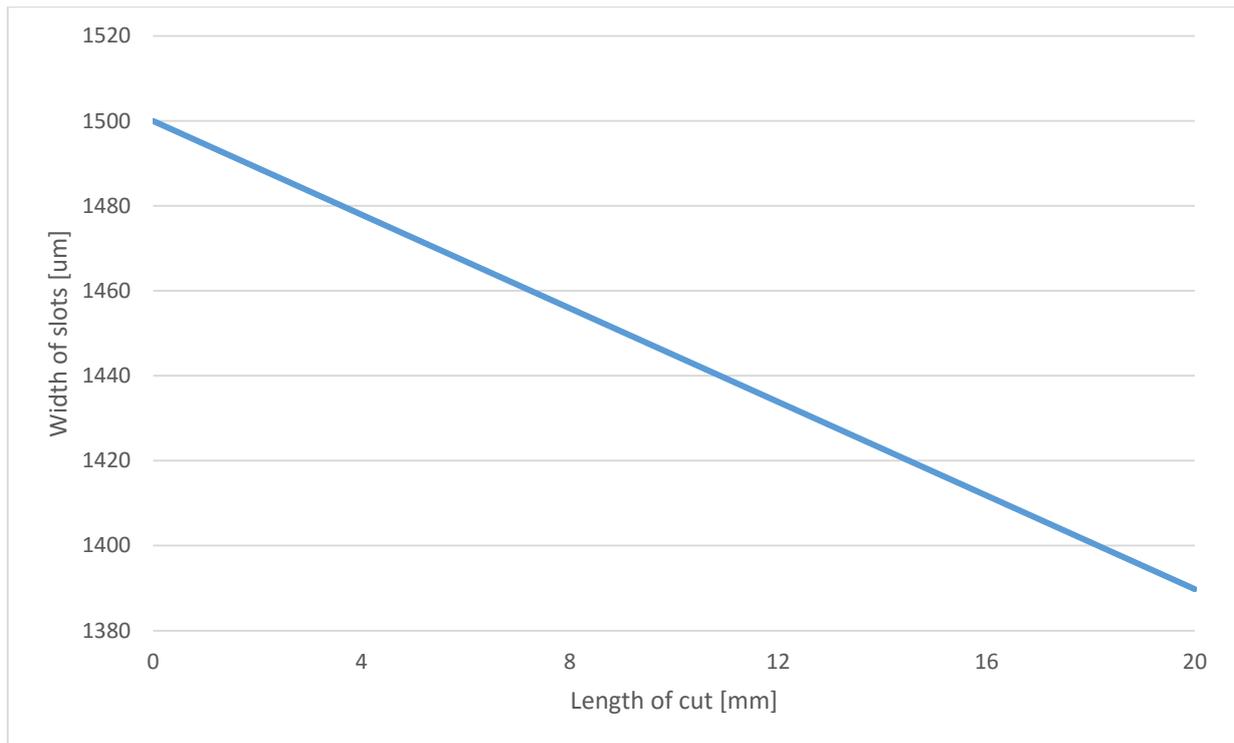
Figure 83: Experimental run 10: Tool wear graph after machining with parameters v_c =70.69 [m/min], v_f =827.03 [mm/min] and a_p =106.42 [μm]
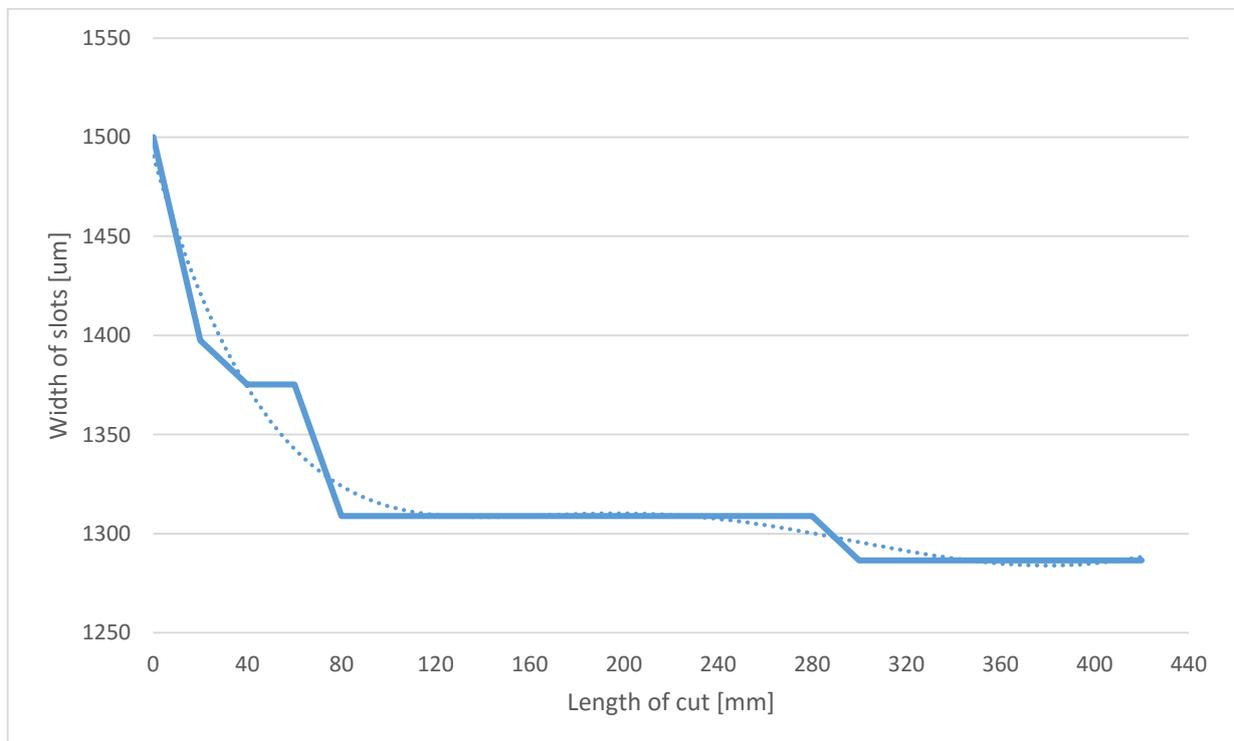
Figure 84: Experimental run 11: Tool wear graph after machining with parameters v_c =70.69 [m/min], v_f =612.97 [mm/min] and a_p =143.58 [μm]
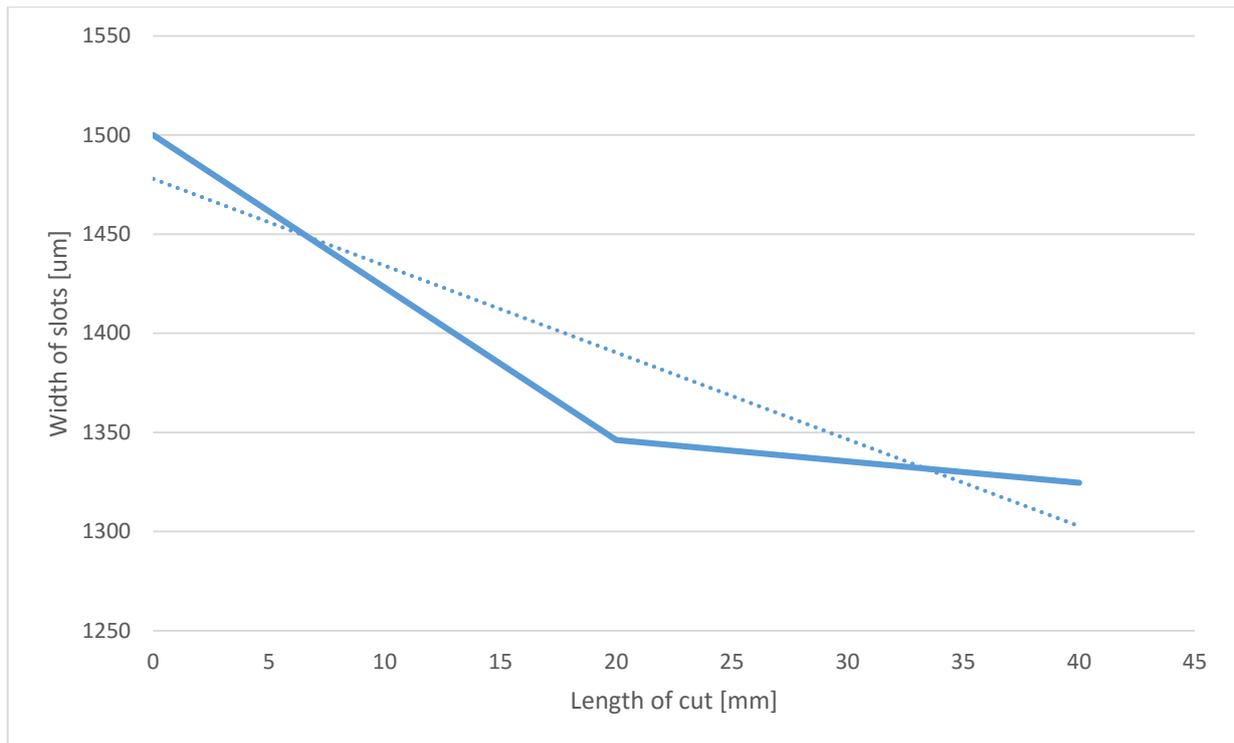
Figure 85: Experimental run 12: Tool wear graph after machining with parameters v_c =75.4 [m/min], v_f =768 [mm/min] and a_p =125 [μm]
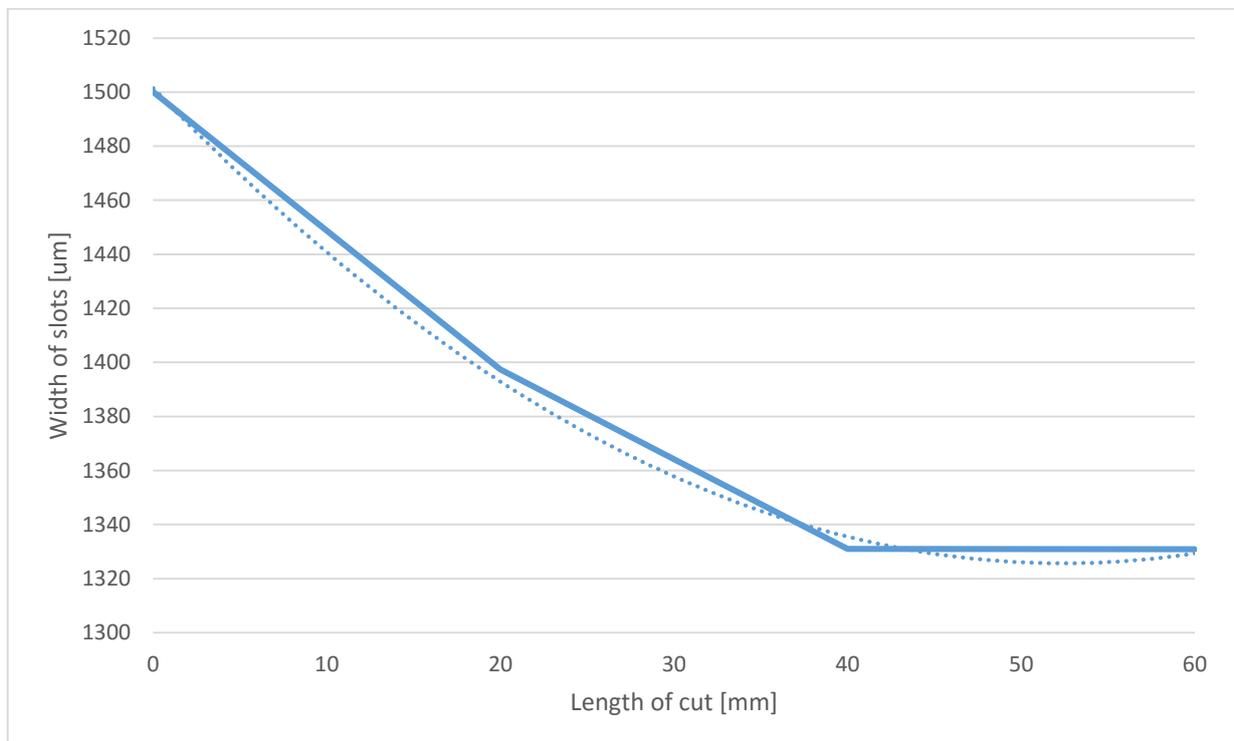
Figure 86: Experimental run 13: Tool wear graph after machining with parameters v_c =84.82 [m/min], v_f =864 [mm/min] and a_p =125 [μm]
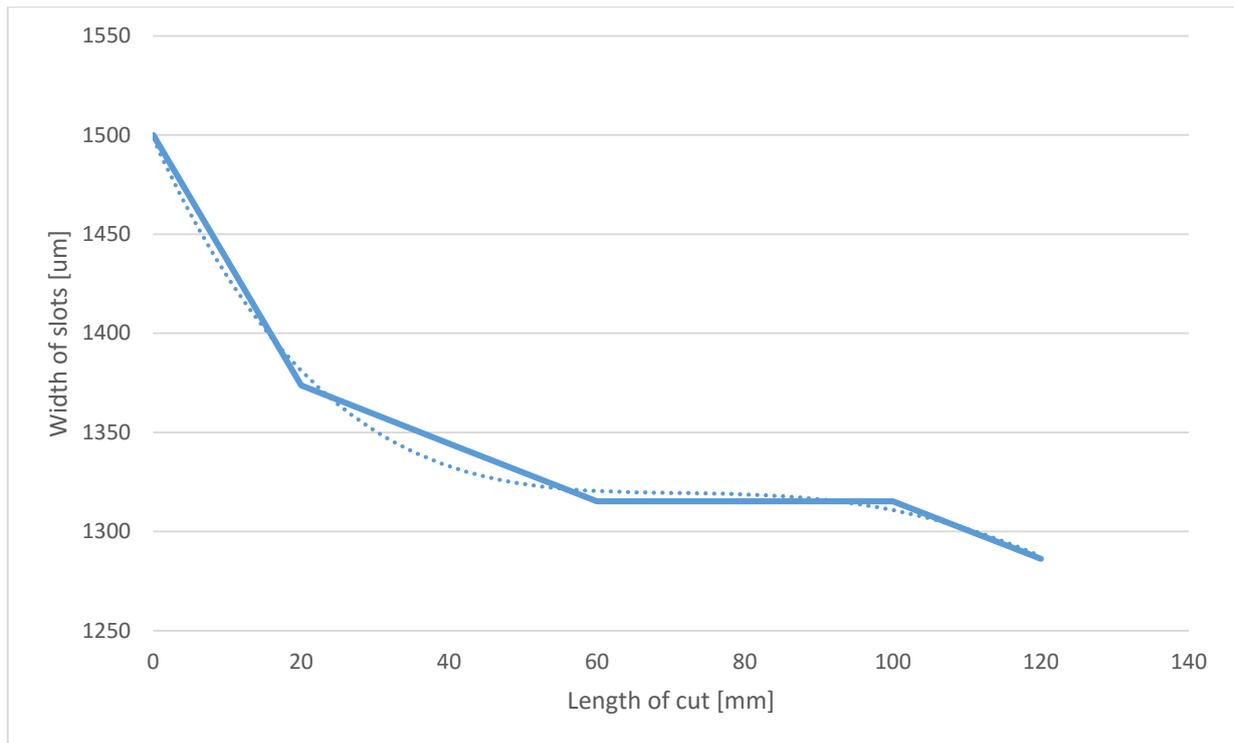
Figure 87: Experimental run 14: Tool wear graph after machining with parameters v_c =80.11 [m/min], v_f =937.3 [mm/min] and a_p =106.42 [μm]
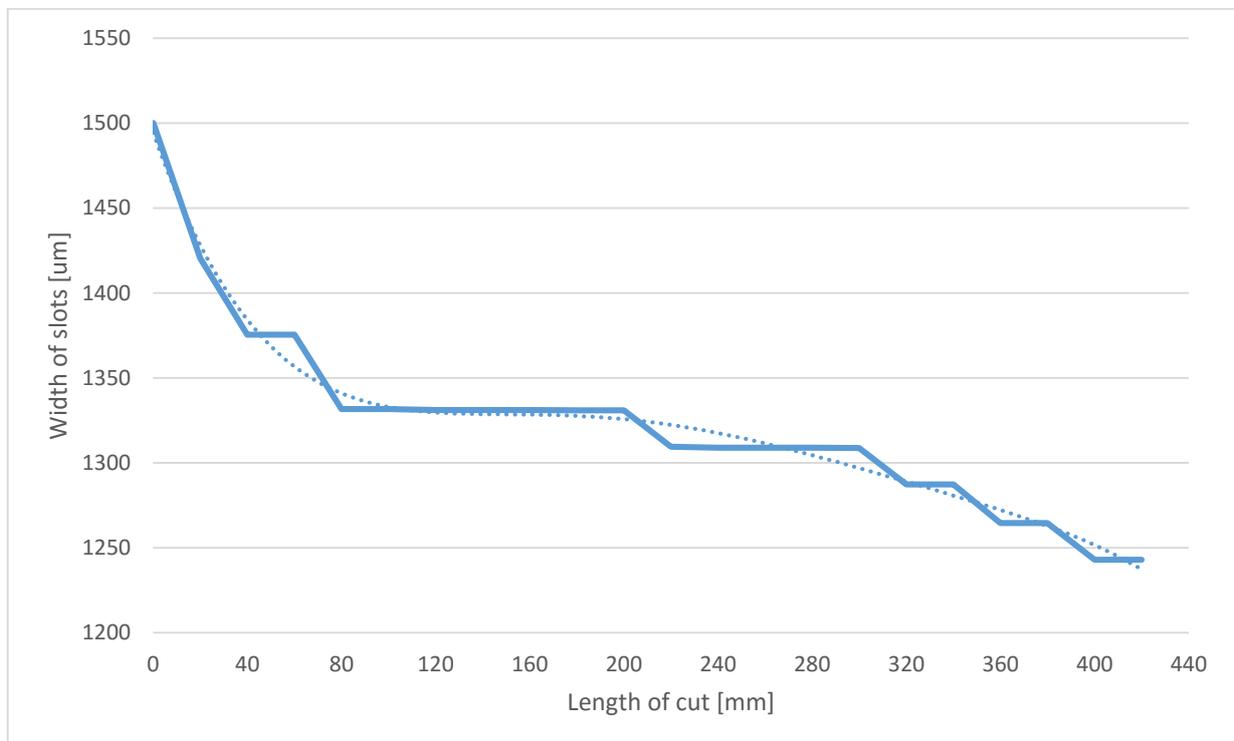

Figure 88: Experimental run 15: Tool wear graph after machining with parameters v_c =75.4 [m/min], v_f =768 [mm/min] and a_p =125 [μm]
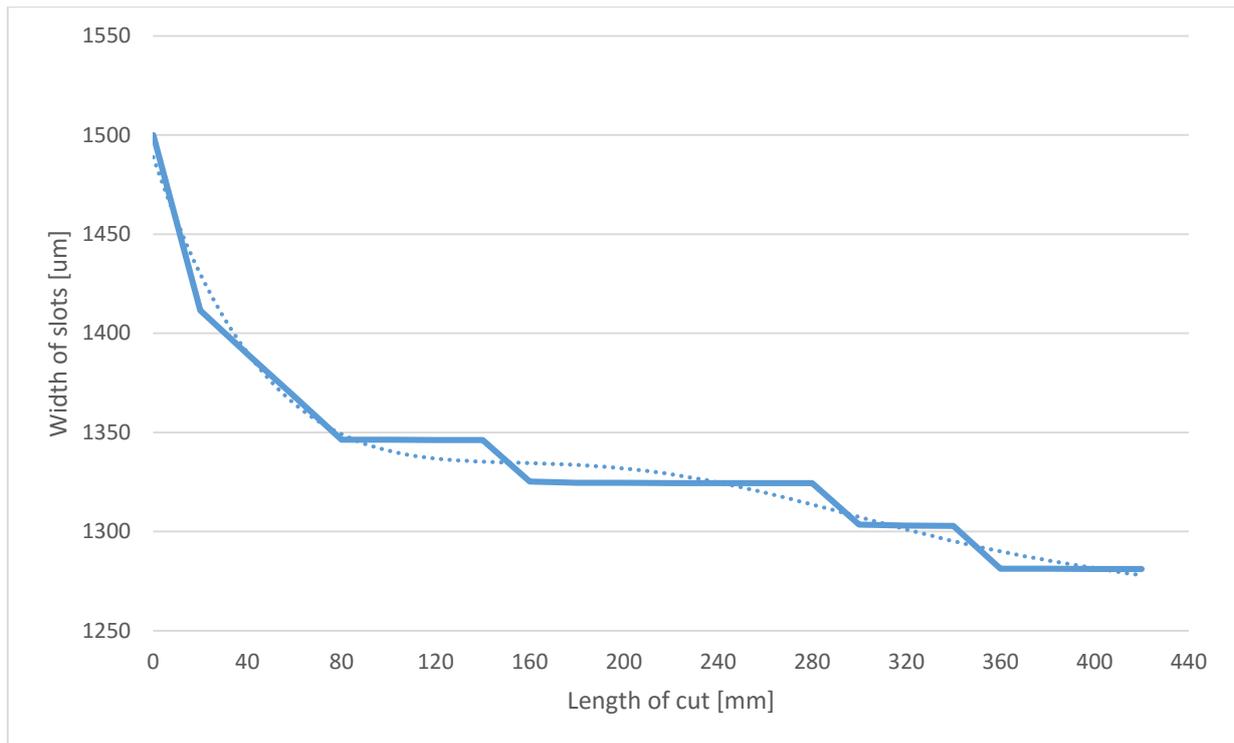
Figure 89: Experimental run 16: Tool wear graph after machining with parameters v_c =75.4 [m/min], v_f =768 [mm/min] and a_p =125 [μm]
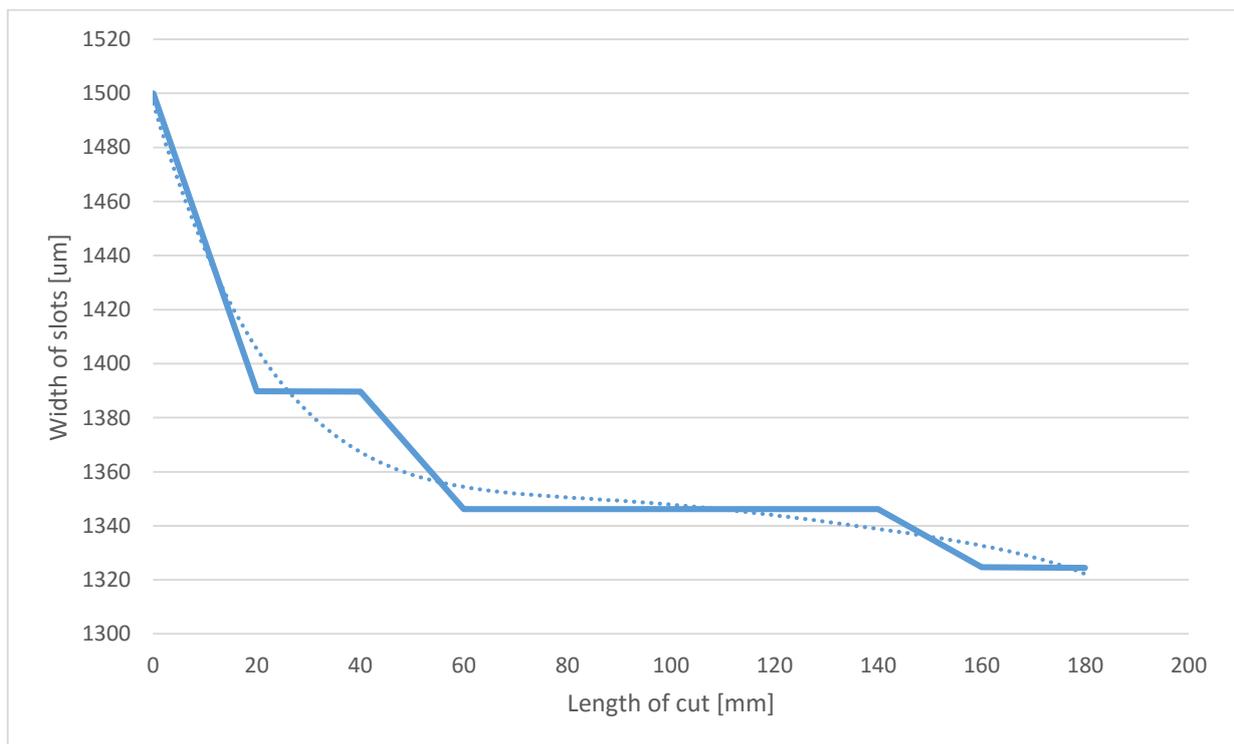

Figure 90: Experimental run 17: Tool wear graph after machining with parameters v_c =75.4 [m/min], v_f =768 [mm/min] and a_p =125 [μm]
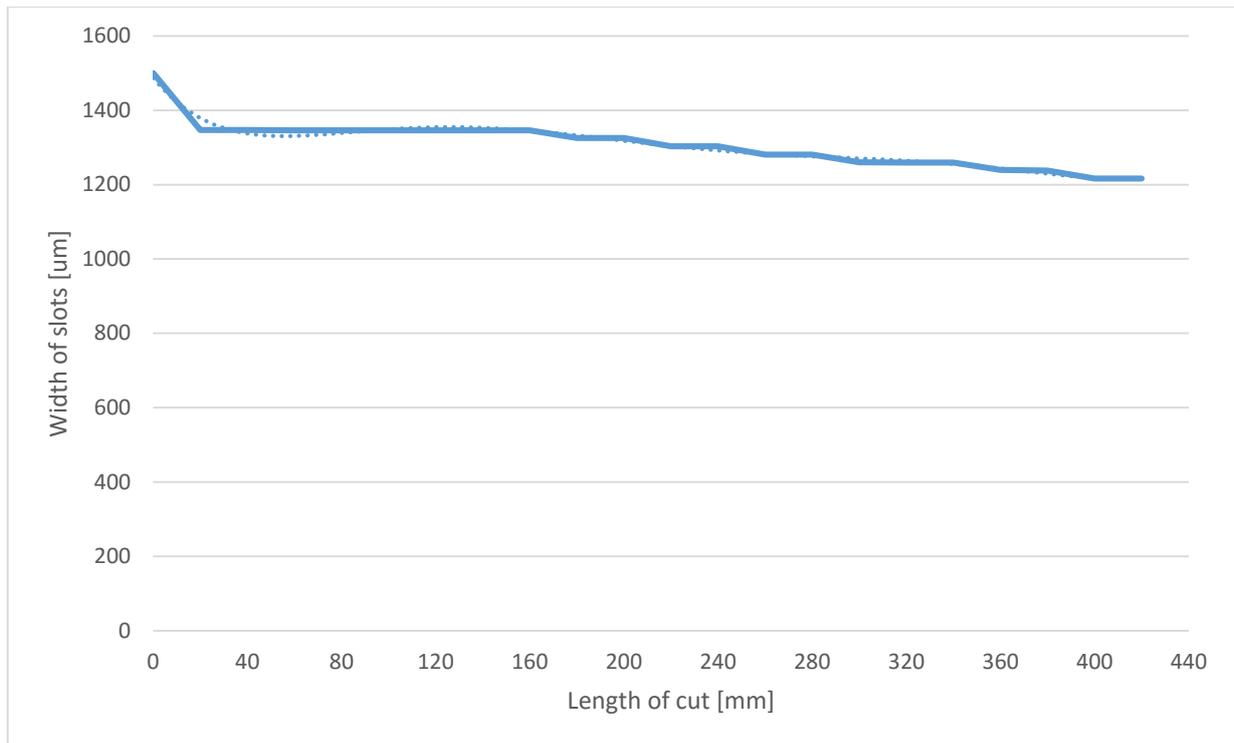
Figure 91: Experimental run 18: Tool wear graph after machining with parameters v_c =70.69 [m/min], v_f =827.03 [mm/min] and a_p =143.58 [µm]
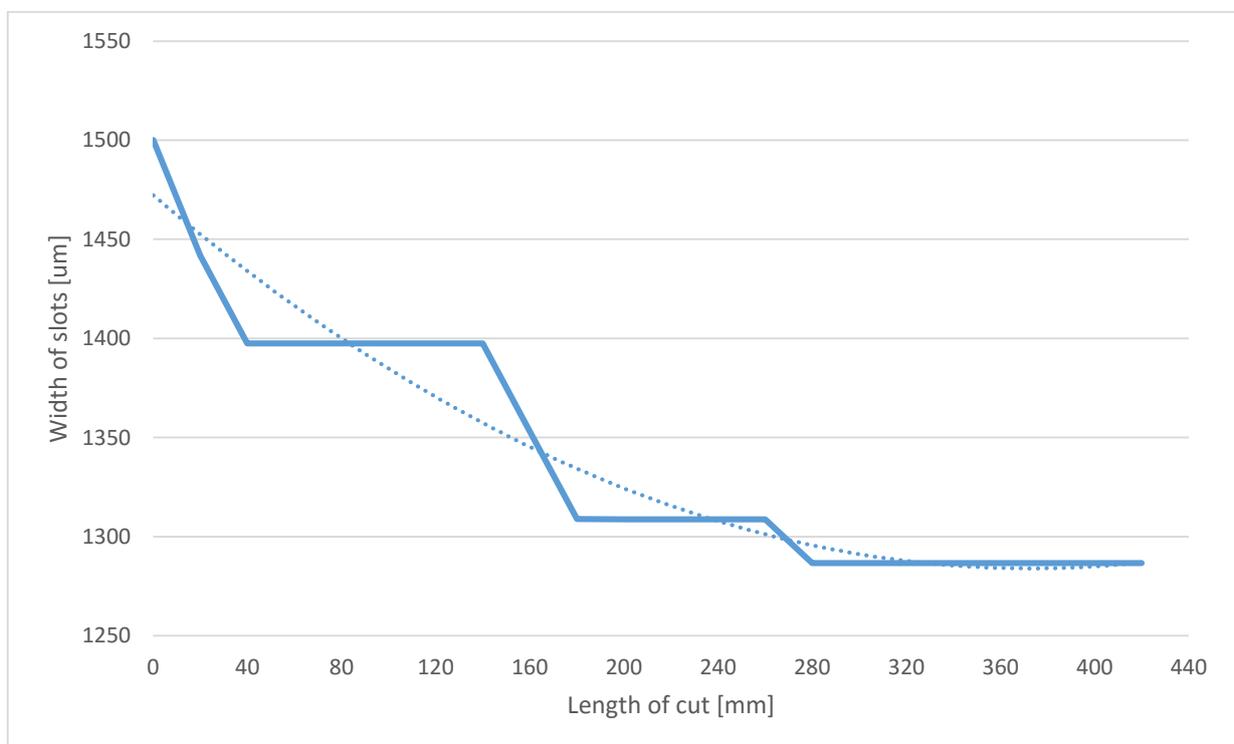

Figure 92: Experimental run 19: Tool wear graph after machining with parameters v_c =75.4 [m/min], v_f =768 [mm/min] and a_p =125 [µm]
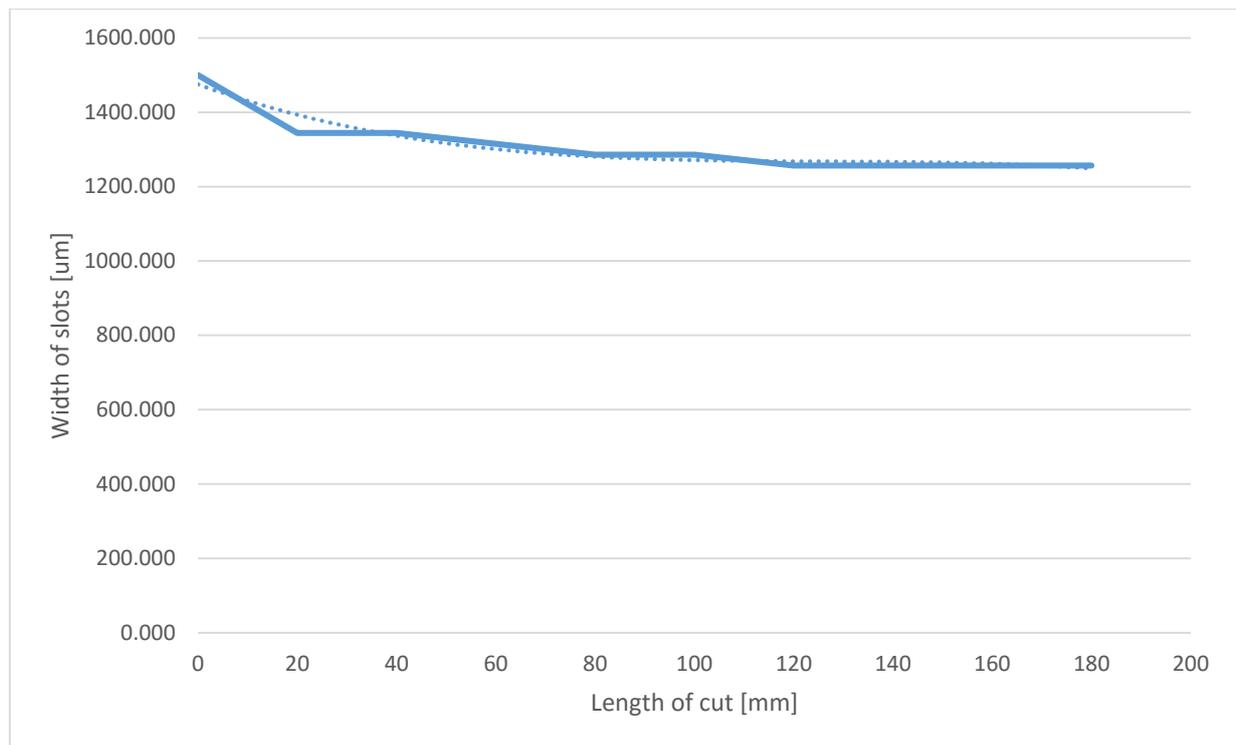
Figure 93: Experimental run 20: Tool wear graph after machining with parameters v_c =75.4 [m/min], v_f =768 [mm/min] and a_p =156.25 [µm]

APPENDIX C

After each experiment the chips for that experiment was gathered and microscope images was taken of each set of chips. The chip sets were then categorised from 0 – 2 depending on what they looked like. A score of zero was given to chip sets who were relatively large and well formed. A score of 2 was given to chip sets who were extremely fragmented and broken into very small bits. A score of 1 was given to chip sets who contained elements of both. Appendix C shows all of the experimental chip sets with their scores and parameters used.

Figure 94: Experimental run 1: Chip set with score after machining with parameters v_c =65.97 [m/min], v_f =672 [mm/min] and a_p =125 [μm]

Figure 95: Experimental run 2: Chip set with score after machining with parameters v_c =75.4 [m/min], v_f =768 [mm/min] and a_p =93.75 [μm]

XXIII

Figure 96: Experimental run 3: Chip set with score after machining with parameters v_c =75.4 [m/min], v_f =768 [mm/min] and a_p =125 [μm]

Figure 97: Experimental run 4: Chip set with score after machining with parameters v_c =80.11 [m/min], v_f =937.3 [mm/min] and a_p =143.58 [μm]

Figure 98: Experimental run 5: Chip set with score after machining with parameters v_c =80.11 [m/min], v_f =694.7 [mm/min] and a_p =143.58 [μm]

Figure 99: Experimental run 6: Chip set with score after machining with parameters v_c =80.11 [m/min], v_f =694.7 [mm/min] and a_p =106.42 [μm]

Figure 100: Experimental run 7: Chip set with score after machining with parameters v_c =75.4 [m/min], v_f =576 [mm/min] and a_p =125 [μm]

Figure 101: Experimental run 8: Chip set with score after machining with parameters v_c =70.69 [m/min], v_f =612.97 [mm/min] and a_p =106.42 [μm]

Figure 102: Experimental run 9: Chip set with score after machining with parameters v_c =75.4 [m/min], v_f =960 [mm/min] and a_p =125 [μm]

Figure 103: Experimental run 10: Chip set with score after machining with parameters v_c =70.69 [m/min], v_f =827.03 [mm/min] and a_p =106.42 [μm]

Figure 104: Experimental run 11: Chip set with score after machining with parameters v_c =70.69 [m/min], v_f =612.97 [mm/min] and a_p =143.58 [μm]

Figure 105: Experimental run 12: Chip set with score after machining with parameters v_c =75.4 [m/min], v_f =768 [mm/min] and a_p =125 [μm]

Figure 106: Experimental run 13: Chip set with score after machining with parameters v_c =84.82 [m/min], v_f =864 [mm/min] and a_p =125 [μm]

Figure 107: Experimental run 14: Chip set with score after machining with parameters v_c =80.11 [m/min], v_f =937.3 [mm/min] and a_p =106.42 [μm]

Figure 108: Experimental run 15: Chip set with score after machining with parameters v_c =75.4 [m/min], v_f =768 [mm/min] and a_p =125 [μm]
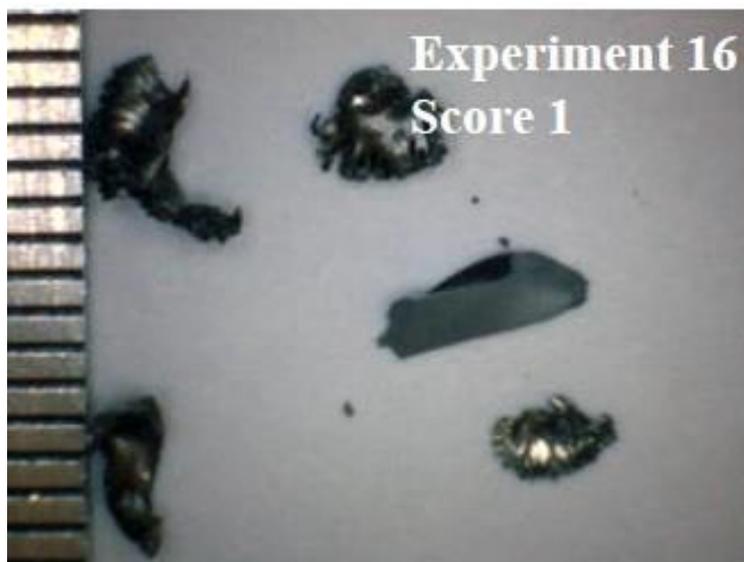
Figure 109: Experimental run 16: Chip set with score after machining with parameters v_c =75.4 [m/min], v_f =768 [mm/min] and a_p =125 [μm]

Figure 110: Experimental run 17: Chip set with score after machining with parameters v_c =75.4 [m/min], v_f =768 [mm/min] and a_p =125 [μm]

Figure 111: Experimental run 18: Chip set with score after machining with parameters v_c =70.69 [m/min], v_f =827.03 [mm/min] and a_p =143.58 [μm]

Figure 112: Experimental run 19: Chip set with score after machining with parameters v_c =75.4 [m/min], v_f =768 [mm/min] and a_p =125 [μm]

Figure 113: Experimental run 20: Chip set with score after machining with parameters v_c =75.4 [m/min], v_f =768 [mm/min] and a_p =156.25 [μm]